GREEN BASED SORPTION TECHNOLOGY FOR REMOVAL OF SELECTED PHARMACEUTICALS FROM WASTEWATER AND THEIR DISCHARGE LOADS WITHIN LAKE VICTORIA BASIN, KENYA

Selly Jemutai Kimosop

A THESIS SUBMITTED IN PARTIAL FULFILLMENT FOR THE REQUIREMENT OF THE DEGREE OF DOCTOR OF PHILOSOPHY (PHD) IN CHEMISTRY OF MASINDE MULIRO UNIVERSITY OF SCIENCE AND TECHNOLOGY

March, 2018

DECLARATION

Declaration by Candidate

This thesis is my original work prepared with no other than the indicated sources and support and has not been presented elsewhere for a degree or any other award.

Signature..... .Date….....

KIMOSOP SELLY JEMUTAI

SCH/H/01/13

Declaration by Supervisors

The undersigned certify that they have read and hereby recommend for acceptance of Masinde Muliro University of Science and Technology a thesis entitled:

"Green Based Sorption Technology for Removal of Selected Pharmaceuticals from Wastewater and their Discharge Loads within Lake Victoria Basin, Kenya."

Signature…….. Date……

Dr. Francis Orata Omoto,

Senior Lecturer, Department of Pure and Applied Chemistry,

Masinde Muliro University of Science and Technology

Signature…….....…….. Date…….....

Dr. Veronica A. Okello,

Lecturer, Department of Physical Sciences,

Machakos University College

Signature……..... Date…….....

Prof. Zachary M. Getenga,

Professor, Department of Chemistry,

Chuka University

COPYRIGHT

DEDICATION

I dedicate this work to my beloved family

ACKNOWLEDGMENT

Most of all, my gratitude is to God Almighty for granting me good health throughout the period of my studies.

My sincere gratitude goes to my Supervisors Dr. Francis Orata, Prof. Zachary Getenga and Dr. Veronicah Okello for their superb guidance and support for the entire study period. I am grateful for their valuable criticism, encouragement and great motivation that enabled smooth running of the research.

I would like to express my earnest appreciation to DAAD for award of a scholarship to enable completion of this work. I also thank the International Foundation for Science (IFS) for research grant towards this study. My sincere gratitude goes to the Alexander von Humboldt for research grant. I thank Chuka University for allowing the use of their high performance liquid chromatography (HPLC) instrument and Kenya Industrial Research and Development Institute (KIRDI) for assistance in carbonization.

I appreciate the support of many colleagues and friends namely Mr. Victor Shikuku, Dr. Jackson Cheruiyot, Ms. Agnes Muyale and Dr. Dickson Andala who assisted in analysis.

My Sincere thanks also go to all staff of the Department of Pure and Applied Chemistry, Masinde Muliro University of Science and Technology.

Finally, special thanks go to my family, especially my husband for his endless support, continued patience and love throughout the course of my studies.

ABSTRACT

The presence of pharmaceuticals (PHCs) in wastewater, surface and ground water systems has instigated great environmental concern due to the toxicological effects associated with these compounds. Conventional wastewater treatment technologies have been shown to be inadequate in removing these chemicals. It is therefore imperative to incorporate efficient, cost-effective and green remediation technologies in treatment of wastewater to maintain a safe and sustainable environment. In this study, novel magnetically engineered green adsorbent composites of diatomaceous earth (α-Fe_2O_3-DTE), carbonized bagasse (α-Fe_2O_3-CBG) and carbonized maize cobs (β-FeO(OH)-CMC) were developed for removal of selected PHCs in wastewater. The synthesized composites were characterized. The concentrations and discharge loads of selected PHCs (ampicillin, sulfamethoxazole, chloramphenicol, carbamazepine, lamivudine, aspirin and diclofenac) within Lake Victoria Basin of Kenya were determined. Samples were extracted by solid phase extraction and analyzed using hyphenated liquid chromatography-mass spectrometry (LC-MS). Residue levels of selected PHCs from Wastewater Treatment Plant (WWTP) effluents ranged from <0.05±0.02 to 0.36±0.04 µg/L. Hospital effluents had levels between <0.05±0.02 to 0.79±0.07 µg/L. PHC concentrations in water from streams and rivers receiving water from WWTPs ranged from <0.05±2 to 0.29±0.02 µg/L. Sediments collected from the riverbeds recorded PHC levels of <50±2 to 94±3 ng/g. Sludge samples from WWTPs had PHCs between <50±2 to 154±9 ng/g, while hospital lagoons had residues between <50±2 to 276±12 ng/g. The daily discharge loads of selected PHCs from the nine WWTPs studied ranged from 123.3±0.3 mg/L to 3130.0± mg/L. The mean percentage removal of the selected PHCs in conventional aerated lagoons was 36.92±0.78 % for the selected WWTPs. Adsorbent properties were determined. Powder X-ray diffraction (XRD) results showed the crystalline structure of α-Fe_2O_3 and β-FeO(OH) in modified composites of α-Fe_2O_3-DTE, α-Fe_2O_3-CBG and β-FeO(OH)-CMC, respectively. The scanning electron microscopy coupled with energy dispersive analysis X-ray (SEM-EDAX) together with X-ray fluorescence (XRF) spectroscopic results showed increased percentage of iron in the modified adsorbents indicating successful impregnation with iron. Fourier transform infrared (FTIR) spectroscopy revealed the presence of hydroxyl, carbonyl and iron oxide groups on the modified sorbents. The Brunauer–Emmet–Teller (BET) surface areas for the three modified adsorbents were 22.0097 m^2g^{-1}, 2.0741 m^2g^{-1} and 2.58 m^2g^{-1}, respectively. The Barrett-Joyner-Halenda (BJH) desorption surface areas were 20.4619 m^2g^{-1}, 1.2504 m^2g^{-1} and 2.0601 m^2g^{-1}. Gibbs free energy calculations confirmed the adsorption was energetically favourable and spontaneous with a high preference for adsorption on α-Fe_2O_3-DTE. Kinetic results showed multi-mechanistic adsorption sequences with the data tending to conform with the Langmuir model for α-Fe_2O_3-DTE while α-Fe_2O_3-CBG and β-FeO(OH)-CMC best fitted the Freundlich model. The adsorption capacity of carbamazepine was 90.15 %, 60.9 % and 43 % within a period of 180 minutes for the three sorbents, respectively. CBZ adsorption obeyed pseudo-second-order kinetics for all the composites with R^2 values of 1.000, 0.998 and 0.976 for the tree composites, respectively. The fabricated composites exhibited excellent ferromagnetic properties thus providing alternative cost-effective technology for the efficient management of CBZ and other toxic organic pollutants in the environment.

TABLE OF CONTENTS

CHAPTER FOUR

LIST OF APPENDICES

LIST OF TABLES

LIST OF FIGURES

LIST OF ABBREVIATIONS AND ACRONYMS

BET	Brunauer Emmett and Teller
BJH	Barrett Joyner and Halenda
CBG	Carbonized Bagasse biochar
CMC	Carbonized Maize Cob biochar
DTE	Diatomaceous Earth adsorbent
EPA	Environmental Protection Agency
EU	European Union
FT-IR	Fourier Transform Infrared
GC-MS	Gas Chromatography Coupled with Mass Spectroscopy
HIV	Human Immune-deficiency Virus
HPLC-MS	Liquid Chromatography Coupled with Mass Spectroscopy
LVB	Lake Victoria Basin
NRDB	Nzoia River Drainage Basin
PHCs	Pharmaceuticals
PVC	Polyvinyl Chloride
SEM	Scanning Electron Microscopy
EDAX	Energy dispersive Analysis X-ray
SPE	Solid Phase Extraction
TEM	Transmission Electron Microscopy
UV-Vis	Ultra violet Visible
WWTPs	Wastewater Treatment Plants
XRD	X-ray Diffraction
SMX	Sulfamethoxazole
CBZ	Carbamazepine

AMP	Ampicillin
LMV	Lamivudine
ASA	Aspirin
DCF	Diclofenac
CAP	Chloramphenicol
BB	Bagasse biochar (unmodified)
MBB	Modified bagasse biochar
MCC	Maize cob biochar (unmodified)
MMCC	Modified maize cob biochar
DE	Diatomaceous earth
MDE	Modified diatomaceous earth

CHAPTER ONE

1.0 INTRODUCTION

1.1 Background Information

Pharmaceuticals (PHCs) are a group of emerging contaminants and their use is continuously increasing around the world. They are extensively used in human and veterinary medicine to prevent illness and promote growth in fish and livestock farming as well as in agriculture. After administration, these chemicals can transform into more polar and soluble forms as metabolites or as conjugates of glucuronic and sulphuric acid (Heberer, 2002a; Nikolaou *et al.,* 2007). Pharmaceuticals and their metabolites are readily excreted with urine and faeces and enter into urban WWTPs (Kummerer, 2001; Ellis, 2010). These compounds find their way into the aquatic environment through discharge of treated wastewater, seepage from landfills, septic systems, sewer lines and disposal of expired drugs into water systems among other pathways (Glassmeyer *et al.,* 2005; González-Naranjo *et al.,* 2013; Golovko *et al.,* 2014). Most of these compounds are found in hospital effluents and municipal sewage in high concentrations (Watkinson *et al.,* 2009; Michael *et al.,* 2013). This provides a potential route for PHCs loading into the aquatic environment. Hence, raising concerns due to recalcitrance of PHCs to conventional water treatment technologies (Clara *et al.,* 2005; Aga, 2008; Santos *et al.,* 2010; Li, 2014).

A wide range of PHCs have been detected in a variety of environmental samples such as wastewater and drinking water (Hutchinson *et al.,* 2009; Kern *et al.,* 2009; Watkinson *et al.,* 2009; Cai *et al.,* 2014; Matozzo, 2014). Reports indicate the accumulation of some pharmaceuticals in sewage sludge (Jelic *et al.,* 2011), while other studies show the presence of organic compounds such as perfluorosurfactants, pharmaceuticals, and flame retardants in

public drinking water wells where septic systems are prevalent (Ternes *et al.*, 2001; Kolpin *et al.,* 2004; Dinsdale *et al.,* 2009; Schaider *et al.,* 2014). The presence of PHCs in aquatic environment is of great concern since they have explicitly been shown to be toxic to aquatic organisms and may induce development of drug resistant organisms (Li *et al.,* 2009a). Current studies show that effluents from wastewater treatment plants contain xenobiotic organic compounds which can have a lot of ecotoxicological effects thus impacting negatively on environmental systems (Brown *et al.,* 2003; Singer *et al.,* 2011). For example endocrine disrupting chemicals such as bisphenol A are reported to impair reproductive development and hormone production in some organisms such as fish and amphibians (Snyder *et al.,* 2003). Other PHCs are reported to have adverse effects on the renal system resulting in kidney failure, while others are shown to be carcinogenic and mutagenic (Robertson, 1994; Oaks *et al.,* 2002; Matozzo, 2014). Given the ubiquitous use and prevalence of PHCs in aqueous environmental systems, there is great need for determination of their respective levels and further devise mechanisms of minimizing their release to the environment.

In today's world, hazardous waste management is among the most challenging tasks to technological advances due to continuous release of tons of organic contaminants and other toxicants into water systems. Several organo-remediation techniques have been reported in literature. Some of these include but not limited to oxidation technologies and reverse osmosis (Clara *et al.,* 2005; Al-Rifai *et al.,* 2011; Li *et al.,* 2011). Nevertheless, the metabolites formed in these processes may be more toxic than the parent compounds coupled with the enormous operational costs involved (Lamm *et al.,* 2009). Modified and untreated agricultural wastes, such as fruit wastes, coconut shells, maize cobs, seaweed and algae have been demonstrated as efficient and low cost adsorbents for removal of various organic pollutants from wastewater (Ribeiro *et al.,* 2011; Ali *et al.,* 2012; Al-Othman *et al.,* 2012).

Similarly, nanoparticles have been found to be efficient in removing organic pollutants from water (Attia *et al.,* 2013; Choina *et al.,* 2014; Hicks *et al.,* 2014). For example commercial azo dyes such as methylene blue and reactive red 195 have been removed using magnetic Fe_3O_4@C nanoparticles with great success (Belessi *et al.,* 2009; Thattai *et al*; 2014; Wu *et al.,* 2014). Another study by Kim *et al.,* (2014) reported the potential of granular mesoporous silica nanoparticles in adsorption of twelve pharmaceuticals from aqueous solutions.

Population pressures, rapid urbanization and industrialization in Kenya are causing strain to the limited waste disposal facilities available in urban centers. Kisumu, Kakamega, Bungoma and Eldoret towns are located within the Lake Victoria Drainage Basin. The proximity of these towns to Lake Victoria has resulted in anthropogenic inputs of pollutants into the lake. These compounds find their way into the aquatic environment through discharge of treated wastewater, seepage from landfills, septic systems, sewer lines and disposal of expired drugs into water systems among other pathways (Glassmeyer *et al.,* 2005; Jain *et al.,* 2013; González-Naranjo *et al.,* 2013). Most of these compounds are found in hospital effluents and municipal sewage in high concentrations (Watkinson *et al.,* 2009; Michael *et al.,* 2013).

Trace micro pollutants such as perfluorinated surfactants, polyaromatic hydrocarbons and pesticides have been detected within the Lake Victoria basin indicating pollution of the region (Getenga *et al.,* 2004; Werimo *et al.,* 2009; Orata *et al.,* 2009; Lisouza *et al.,* 2011). Most wastewater treatment plants such as those in Kenya are not designed to remove highly polar micro pollutants and as such, they have become point sources of PHCs loading into surface waters (Michael *et al.,* 2013). Consequently, PHCs including antibiotics, analgesics and antiretrovirals have been detected in surface and treated wastewaters in Kenya (K'oreje *et al.,* 2012; Kimosop *et al.,* 2016). This poses a great risk of exposure to these chemicals.

Therefore, there is an urgent need to document the levels of these chemicals and develop effective and sustainable wastewater treatment technologies to achieve quality environment.

1.2 Statement of the problem

The presence of PHCs in the aquatic environment has caused great concern since these chemicals have been shown to be toxic to aquatic organisms. These compounds have been linked to the development of drug resistant bacteria and viruses making it difficult to treat diseases (Li *et al.*, 2009b). In addition, WWTPs are inefficient in removal of PHCs leading to dispersion of these compounds in the environment through discharged effluents. PHCs have been polluting the environment since their introduction through human and animal wastes (Li, 2014; Liu *et al.*, 2014). Studies on the levels of PHCs in Kenya reported alarming concentrations of these compounds (K'oreje *et al.*, 2012). However, there are limited data on the levels of these compounds within the Lake Victoria Basin (LVB) of Kenya. Therefore, this study sought to document the levels of frequently used PHCs in WWTPs within LVB in order to assess the potential risks and devise ways of minimizing release of PHCs into the environment. Various scientific methods of removal of PHCs have been studied; the metabolites formed in these processes are more toxic than the parent compounds (Clara *et al.*, 2005; Lamm *et al.*, 2009). Adsorption is one of the emerging technologies for remediation of contaminants in the environment. This study aimed at developing a novel approach using magneto responsive adsorbents for removal of selected PCHs from aqueous media as a cost-effective green technology.

1.3 JUSTIFICATION

Lake Victoria is the second largest fresh water lake worldwide with a surface area of 68,000km^2. The major towns around the lake are Kisii, Homabay, Kisumu, Busia, Kakamega, Mumias, Bungoma and Eldoret. Rapid urbanization and industrialization is

causing strain to the limited waste disposal facilities available in these urban centers resulting in anthropogenic inputs of pollutants such as PHCs into the lake. PHCs such as carbamazepine are some of the emerging pollutants in the environment with carcinogenic degradation products, hence the need for their removal from wastewater (Kosjek *et al.*, 2009a). The use of low-cost adsorbents from natural organic origin is essential in ensuring green environmentally friendly technology. Impregnation with iron, an essential metal, induces magnetic properties making the adsorbents easy to reuse.

1.4 General objective

Determination of concentrations and discharge loads of selected PHCs in effluent generated by WWTPs within Lake Victoria Basin, Kenya and to investigate their removal by novel magneto responsive adsorbents.

1.5 Specific objectives

1. To determine the concentrations and discharge loads of ampicillin, sulfamethoxazole, chloramphenicol, carbamazepine, lamivudine, aspirin and diclofenac in wastewater and sludge from water systems in main towns (Kisii, Homabay, Kisumu, Kakamega, Mumias, Bungoma, Webuye and Eldoret) within Lake Victoria Basin of Kenya.
2. To develop a novel approach for preparing magneto responsive adsorbent composites of Diatomaceous Earth (α-Fe_2O_3-DTE), Carbornized Bagasse (α-Fe_2O_3-CBG) and Carbonized Maize Cobs (β-FeO(OH)-CMC).
3. To characterize the physicochemical properties of the unmodified and iron modified (α-Fe_2O_3-DTE, α-Fe_2O_3-CBG and β-FeO(OH)-CMC) adsorbent composites.

4. To determine the sorption kinetics, isothermal behaviour, thermodynamics and infer adsorption mechanism of the three adsorbents in remediation of carbamazepine (CBZ) in synthetic wastewater.
5. To determine the efficacy of removal of carbamazepine in synthetic wastewater by the three magneto responsive adsorbent composites

1.6 Significance of the study

(i) Findings from this study provide scientific information on the efficiency of the WWTPs in pharmaceuticals remediation and extent of pollution. This forms a basis for setting up policies for meeting targets to maintain a green and healthy environment.

(ii) The properties of the magneto responsive adsorbent composites were established leading to academic advancement in understanding their utilization based on their characteristics.

(iii) The potential of the synthesized iron-modified green adsorbents (diatomaceous earth, carbonized bagasse and maize cob) for remediation of the selected PHCs from water was established and would help in treatment of these chemicals in water systems.

(iv) The study for the first time reports the effectiveness in the removal of PHCs from the effluents generated by WWTPs by green technology thus minimizing negative environmental impacts caused by the widespread use of the PHCs.

CHAPTER TWO

2.0 LITERATURE REVIEW

2.1 Introduction

The widespread use of organic compounds in modern society and their dispersion through wastewater have resulted in pollution of both ground and surface water systems worldwide (Bottoni *et al.,* 2010). Despite the great impact that may be caused by these compounds, a vast majority of them are not regulated in wastewater outfalls. Some of these chemicals include poly aromatic hydrocarbons, pesticide, pharmaceuticals, per-fluorinated compounds and flame retardants (Werimo *et al.,* 2004; Orata *et al.,* 2009; Lisouza *et al.,* 2011; Kim *et al.,* 2013). Though used for beneficial purposes, pharmaceuticals (PHCs) have been shown to be emerging surface water, groundwater and drinking water contaminants raising international concern (Kolpin *et al.,* 2002; Wick *et al.,* 2011; Schaider *et al.,* 2014). These compounds find their way into the aquatic environment through discharge of treated wastewater, seepage from landfills, septic systems and sewer lines and disposal of expired drugs into water systems among other pathways (Glassmeyer *et al.,* 2005; Kummerer, 2009).

Pharmaceutical compounds have adverse effects, such as disturbance of reproductive and hormone systems, neurobehavioural changes among others, on aquatic organisms even at low concentrations (Christen *et al.,* 2010). The presence of these compounds in the environment has also been shown to induce development of resistant bacterial strains and viral resistance (Singer *et al.,* 2007; Straub, 2009; Li *et al.,* 2009a; Jain *et al.,* 2013). The removal efficiencies in wastewater treatment plants are dependent on several factors, which include; the physico-chemical properties of the compound, method of treatment employed, climatic conditions,

operational conditions of the treatment process and the age of the activated sludge used in the treatment plant (Miège *et al.,* 2009). Conventional wastewater treatment plants consist of a primary sedimentation process followed by secondary treatment and final sedimentation. Organic pollutants can be transformed from the aqueous phase by hydrolysis, biotransformation or sorption to sludge (Le-Minh *et al.*, 2010). Nevertheless, the removal efficiency may vary based on compound affinity to the aqueous phase (hydrophilic pharmaceuticals) or adsorption onto sludge (hydrophobic chemicals). The utilization of sewage sludge as a fertilizer may lead to dispersion of these compounds into various environmental compartments (Kim *et al.,* 2007b; Phillips *et al.,* 2010; Daneshvar *et al.,* 2012; Michael *et al.,* 2013). As a result, PHCs have often been detected in treated drinking water (Kim *et al.,* 2007a; Magnér *et al.,* 2010). Among the PHCs detected in Kenyan treated wastewater effluents include lamivudine, sulfamethoxazole, ibuprofen and sulfadoxine representing antiretrovirals, antibiotics, analgesics and antimalarials, respectively (K'oreje *et al.,* 2012).

2.2 Pharmaceuticals in the environment

The presence of PHCs in the environment has raised international concern with various researchers showing that a variety of these chemicals enter water bodies as a result of inadequate wastewater treatment (Luo *et al.,* 2014). Most human and veterinary pharmaceuticals are incompletely metabolized in treated patients and animals, as such a large fraction of these compounds are excreted unchanged via faeces or urine (Lamm *et al.,* 2009). Other sources of contamination include improper disposal of expired pharmaceutical stocks, leachate from pharmaceutical landfilling or pit latrines (Peng *et al.,* 2014; Graham and Polizzotto, 2013).

Among the frequently detected PHCs in water resources worldwide are antibiotics, analgesics, personal care products and anti-retroviral compounds (Ternes *et al.,* 1999; Wiegel *et al.,* 2004; Bendz *et al.,* 2005; Zuccato *et al.,* 2010; Escher *et al.,* 2010; Chen *et al.,* 2011; K'orenje *et al.,* 2012; Anumol *et al.,* 2013). A study by Wood *et al.,* (2015) reported high levels of antiretroviral drugs in surface water bodies in South Africa with average concentrations ranging from 26.5 ng/L to 430 ng/L. Nevirapine and zidovudine were among the frequently detected anti-retrovirals in South African surface waters. In Kenya, some of the widely used PHCs include ampicillin, sulfamethoxazole, chloramphenicol, carbamazepine, lamivudine, zidovudine, aspirin, diclofenac and caffeine which have been detected in water systems within Nairobi River (K'orenje *et al.,* 2012). Some of the PHCs that were studied are shown in compounds 2.1.

The study focused on selected pharmaceuticals based on their wide utilization in Kenya and toxicities and are described below. Ampicillin (AMP) [**1**], (2S,5R,6R)-6-[[(2R)-2-amino-2-phenylacetyl]amino]-3,3-dimethyl-7-oxo-4-thia-1-azabicyclo[3.2.0]heptane-2-carboxylic acid, is a broad spectrum beta-lactam antibiotic used for the treatment of various bacterial infections. It can either be taken orally or intravenously to act against both Gram-negative and Gram-positive bacteria (Gao *et al.,* 2012b). It is effective for ear, respiratory, urinary tract and salmonella infections. The widespread use of ampicillin has led to its detection in various environmental compartments (Heberer *et al.,* 2001; Kolpin *et al.,* 2002; K'oreje *et al.,* 2012). Antibiotics such as ampicillin have been shown to induce antibiotic resistance genes in bacteria making it difficult to control diseases caused by these organisms (Gao *et al.,* 2012a), hence, there is need to minimize their release into the environment.

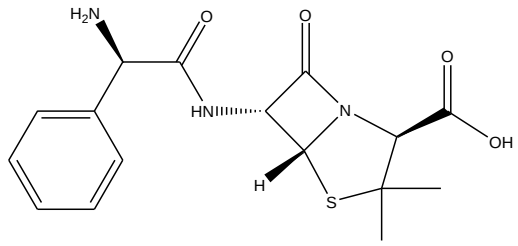

1

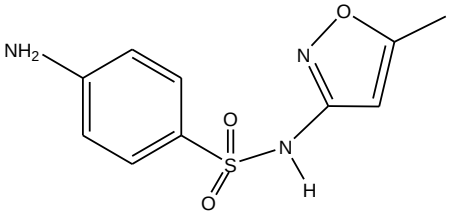

2

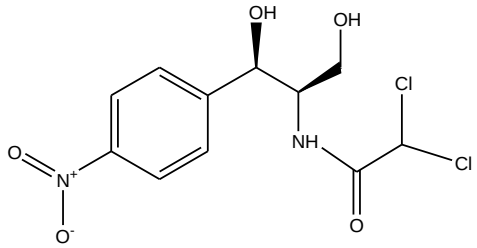

3

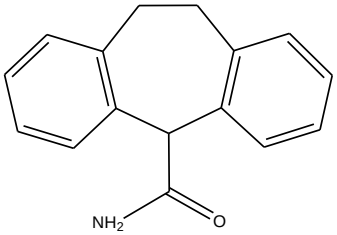

4

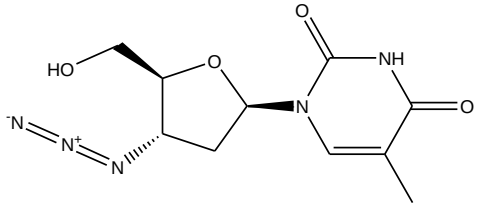

5

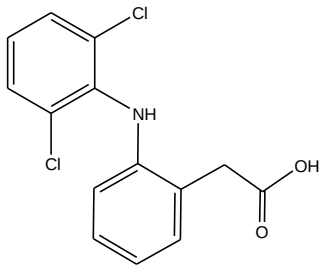

6

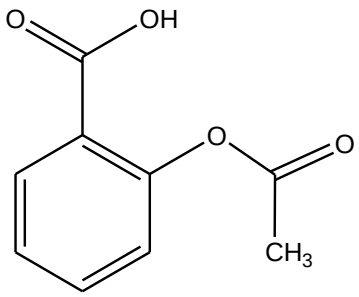

7

(Tenenbaum *et al.*, 2014)

Compounds 2.1: Selected Pharmaceuticals in this Study

Sulfamethoxazole (SMX)[**2**], 4-amino-N-(5-methyl-1,2-oxazol-3-yl)benzene sulfonamide, is an antibiotic used to treat a variety of bacterial, fungal, and protozoan infections. Its mode of action is by inhibiting an enzyme involved in the synthesis of tetrahydrafolic acid (Burchall, 1973; Seydel *et al.,* 1972). It is marketed all over the world in generic preparations and under various trade names. It is among the antibiotics of great concern to scientists worldwide due to its consumption, discharge, persistence and toxic properties (Jones *et al.,* 2002; Hughes *et al.,* 2013; Lienert *et al.,* 2007a). Sulfamethoxazole is used for both human and veterinary purposes hence its high detection in various environmental compartments all over the world (Kaplan, 2013; de García *et al.,* 2013; Johnson *et al.,* 2015). The detection of these compounds in water systems is of great environmental concern since they may result in development of resistant bacteria (Li *et al.,* 2009b). Therefore, there is need to quantify the levels of these pharmaceuticals in the environment and develop methods of reducing their discharge into water bodies.

Chloramphenicol (CAP)[**3**] 2,2-dichloro-N-[(1R,2R)-1,3-dihydroxy-1-(4-nitrophenyl)propan-2-yl]acetamide, is a broad-spectrum antibiotic which is considered both cheap and easy to manufacture, and thus frequently used in the developing world. It is effective against a wide variety of Gram-positive and Gram-negative bacteria, including most anaerobic organisms. Chloramphenicol is used for the treatment of cholera, staphylococcal brain abscesses and meningitis It is also used for veterinary purposes for the treatment of chlamydial disease (Li., 2014). Exposure to chloramphenicol results in bone marrow suppression and aplastic anaemia, which is idiosyncratic. The intravenous utilization of chloramphenicol is associated with gray baby syndrome (Kummerer, 2008).

Carbamazepine (CBZ) [**4**], benzo[b][1]benzazepine-11-carboxamide, is a human pharmaceutical for treating epileptic seizures, trigeminal neuralgia, bipolar depression, excited psychosis, and mania (Thacker, 2005). Global consumption is estimated at 2.2 million pounds yearly. In humans, it is excreted along with its major metabolites 5,6-dihydroxy-5,6-dihydrobenzo[b][1]benzazepine-11-carboxamide (carbamazepine-diol) and 10,11-dihydro-5H-debenz(b,f)azepine-5-carboxamide 10,11-epoxide (carbamazepine-epoxide). Carbamazepine is not degraded in WWTP processes due to its resistance to microbial biodegradation and thus most removal efficiencies are below 10% (Zhang *et al.*, 2008). Sorption of carbamazepine onto sewage sludge is not an effective removal pathway because of the low affinity for organic matter (Kd = 1.2 L/kg). Since it is poorly removed during wastewater treatment, carbamazepine is commonly found in WWTP effluent around the world. Studies have reported carbamazepine in effluent at concentrations up to 1.6 µg/L (Heberer *et al.,* 2002b; Glassmeyer *et al.,* 2005). Effluent concentrations of carbamazepine occasionally exceed influent concentrations, which may be due to fluctuations in concentrations that are not accounted for in short term studies, or may be caused by processes in the treatment plant that convert some metabolites back into carbamazepine (Zhang *et al.,* 2008). Some of the potential carbamazepine degradation products such as aza-arenes may be toxic and carcinogenic (Kosjek *et al.,* 2009a). Studies by Oetken *et al.* (2005) show the toxicity of carbamazepine to aquatic insects. There is need to eliminate this xenobiotic compound in aqueous systems to avoid their detrimental effects to flora and fauna.

Lamivudine (LMV) [**5**], 4-amino-1-((2S,5R)-2-(hydroxymethyl)-1,3-oxathiolan-5-yl) pyrimidin-2(1H)-one, is a nucleoside analog reverse transcriptase inhibitor which is marketed under the trade name Epivir and Epivir-HB. It is used for treatment of

chronic hepatitis B and in combination with zidovudine for treatment of human immunodeficiency virus (HIV) (Gathe *et al.,* 2002; Koziel and Peters, 2007). Although the long-term use of lamivudine results in the emergence of resistant hepatitis B virus mutant, it is still widely used as it is well tolerated (Lok *et al.,* 2003). Consequently, lamivudine has been detected in wastewater treatment plants and rivers (K'oreje *et al.*, 2012).

Diclofenac (DCF) [**6**], 2-[2-(2,6-dichloroanilino)phenyl]acetic acid, is a nonsteroidal anti-inflammatory drug used to reduce inflammation and as an analgesic reducing pain in certain conditions. It is also used in the treatment of acute migraines (Mueller *et al.,* 2012). Diclofenac is available as a generic drug in a number of formulations, including diclofenac diethylamine, which is applied topically. Over-the-counter use is approved in some countries for minor aches and pains and fever associated with common infections. Long-term use of diclofenac has been linked to liver toxicity (Boelsterli, 2003; Mueller *et al.,* 2012). A study by Juhlin *et al.,* (2004) showed that acute administration of diclofenac deteriorated renal function in patients with coronary artery disease and heart failure. Diclofenac has been linked to cause decline of vultures in Asia (Arun and Azeez, 2004). Yet, diclofenac and its metabolites have been detected in the environment in significant concentrations (Zhang *et al.,* 2008; Kosjek *et al.,* 2009a; Vieno and Sillanpää, 2014). Microbial degradation of diclofenac was reported to be very slow resulting in formation of two metabolites; 4′-hydroxy-diclofenac and diclofenac β-*O*-acyl glucuronide (Kosjek *et al.,* 2009b; Lee *et al.,* 2012). The later was reported to be deconjugated to form diclofenac within seven days. Hence, indicating that the biological removal of diclofenac is not likely to occur in conventional WWTPs (Lee *et al.,* 2012). Besides, water treatment technologies such as chlorination have been shown to result in formation of highly stable chlorinated derivatives

that are carcinogenic (Soufan *et al.,* 2012). Hence, there is need to minimize discharge of diclofenac and other toxic organic chemicals into the environment using greener methods.

Aspirin [**7**], 2-acetyloxybenzoic acid, is among the non-steroidal anti-inflammatory drugs which exhibits a broad range of pharmacological activities, including analgesic, antipyretic, and anti-platelet properties (Adebayo *et al.,* 2007). It is also used to help prevent heart attacks, strokes, and blood clot formation in people at risk of developing blood clots (Cambria-Keily and Gandhi, 2002; Wong *et al.,* 2004). It has been found to be persistent in the environment (de García *et al.,* 2013).

The WWTP effluents generated in Kisii, Homabay, Kisumu, Kakamega, Mumias, Bungoma, Busia and Eldoret towns which are within the Lake Victoria Basin (LVB) in Kenya are disposed of into rivers which are discharged into Lake Victoria. The Lake is known to be highly polluted (Getenga *et al.,* 2004; Werimo *et al.,* 2009; Orata *et al.,* 2009). However, little information has been published on the levels of PHCs within the region. Most of the WWTPs within the LVB use conventional treatment methods which are not designed for removal of PHCs (Clara *et al.,* 2005). These chemicals are therefore potential pollutants in rivers within LVB ending up in the lake. Elsewhere PHCs have been reported in the environment and have led to development of antibiotic and antiviral resistant bacteria posing great risk to human health (Crane *et al.,* 2006; Caracciolo *et al.,* 2010; Huang *et al.,* 2014). There is need to determine the residue levels of these compounds in water systems within LVB and hence, carry out an investigation into an effective and eco-friendly technology for their removal.

2.3 Occurrence and ecological risk associated with presence of PHCs

As pharmaceuticals do not occur individually in the environment, but as complex mixtures, the interaction of these compounds with wildlife that might have high similarity with the molecular targets, the so-called non-target organisms (Rand-Weaver *et al.,* 2013), may occur at relevant environmental concentrations, due to combined and synergistic effects (Calisto and Esteves 2009);

Anthropogenic organic xenobiotics such as industrial chemicals and biocides are ubiquitously present in the environment (Kolpin *et al.,* 2004; Schaider *et al.,* 2014). Pollution of freshwater resources has become an issue of great concern considering the ever rising demand for clean water. The predicted increase in the population of the world in the next few decades may result in increased consumption of pharmaceuticals which further worsens the situation (Kummerer, 2008; Vazquez-Roig *et al.,* 2014). Most human and veterinary pharmaceuticals are incompletely metabolized in treated patients and animals, as such a large fraction of these compounds are excreted unchanged via faeces or urine (Lamm *et al.,* 2009). Moreover, disposal of unused medicines contributes to the release of these chemicals into sewer systems.

Most pharmaceuticals are designed to retain their chemical structure for long in order to allow reaction time for their therapeutic work. This property, together with their continuous discharge, results in extended residence time of PHCs in the environment (Kasprzyk *et al.*, 2009). Consequently, PHCs and their transformation products are detected in wastewater treatment plants, surface, ground and drinking water (Stackelberg *et al.,* 2004; Phillips *et al.,* 2010). For instance, Kosma *et al.,* (2010) reported the presence of diclofenac, caffeine and ibuprofen in municipal and hospital wastewaters in Greece. Similarly, significant concentrations of carbamazepine, ibuprofen and tetracycline have been detected in biosolids

and sludge samples (Chenxi *et al.,* 2008; Yu and Wu, 2012). In Kenya, K'oreje *et al.,* (2012) reported the presence of ten pharmaceutically active compounds belonging to different classes in Nairobi River, Kenya. Some of the compounds detected in high concentrations (10–30μg/L) were lamivudine, zidovudine and nevirapine antiretrovirals which were higher than those reported in other parts of the world. Other classes of pharmaceuticals reported were antibiotics, analgesics/anti-inflammatory, anti-epileptic drugs and antimalarials. This is of great concern due to the toxicological effects of these compounds on flora and fauna (Farré *et al.,* 2001; Crane *et al.,* 2006; Enick and Moore, 2007).

Effects of PHCs are diverse and may be categorized as direct or indirect. The former include acute toxicity while the later involves impacts on the reproduction ability (Bruce *et al.,* 2010). Synthetic estrogens, which are used as contraceptives such as ethinylestradiol, have been reported as strong endocrine disruptors, which cause feminization of fish (Brown *et al.,* 2003). Other biologically active compounds such as antibiotics have a direct impact on organisms after their release into the environment (Gao *et al.,* 2012b). However, they can also indirectly influence humans if the chronic exposure of bacteria and viruses to these substances result in the formation of antibacterial and antiviral resistant strains (Caracciolo *et al.,* 2010; Huang *et al.,* 2014). For example the use of the antiviral drug Tamiflu during pandemic influenza medical response was reported to induce resistance genes of influenza A virus in wild birds (Olsen *et al.,* 2006; Singer *et al.,* 2007; Singer *et al.,* 2011). Diclofenac, a commonly used analgesic, has been linked to histopathological alterations in kidneys and gills of rainbow trouts (Schwaiger *et al.,* 2004). It has been reported to be the major cause of decrease in vulture populations in Pakistan (Oaks *et al.,* 2002). Other effects of PHCs include alteration of proper functioning of hormonal systems, which may result in obesity, reduced fertility, learning and memory difficulties and cardiovascular diseases (Zhang and Zhang, 2011).

Additionally, PHCs and their metabolites can form toxic by-products during disinfection of drinking water by ozonation or chlorination (Richardson *et al.,* 2007; Bond *et al.,* 2011). For example chloramination of compounds containing dimethylamine moieties such as ranitidine, results in formation of N-nitrosodimethylamine, a strong carcinogen (Le Roux *et al.,* 2011; Shen and Andrews, 2011). Similarly, this carcinogenic compound has been reported during ozonation of N,N-dimethylsulfamide, a degradation product of tolylfluanide fungicide (Schmidt and Brauch, 2008). Another report by Kumar *et al.,* (2014) showed that chlorination could not remove the antiretroviral drug, zidovudine from water. Therefore, understanding the fate of PHCs in the environment is critical in assessing the potential risks caused and possible remediation strategies.

2.4 Strategies employed in minimizing discharge of PHCs

The occurrence of a large spectrum of PHCs in the environment indicates that conventional wastewater treatment plants are associated with incomplete degradation of these compounds (Stackelberg *et al.,* 2004; Al-Rifai *et al.,* 201I). Degradation of PHCs in wastewater treatment plants involves a limited number of biochemical reactions such as hydroxylation, oxidation and de-alkylation resulting in small structural changes of the parent compound (Helbling *et al.,* 2010). Most wastewater treatment plants are designed to reduce effluent nutrient loads, particularly nitrogen and phosphorous in order to prevent eutrophication of receiving waters. Therefore, there is need to develop sustainable strategies to minimize the release of PHCs into the environment.

Recently, studies have focused on new, advanced wastewater treatment technologies. Reports have shown that treatment by ozonation efficiently eliminates a large spectrum of PHCs from water (Hollender *et al.,* 2009; Yang *et al.,* 2011). However, ozonation leads to

the formation of oxidation products, which are potentially toxic (von Gunten, 2003; Teixeira *et al.,* 2011). Halogenated compounds such as iodinated X-ray contrast media and their transformation products are reported to be recalcitrant (Zimmermann *et al.,* 2011). The use of biofilms for degrading PHCs from aqueous systems has also been studied. For instance, *Trichosporon asahii* yeast isolated from caffeine contaminated soil was used to remove caffeine from industrial wastewater (Lakshmi and Das, 2013). Moreover, the degradation of tetracycline was enhanced using enzyme extract from spent mushroom compost of *Pleurotus eryngii* (Chang *et al.,* 2014).

Other treatment techniques, which include advanced oxidation processes, membrane bioreactors, photocatalysis and electrochemical methods, have been shown to eliminate various organic compounds (Basile *et al.,* 2011; Oller *et al.,* 2011). Nonetheless, these treatment techniques may result in formation of toxic by-products during disinfection of drinking water (Richardson *et al.,* 2007; Yang *et al.,* 2011). Moreover, most of the studies have only been tested under laboratory conditions and therefore facing a lot of technical difficulties in application to full scale water treatment. These methods are also expensive compared to existing treatment technologies, at least at the current state of knowledge and technology. However, this might change in the future. Other attempts to minimize PHCs loading from hospitals include on-site separation and treatment of urine with high loads of pharmaceuticals (Lienert and Larsen 2007b; Beier *et al.,* 2011). Nonetheless, this technique has been associated with high costs and lacking in practicability.

2.5 Adsorption cleanup technology

Adsorption is one of the promising cleanup technologies that have attracted the interest of researchers (Ruiz *et al.,* 2010). A study by Genc and Dogan, (2015) reported adsorption of ciprofloxacin antibiotic onto bentonite, activated carbon, zeolite and pumice. Similarly,

pumice was shown to be efficient in removing tetracycline from aqueous media (Guler and Sarioglu, 2014). Other adsorbents such as coal, geothite and graphene oxide have also been used for removal of tetracycline from water systems (Sun *et al.,* 2010; Zhao *et al.,* 2011; Gao *et al.,* 2012a). Nanoparticles have also been used for removal of trace organic pollutants such as pesticides, halogenated organics and microorganisms from water (Pradeep and Anshup, 2009). For example, chlorotetracycline was adsorbed onto magnetite nanoparticles (Zhang *et al.,* 2011a). Other studies have reported degradation of PHCs in nanoparticle treated water samples. Ofloxacin antibiotic was degraded in water using titanium oxide nanoparticles resulting in formation of demethylated and de-carboxylated fluoroquinolone species (Wieren *et al.,* 2012). Photocatalytic degradation of tetracycline and ibuprofen was also reported on the surface of zinc oxide nanoparticles (Choina *et al.,* 2014). Furthermore, Al-Khateeb *et al.,* (2014) reported great success in adsorption of aspirin, caffeine and acetaminophen onto graphene nanoplatelets in real environmental samples.

Similarly, agricultural wastes such as fruit wastes, coconut shells and wheat straw have been demonstrated to be efficient low cost adsorbents for removal of various organic pollutants from wastewater (Ribeiro *et al.,* 2011; Ali *et al.,* 2012). A study by Mestre *et al.,* (2011) reported adsorption of paracetamol and ibuprofen onto activated carbon derived from sisal waste.

2.6 Methods of characterization of adsorbents

The characterization of adsorbents is crucial in understanding their properties and potential applications. The choice of characterization methods was dependent on the intrinsic properties of the sample under investigation and available instruments. Techniques capable of analyzing the size, morphology, structure, chemical and physical properties of the

adsorbents were applied in characterization of the synthesized materials. The techniques used in this study include;

2.6.1 Scanning Electron Microscopy (SEM)

In this technique, finely focused electron beam is rastered across the surface of specimen. The interaction of the primary electron beam with surface atoms excites several types of scattered or emission electrons which can be used to map the surface topography (image) or to obtain elemental information (Hornyak *et al.*, 2008). The most important secondary beam effects exploited in SEM investigations are: the secondary, backscattered electrons (both for imaging) and characteristic x-rays (for simultaneous elemental analysis with EDAX). Figure 2.1 shows types of electron-matter interactions caused by primary electron beam during SEM analysis.

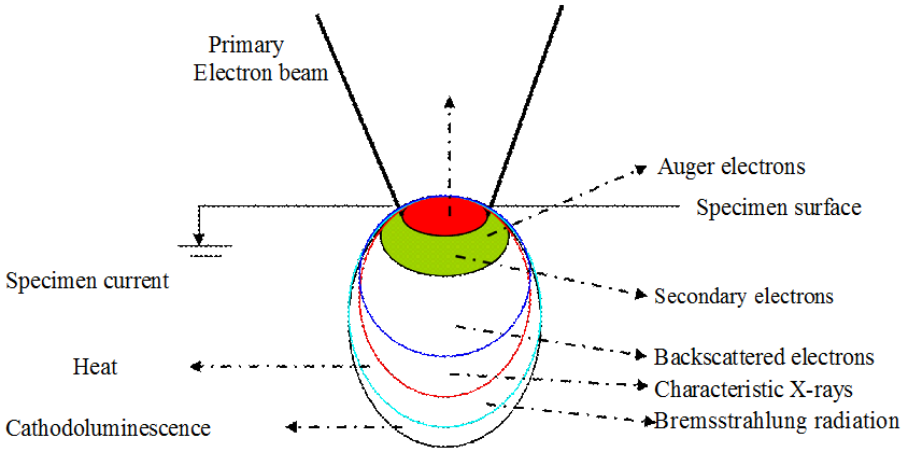

Figure 2.1: Schematic presentation of electron-specimen interaction of primary electron beam with a surface during Scanning Electron Microscopy and X-ray Microanalysis (Hornyak *et al.*, 2008).

The backscattered electrons originate from an elastic scattering of the primary beam

electrons by nuclei on the specimen surface. On the other hand, secondary electrons are due to inelastic scattering following interaction with specimen electrons. Since backscattered electrons originate from elastic scattering event they are equivalent in energy to primary electrons compared to inelastically scattered secondary electrons. The image from backscattered electrons gives excellent compositional contrast since backscattered electrons yield depends on atomic number (Z). Given that the high-energy backscattered electrons can escape from a larger interaction volume of the specimen than secondary electrons, the resolution is lower at fixed accelerating voltages. This is as a result of knock out effect of electrons from beam trajectory during elastic scattering (Mohan *et al.,* 2014).

The SEM image is formed from low-energy secondary electrons after they exit from sample surface and are collected. Since the scattering event is inelastic the energy of the secondary electrons is reduced relative to that of primary beam electrons. In addition, secondary electrons originate from few nanometers (1 - 50 nm in depth) and can be used to determine the surface morphology and topography. The resolution of secondary electrons depends on the beam spot size, the interaction volume, and the incident angle of the beam. A tilted surface enhances secondary electron generation because a larger specimen volume interacts with the beam, resulting in increased secondary electron emission. If the primary electron beam falls into a pit or cavity, fewer secondary electrons can escape because the specimen reabsorbs the electrons. The difference in density of generated secondary electrons reaching the detector is responsible for topographical contrast during SEM imaging (Zhang *et al.,* 2013).

The electron beam-specimen interaction equally generates x-ray photons. These characteristic x-rays are caused by the ionization of inner shell electrons when the electron beam energy exceeds critical ionization energy. The relaxation of outer shell

electrons into vacancy generated by ejected inner shell electron (usually K shell) yields characteristic x-rays, specific to each element. Energy-dispersive x-ray (EDAX) spectroscopy measures the x-ray intensity as a function of energy whereas wavelength dispersive x-ray spectroscopy measures x-ray intensity as a function of wavelength dispersion based on Bragg's diffraction (Song *et al.*, 2014).

2.6.2 X-ray diffraction (XRD)

Electromagnetic radiation interaction with adsorbent composites may result in several secondary physical effects including: vibration, rotation, electronic transitions, scattering, diffraction and/or non-radiative processes. Electronic transitions between energy states are analyzed by absorption, emission or fluorescence spectroscopy. The scattering of x-rays by a crystal lattice was analyzed by powder X-ray Diffraction (XRD). The x-rays, similar to electron beams, can also be reflected (diffracted) at the net plane of a crystal lattice. The spacing between atoms and planes in crystalline solids show long-range periodic structure on the order of the wavelength of x-rays exhibited as Bragg diffraction peaks. Bragg‟s law forms the foundation of x-ray diffraction, equation 2.1:

$$n\lambda = 2d\sin\theta \qquad \text{equation } \mathbf{2.1}$$

where; λ is the wavelength of the x-rays, d is the inter-lattice spacing, θ is the incident angle and n is an integer. Irradiating a crystal with a collimated and mono-energetic x-ray source gives rise to constructive and destructive interference via scattering of the x-rays at the crystal planes. Figure 2.2 illustrates how Bragg's law is met, whereby the crystal planes of the sample make an angle of θ in respect with the x-ray source and the detector is situated at an angle of 2θ relative to the x-ray source. To obtain constructive interference the path length A-B-C has to be equal to an integer multiple of the incident wavelength. Different

crystal planes usually have different diffraction angles (Zhang *et al.*, 2012).

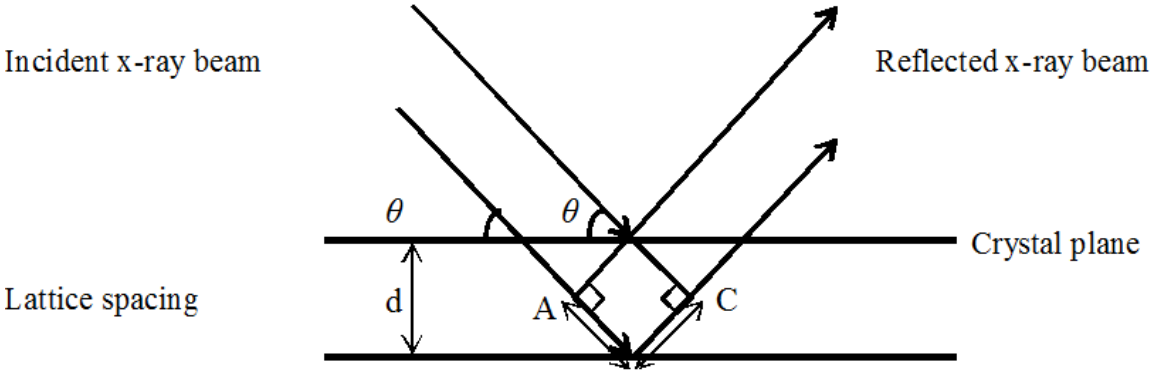

Figure 2.2: Diffraction of x-rays from a set of crystal planes (Zhang *et al.*, 2012)

2.6.3 Infrared Spectroscopy

Fourier Transform Infrared (FTIR) spectroscopy provides information on fundamental vibrations of characteristic functional groups within polymeric and metal oxide materials fabricated. Analysis by IR spectroscopy is usually limited to energies between 4000 – 400 cm^{-1} and to some extent the far IR region of electromagnetic spectrum (Choina *et al.*, 2014). Functional groups common in organic materials include: hydroxyl, carbonyl, ester, methyl, epoxy, phenol and aromatic ring. For inorganic materials (metal oxides) lattice vibrations were responsible for the observed IR active bands (Kloss *et al.*, 2012). The analysis by FTIR spectroscopy is limited to molecules having a permanent dipole moments or phonons in crystalline materials. The FTIR spectrum is collected as absorbance or the percent transmittance of light as a function of wavelength (λ) or often its inverse that is the wave number (cm^{-1}) is usually used. Quantitatively, the amount of energy absorbed at a given frequency depends on both molecular concentration and molecular structure. FTIR is used to identify functional groups in the adsorbents. Data interpretation of characteristic bands is carried out by simple inspection and reference to generalized charts of characteristic

group frequencies ((Yuan *et al.,* 2013).

2.6.4 Ultra-Violet/Visible Spectroscopy

The Ultra-Violet/Visible spectrum of a material provides information about its optical properties, which are directly related to its electronic properties. These include the optical band gap and sub-band gap absorptions. The optical transitions across the fundamental band gap of semiconductors can be related to band structure and in particular to the density of states in nanostructured and doped semi-conductors (van de Steene *et al.,* 2006).

2.6.5 Magnetic Measurements

Magnetic measurements are performed by using a Superconducting Quantum Interference Device, SQUID. SQUID is a sensitive magnetometer used to detect magnetic flux density as a voltage (Han *et al.,* 2016). The device is composed of a ^{4}He cryostat with a superconducting magnet wherein the sample temperature can be controlled by a ^{4}He gas flow control system. At the core of the SQUID detector are two Josephson junctions connected in parallel in a closed superconducting loop, which serves to precisely measure the induced currents (Hu *et al.,* 2014).

2.6.6 Surface Area and Porosity

Gas sorption (both adsorption and desorption) is the most popular method for determining the surface area and pore size distribution of nanostructured materials especially catalysts. Specific surface area of a material is usually determined by physical adsorption of a gas in Brunauer-Emmet-Teller Method (BET). The material is first heated and degassed by vacuum force or inert gas purging to remove adsorbed foreign molecules. The sample

material is then placed in a vacuum chamber at a constant and very low temperature, usually at the temperature of liquid nitrogen (-195.6 °C), and subjected to a wide range of adsorbate pressures, to generate adsorption and desorption isotherms (Wu *et al.*, 2014). The amount of gas molecules adsorbed or desorbed is determined by the pressure variations due to the adsorption or desorption of the gas molecules by the material (the adsorbent). Knowing the area occupied by one adsorbate molecule, σ (for example, σ= 16.2 $Å^2$ for nitrogen), and using an adsorption model, the total surface area of the material can be determined. The most well-known and widely used is the BET equation for multilayer adsorption, 2.2.

$$\frac{P}{V(P_o - P)} = \frac{P/P_o}{V(1-P/P_o)} = \frac{1 + c - 1(P/P_o}{cV_m \quad cVm}$$

Eq. 2.2

Where P is the equilibrium experimental pressure, Po is the vapour pressure of the adsorbate gas at the experimental temperature, V ($m^3.g^{-1}$) is the standardized experimental volume of the adsorbed gas per gram of adsorbant, V_m ($m^3.g^{-1}$) is the volume of the adsorbate monolayer per gram of adsorbent and *c* is the a constant that relates to heat of adsorption.

BET is based on assumptions that: (a) the surface is energetically homogenous (b) only vertical interactions between adsorbed molecules are considered, and (c) the molecules adsorbed on the surface demonstrate the strongest energy of adsorption and heat of adsorption of the subsequent layers is the same as the latent heat of condensation of the adsorbate gas (Chaukura *et al.*, 2016).

2.7 Extraction and Analysis of samples

Various methods for PHCs extraction have been employed (Steene and Lambert, 2008). Solid phase extraction is one of the most versatile methods of extraction and cleaning of environmental samples (Kelly, 2000; Zhu *et al.,* 2010). A study by Ben *et al.,* (2008) reported good recoveries of tetracycline and tiamulin sulfonamides in swine wastewater using solid phase extraction. Among the methods widely used for determination of concentrations of pharmaceuticals are ultra-violet and visible spectrophotometry (UV-Vis), Gas chromatography hyphenated to mass spectrometry (GC-MS/MS) and high performance liquid chromatography tandem mass spectrometry (HPLC-MS) (van de Steen *et al.,* 2006; Zhu *et al.,* 2010; Magnér *et al.,* 2010). Quantitative analysis using UV-Vis is usually based on Beer Lambert's law and in many cases the presence of stray radiation makes the direct application of Beer's law inaccurate. Therefore, GC-MS and HPLC-MS methods have been employed due to their low detection limits (van de Ven *et al.,* 2004; Chenxi *et al.,* 2008). The use of GC-MS technique limits the spectrum of the analyzed chemicals to non-ionic and thermally stable substances. However, derivatization methods such as acylation or methylation and hydrolysis can be employed to enable analysis by GC-MS (Jeannot *et al.,* 2002). Ultra high performance liquid chromatography has also been used for analysis of trace organic pollutants including pharmaceuticals (Li *et al.,* 2009a; Magnér *et al.,* 2010; Anumol *et al.,* 2013).

CHAPTER THREE

3.0 MATERIALS AND METHODS

3.1 Study Area

This study was carried out within Lake Victoria Basin (LVB) of Kenya (Figure 3.1). Lake Victoria is the second largest fresh water lake worldwide with a surface area of 68,000km^2. It is situated within three countries; Kenya, Uganda and Tanzania. The lake has a catchment area of 193,000 km^2 of which Kenya occupies about 22 %. The basin lies between latitude $1^0$30'N and $0^0$05'S and longitude 34^0 and $35^0$45'E. The major towns around the lake are Kisii, Homabay, Kisumu, Busia, Kakamega, Mumias, Bungoma and Eldoret. Effluents from WWTPs in these towns are disposed of into rivers which discharge directly or indirectly into Lake Victoria. The major rivers that drain into Lake Victoria include; Nzoia,Yala and Sondu which may be sources of PHCs loading into the lake. The watewater treatment plants which located in major towns within the basin and their daily capacities are shown in Table 3.1.

3.2 Chemicals, Standards Reagents

High purity standards (>99 %) for ampicillin, sulfamethoxazole, carbamazepine, lamivudine, aspirin, diclofenac and chloramphenical were purchased from Sigma Aldrich, Augsburg Germany. Analytical grade and HPLC grade solvents for extraction and analysis were also purchased from Fluka Chemicals, Germany. Other expendables such as solid phase extraction cartridges and nylon microfilters were bought from Merck Chemicals through Estec Kenya Limited. All stock solutions were prepared using HPLC grade solvents.

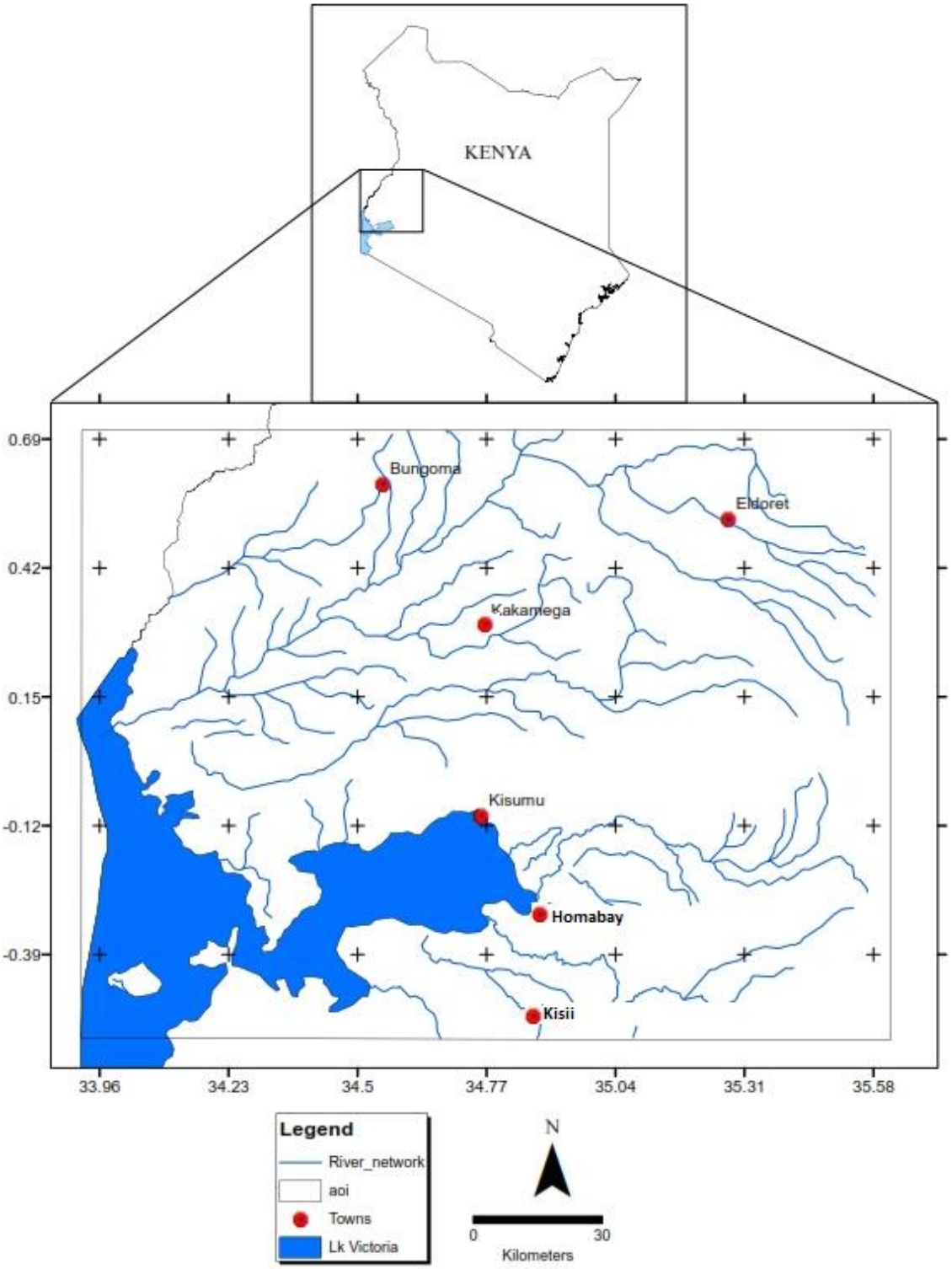

Figure 3.1: The map of Lake Victoria Basin (Kenya) showing the study area.

Table 3.1: Waste water treatment plants in major towns within LVB

Location of WWTP		**Population served**	**Type of watewater treated**	**Capacity (C_{WWTP})(M^3day^{-1})**
Eldoret		165,450	Domestic	1600
Eldoret hospital			Hospital	_
Bungoma		81,151	Domestic	1500
Bungoma Hospital			Hospital	_
Busia		61,715	Domestic	600
Kakamega	Kakamega hospital	99,987	Hospital	_
	Shirere		Domestic	800
	Nabongo		Domestic	_
	MMUST		Institutional	425
Kisumu	Nyalenda	409,908	Domestic	6050
	Kisat		Domestic and industrial	2450
Homabay		54,040	Domestic	720
Kisii		83,460	Domestic	1400

- Daily capacities not known.

Source: Lake Victoria North and Lake Victoria South Water Services Board Technical Report, 2012.

3.3 Analytical Instruments used in the study

The instruments used in the study are described giving their models. A Shimadzu LC-20AD fitted with a SIL-20A (HT) autosampler and a SPD-20A prominence ultraviolet-visible (UV) detector were used for HPLC analysis of PHC residues. Functional group determination was carried out using a Thermofischer, Nicolet iS5 (USA) FTIR. Surface morphology was

determined using SEM (BITRI BSM 6460LV) coupled with an EDAX instrument. For XRD analyses,a PANalytical X'Pert Pro powder instrument was used. A DC SQUID magnetometer system (model XL-5, manufactured by Quantum Design, USA) incorporating a high-temperature superconductor thin film SQUID sensor was used to determine adsorbent magnetic properties. A water deionizer (milliQ water) and water still were used. Surface area was determined by Micromeritics ASAP 2020 BET analyzer.

3.4 Collection of samples from WWTPs and rivers for analysis of PHC residues

Waste water samples for residue analysis were collected from hospitals and municipal wastewater treatment plants and within major towns within LVB of Kenya (Figure 3.1). Slu dge and wastewater were collected from hospital lagoons and WWTPs between October, 2014 and September, 2015. Both untreated samples (influent) and treated samples (effluent) from the WWTPs were collected (appendix 1 and 2, respectively). Appendix 3 shows a photograph taken during sampling of sludge from Kipkenyo WWTP in Eldoret. Water and sediment samples from receiving rivers were also sampled (Sosiani River). Wastewater samples were collected in 2 L amber glass bottles and taken to the laboratory in an ice box. Samples were then refrigirated at -4 ^{o}C prior to extraction within 48 hours. Sludge samples were also collected, air-dried, ground and passed through 200 mm sieve prior to extraction. The selected WWTPs were used to treat wastewaters originating from domestic, hospital and industrial areas, and their characteristics are presented in Table 3.1.

During sampling, it was noted that effluents from the WWTPs were being discharged into rivers which discharge water into Lake Victoria. An example is Auji River which receives discharge from Nyalenda WWTP and dicharges its water to Lake Victoria where water samples were collected (appendix 4).

3.5 Collection of adsorbent samples

The diatomaceous earth (DTE) adsorbent was obtained from Naivasha (Kenya). DTE is the fossilized remnants of diatoms, tiny planktonic algae residing in all of the earth's waters (Yu *et al.,* 2015). Diatoms are single celled organisms that belong to the phylum Bacillariophyta and which possess a cell wall made of silica (SiO_2). The death of large numbers of diatoms in an area leads to sedimentation of the minerals present in the cell walls resulting in large deposits which can be mined. The remarkable property of these deposits is their high purity, often greater than 85% silica. As a result diatomite is non-toxic and odourless, which is present naturally in large quantities and available at low cost (Danil *et al.,* 2012).

The biomass for generation of biochar was sugarcane bagasse and maize cobs. Sugarcane bagasse is the waste generated during processing of cane. In this study, sugarcane bagasse was obtained from Mumias Sugar Company. On the other hand, maize cobs were collected from farmers within the Lake Victoria Basin in Kenya. It is an agricultural waste which is abundant within the region.

3.6 Production of unmodified and iron modified adsorbent composites

The unmodified bagasse (CBG) and maize cob (CMC) biochars were prepared by chopping the biomass into pieces then thoroughly washed with de-ionized water to remove all adhering dirt and air dried before pyrolysis. Carbonization was achieved by slow-pyrolysis at 350 °C and at a heating rate of 10 °C $minute^{-1}$ and a residence time of 1 h in a furnace under nitrogen stream. The biochar was then washed with deionized water until the effluent from it was neutral to litmus and oven-dried at 100 °C for 2 h (Ng'eno *et al.,* 2016). Iron modified carbonized bagasse (α-Fe_2O_3-CBG) was then fabricated by direct hydrolysis of an iron salt following the protocol described by Hu *et al.,* (2015) with slight modification. Iron salt solution prepared by dissolving 10 g of $FeCl_3.4H_2O$ in 50 mL of deionized water was mixed

with 10 g of CBG for 8 h under continuous agitation and finally oven dried at 100-120 °C for 12 h. The resultant product, iron modified carbonized bagasse (α-Fe_2O_3-CBG), was sieved to obtain uniform particle size (<220 µm) then stored in air-tight containers (Figure 3.2) for adsorption experiments. Similar treatment was performed using diatomaceous earth (DTE) and carbonized maize cob (CMC) to obtain α-Fe_2O_3-DTE and β-FeO(OH)-CMC composites (Figures 3.3 and 3.4), respectively.

Figure 3.2: Photograph showing unmodified bagasse biochar (CBG)and iron modified bagasse α-Fe_2O_3-CBG adsorbents

Figure 3.3: Photograph showing unmodified (DTE) and iron modified diatomaceous earth (α-Fe_2O_3-DTE) adsorbents

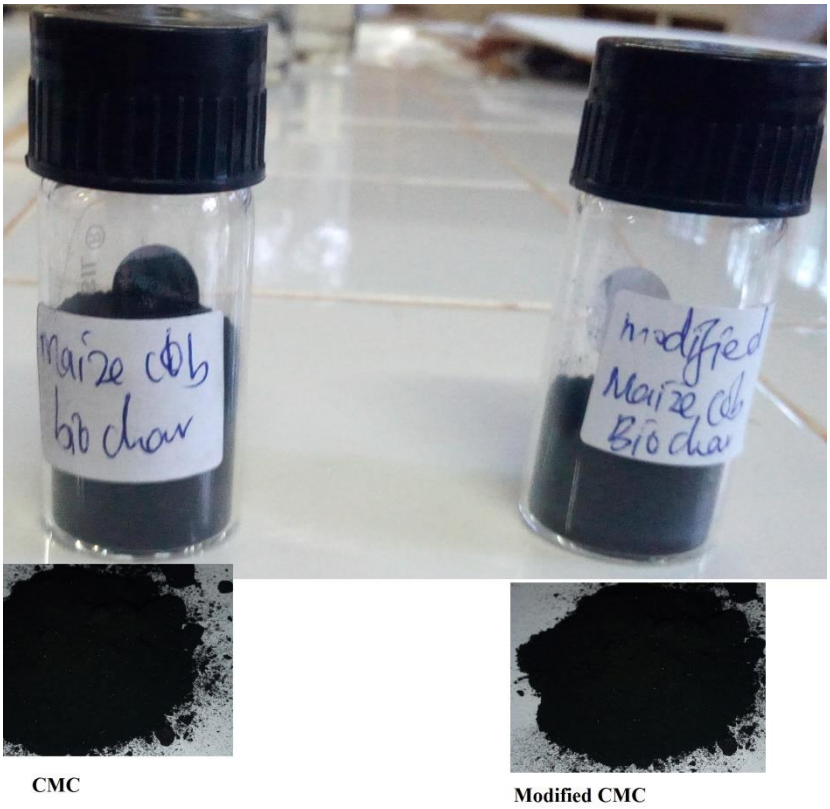

Figure 3.4: Photograph showing unmodified and iron modified maize cob adsorbents

3.5 Extraction of Samples for Residue Analysis

Wastewater samples were extracted by passing 300 ± 3.0 mL aliquots through a 6 mL phenomenex C_{18} solid phase extraction (SPE) cartridge that had been pre-conditioned with 10 mL of methanol and distilled water, successively. Elution was carried out using 10 mL of HPLC grade methanol which was then evaporated to dryness under vacuum. The residue was redissolved to 2 mL with HPLC-grade methanol (Van de Ven *et al.,* 2004). This process was carried out by batch extraction using an SPE mannifold. All samples were filtered using 0.45 µm nylon microfilters prior to injection to LC instrument. Sludge samples were extracted by weighing 0.5 ± 0.05 g of dry sample into a conical flask and adding 15 mL of HPLC grade methanol. Samples were shaken for 8 hours in an orbital shaker at 100 r.p.m. After which the supernatant was filtered through glasswool that had been pre-conditioned with 10 mL of HPLC grade methanol. The filtrate was evaporated to dryness and sample re-dissolved in 100

mL distilled water. Clean up of samples was performed by SPE following the same procedure for wastewater samples (Nguyen *et al.*, 2015).

3.6 Analysis by HPLC

Residue samples and samples from batch adsorption experiments were filtered using 0.45 μm nylon micro filters prior to injection to LC instrument. A Shimadzu LC-20AD fitted with a SIL-20A (HT) autosampler and an SPD-20A prominence ultraviolet-visible (UV) detector was used for HPLC analysis (appendix 5). A reverse phase phenomenex (C_{18}) column (4.6 mm i.d. × 250 mm, 5 μm particle) was used for separation of the analytes (Van de Ven *et al.*, 2004). Injection volume was 10 μL and flow rate of 1 mL per minute.

Gradient elution was carried out using a mobile phase consisting of (50: 50 v/v) HPLC grade acetonitrile: Methanol (A) and water with 0.1 % formic acid (B) at a flow rate of 0.30 mL/min. The gradient programme was set as follows; (0-3 mins) A=90 %, 8 min A=65 %, 17 min A=50 %, 20 min A=0 %, 30 min A=90 %. Quantification was done using a UV detector at 250 nm wavelength (Park and Choung, 2007). Analyte identification was based on comparison of chromatograms of unknowns with those of standards. Standards and blanks were measured periodically throughout the analysis for quality assurance. Quantitative analysis of PHCs was achieved through the integration of selected HPLC chromatograms. All analyses were carried out in triplicate. Mass spectrometric analysis was done with electron impact ionization for identification of analytes (Van de Steen *et al.*, 2008).

3.7 Quality control and assurance

Before analysis, volumetric standards were used to calculate total method recoveries and resolutions. With each set of samples to be analyzed, solvent blank and standard mixtures were run in sequence to check for contamination, peak identification and quantification.

Internal standards and external standard calibration curves were used for PHC residue quantification (Park and Choung, 2007). Limit of detection and limit of quantification are the two important performance characteristics used in method validation for this work. A series of up to six procedural blank samples were extracted along with every batch of sample for assessment of the method detection limits (MDL) of the different target analytes. Method detection limits were set at a signal-to-noise ratio of three in the sample chromatograms. In this study, the limit of detection was the injected amount that resulted in a peak with a height at least three times as high as the baseline-noise level. The quantification limit of the target chemicals was evaluated for each sample based on the average blank concentrations plus five times the standard deviation of the blanks. Precision of a method is the degree of scatter of results which is usually expressed as standard deviation and percentage of relative standard deviation of the retention time and the peak area.

3.8 Discharge loads calculations

The daily discharge load from WWTPs was estimated based on the assumption that the concentration of PHCs in wastewater and sludge recorded are constant throughout the day. This was done using Eq.3.1

$$Dd = (C_w \times C_{wwtp} \times 1000) \times 10^{-3} \ (mg\ day^{-1}) \quad (3.1)$$

Where; Dd=daily discharge of PHCs (mg day^{-1}), C_w=concentration of individual PHC in wastewater (µg L^{-1}), C_{wwtp}=capacity of WWTP (m^3 day^{-1}), 1000=conversion factor from cubic meters to litres, 10^{-3}=conversion from µg to mg.

An estimated total amount of PHCs discharged from the WWTPs were calculated using Eq. 3.2.

$Dd_{Total} = \sum Dd_{WWTPs}$ (3.2)

Where; Dd_{Total} = total amount of PHCs discharged from the WWTPs, $\sum Dd_{WWTPs}$= sum of the daily discharge loads of PHCs in all the WWTPs (mg day^{-1}) (Chirikona *et al.*, 2015).

3.9 Dissipation of Selected pharmaceuticals in WWTPs within LVB

The percentage PHCs lost (dissipation) during treatment by conventional aerated lagoon method was calculated from the concentrations in the effluent and influent using equation 3.3. This gives the efficiency of treatment by conventional method.

$$\%Dissipation = \frac{\left(C_{\text{inf}\,luent} - C_{effluent}\right)100}{C_{\text{inf}\,luent}} \quad (3.3)$$

Where $C_{influent}$ is the concentration of PHCs in the raw (untreated) sewage (entering the WWTP) and $C_{effluent}$ is the concentration of PHCs in the treated sewage (leaving the WWTP).

3.10 Characterization of adsorbents

In order to understand the properties and application potential of the fabricated adsorbents different characterization methods were used. This study utilized various methods for determination of the morphology, structure and physic chemical properties of the adsorbents. Some of the techniques include; scanning electron microscopy (SEM), X-ray diffraction (XRD) method, X-ray fluorescence (XRF) technique, Fourier Transform Infra-red (FTIR) spectroscopy, Brunauer Emmet and Teller (BET) surface area and magnetic measurement techniques.

3.10.1 XRF analysis

For XRF analyses 200 mg of each adsorbent was pelletized and irradiated with X-rays. The elements present in the adsorbent emit a fluorescent-X-ray radiation that is characteristic of those elements which is detected. A spectrum is plotted showing peaks for each element with their percentages in the sample. This provides elemental composition of the adsorbent recorded as mass percent.

3.10.2 XRD analysis of fabricated adsorbent composites (modified and unmodified)

X-ray diffraction (XRD) patterns were determined at room temperature using a PANalytical X'Pert Pro powder) (Copper Kα radiation with k = 1.5406 A˚) equipped with a PSD Lynx-Eye Si-strip detector with 196 channels, in a locked couple mode with an accelerating voltage of 40 kV and an applied current of 40 mA (Yao *et al.*, 2014). A 20 mg sample of each adsorbent was compacted (at least 1 mm in thickness to prevent penetration of the x-ray beam) and mounted on a goniometer. X-rays are directed to hit the surface and interact with electrons in the atoms which are elastically scattered. The diffracted X-rays reveal the distribution of electrons in the adsorbent. These beams are in a specific direction governed by the Bragg's law (Eq. 3.4).

$$2d \sin\Theta = n\lambda \qquad \text{Eq. 3.4}$$

Where; d is the spacing between reflecting planes, Θ is the glancing angle of incident X-ray beam, 2d SinΘ is the path difference for waves reflected by successive planes, n is an integer and λ is the wavelength of the X-ray. The x-ray diffraction spectra were collected from 10 to 90 2θ at rate of 0.5° per minute at room temperature (Chaukura *et al.,* 2016). The patterns obtained were compared with International Centre for Diffraction Data library using High

Score software for qualitative identification of the crystalline compounds. The X-ray pattern is unique for crystalline substance where each peak represents a lattice plane characterized by a miller index. The order of the diffracted waves of each crystallite are described by the miller indices (h,k,l) whose values can be obtained by the Debye-Scherrer method as follows;

$d = a/\sqrt{N}$ Eq. 3.5

But $\Delta \text{ Sin } \Theta = (\lambda/4a^2)(N_2-N_1)$ Eq. 3.6

$N = h^2 + k^2 + l^2$ Eq. 3.7

Where; h,k,l are miller indices representing the position, width and intensity of the crystal, respectively.

The d spacing for the various crystalline structures in the library is guided by the following formulae;

Tetragonal structure: $1/d^2 = ((h^2 + k^2)/a^2) + (l^2/C^2)$ Eq. 3.8

Hexagonal structure: $1/d^2 = 4/3((h^2 + hk + k^2)/a^2) + l^2/C^2$ Eq. 3.9

Cubic structure: $d_{hkl} = a/\sqrt{(h^2 + k^2 + l^2)}$ Eq 3.10

Rhombohedral structure: $\text{Sin}^2\Theta_{\text{nth peak}}/\text{Sin}2\Theta_1{}^{\text{st}}{}_{\text{peak}} = (h^2+k^2+l^2)_n{}^{\text{th}}{}_{\text{peak}}/(h^2 + k^2 + l^2)_1{}^{\text{st}}{}_{\text{peak}}$ Eq. 3.11

The XRD pattern provides information on the properties such as crystallite size, lattice strain, chemical composition and phase diagrams, at atomic level. The identification of crystals was based on their d spacing from the Bragg's law (Eq. 3.4). Each peak in the spectrum represents a lattice plane characterized by a miller index. The miller indices were obtained by Debye Scherrer method and the crystal structure determined using equations 3.8-3.11, respectively.

3.10.3 SEM analysis of synthesized adsorbents

SEM micrographs were obtained using a scanning electron microscope (BITRI BSM 6460LV) coupled to an energy dispersive analysis X-ray (EDAX) instrument. A 5g sample

were mounted on a stub and coated with gold/palladium alloy in a Denton sputter source. Au/Pd coating on non-conducting samples was meant to prevent charging effect in order to achieve better contrast and higher image resolution. A focused electron beam was rastered across the surface of the adsorbent and the backscattered electron signal was detected. The SEM instrument was coupled to Energy Dispersive Analysis X- ray (EDAX) spectroscopy important in elemental analysis. For elemental analysis (EDAX) high acceleration voltages (15 - 20 keV) (voltage applied varied based on extent of sample charging) using a secondary electron detector. Images were taken at several magnifications ranging from 50 to 4000. The micro-porosities of adsorbents were quantified using the image processing software, Pores and Cracks Analysis System (Liu *et al.,* 2011). The SEM images are imported into the software which then converts them into equivalent binary forms based on the gray-level threshold values (T) entered. The microporous regions in the binary images are distinguished by segmenting the image into black and white regions representing solid surfaces and void spaces, respectively (Nizamuddin *et al.,* 2017). The SEM-EDAX micrographs reveal topographical features of the adsorbent, phase distribution, composition difference, presence and location of defects, crystal structure and orientation.

3.10.4 Determination of functional groups by FTIR spectroscopy

The FTIR spectra of the magneto responsive adsorbents were recorded at a range from 400-4000 cm^{-1} with 2 cm^{-1} resolution using a Nicolet iS5 FTIR instrument. Prior to analysis, samples were prepared by milling 0.9 mg of sample with 70 mg of analytical grade potassium bromide (KBr) to form a fine powder and compressing into a pellet for analysis. Over 64 scans were collected for each measurement at 2 cm^{-1} resolution (Yuan *et al.,* 2013). The Infra-red (IR) spectra were used to determine the vibrational frequency changes in the functional groups of the adsorbent (Hu *et al.,* 2015).

3.10.5 Determination of the surface area of unmodified and iron modified adsorbents

The surface area, pore volumes and average pore diameter were determined by nitrogen adsorption method. For each adsorbent, a 150 g sample was outgassed at 350°C for 12 h before measurement. The surface areas were determined on dry adsorbent samples via nitrogen adsorption at 77 K on a Surface Area Analyzer (Micromeritics ASAP 2020 BET). Isotherms were plotted and the total surface area was calculated by the Brunauer, Emmett, and Teller (BET) method using the adsorption isotherms. The BET and Langmuir adsorption isotherms were generated to determine the single-point surface area (Ribeiro *et al.,* 2011). Total pore volume was obtained based on nitrogen uptake at a relative pressure of 0.99 mmHg. The micropore and mesopore size distribution were calculated using the Barrett-Joyner-Halenda (BJH) method (Chaukura *et al.,* 2016).

3.10.6 Determination of magnetic properties of iron modified adsorbent composites

To investigate magnetic properties, a magnetic hysteresis loop for the magneto responsive composites was recorded at room temperature at a constant magnetic field of 1000 Oe. Samples for magnetic studies were ground into a smooth powder, loaded into capsule and weighed prior to analysis (Zhang *et al.,* 2013). The magnetization (M) of 20 mg of each sample was measured as a function of temperature (T) at a constant applied magnetic field (H) using a DC SQUID magnetometer system (Magnetic Property Measurement System (MPSN) magnetometer model XL-5, manufactured by Quantum Design) incorporating a high-temperature superconductor thin film SQUID sensor (Wei *et al.,* 2016). It has the ability of measuring magnetic moments of samples as low as 10^{-8} emu over a wide range of temperature between 2 K to 400 K. Magnetic hysteresis curves were plotted from 0-350 °K based on the Curie law (Eq. 3.12).

$\chi = C/T$ Eq. 3.12

Where; χ is magnetic susceptibility, T is absolute temperature and C is the Curie constant.

Magnetic susceptibility, χ, is dimensionless obtained from equation 3.10

$M = \chi H$ Eq. 3.13

Where; M is the magnetization of sample and H is the magnetic field (1000 Oe).

The shape of the hysteresis loop was used to determine the magnetic property of the adsorbent. A paramagnetic material has no spin order in absence of a magnetic field, while a ferromagnetic material has all spins aligned in the same direction. Conversely, antiferromagnetic materials have all spins align in opposite direction, whereas ferromagnetic ones have spin magnitude greater in one direction. All these magnetic properties can be distinguished by their hysteresis curves.

3.11 Kinetic studies experiments

The kinetic experiments were performed by batch technique. A 0.1 g of the iron modified α-Fe_2O_3-CBG adsorbent were dispersed into 250 mL glass conical flasks containing 1 mg L^{-1} carbamazepine in 50 mL solution at 298 K and agitated at 120 rpm using an overhead temperature-controlled shaker (GFL-3006). At pre-determined regular time intervals (0, 0.5, 1, 2, 3, 4, 5, 6 hours) 0.5 mL aliquots were withdrawn and filtered through 0.22 µm syringe filters into sealed glass vials for residual CBZ analysis. Carbamazepine was detected by HPLC with UV detection (Shimadzu LC 20AT) at 252 nm (Chen *et al.,* 2016). The mobile phase was a mixture of acetonitrile and water (70:30 v/v), with a flow rate of 1 mL min^{-1}. The injection volume was 20 µL. Similar experiments were repeated for the iron modified composites of α-Fe_2O_3-DTE and β-FeO(OH)-CMC.

The amount of CBZ adsorbed per unit mass at pre-equilibrium time (t) was obtained by equation 3.14.

$$q_t = \frac{(C_i - C_e)V}{m} \quad (3.14)$$

Where, q_t is the amount of PHC adsorbed per gram of adsorbent at equilibrium time t, C_i and C_e are the initial and equilibrium concentration (mg L^{-1}), m is the mass of adsorbent (g) and V the volume of the solution (L). To obtain the kinetic parameters, the kinetic data were fitted to three widely used kinetic models, *viz*. pseudo-first order (Ho and McKay, 1998), pseudo-second-order (Ho, 2006), and intra-particle diffusion models (Weber and Morris, 1963) represented in the equations 3.15-3.17, respectively:

Pseudo-first-order model: $$\log(q_e - q_t) = \log q_e - \frac{k_1 t}{2.303}$$ **(Eq. 3.15)**

Pseudo-second-order model: $$\frac{t}{q_t} = \frac{1}{k_2 (q_e)^2} + \frac{t}{q_e}$$ **(Eq. 3.16)**

Intra-particle diffusion model: $$q_t = k_p t^{0.5} + C$$ **(Eq. 3.17)**

Where, qt is the amount of PHC adsorbed per gram of adsorbent at equilibrium time t, q_e is the equilibrium adsorption capacity, k_1, k_2, k_p are rate constants and C is a constant.

3.12 Adsorption isotherm experiments

Adsorption isotherms for CBZ onto adsorbent composites (α-Fe_2O_3-CBG, α-Fe_2O_3-DTE and β-FeO(OH)-CMC) were determined using 0.1g iron-impregnated adsorbents with 50 mL CBZ solutions of varied concentrations (0.25, 0.5, 0.75, 1.00 and 1.25 mgL^1) in a batch mode for a period of 4 hours. The vessels were agitated under similar experimental conditions as in the kinetics experiments described above until equilibration as determined from the kinetic

experiments (4 h). The amount of solute adsorbed per unit mass of adsorbent at equilibrium (q_e) was calculated using the equation 3.18.

$$q_e = \frac{(C_i - C_e)V}{m} \qquad \text{Eq. 3.18}$$

Where; q_e is the solute uptake, Ce is the equilibrium concentration, C_i is the initial analyte concentration, m is the mass of adsorbent and V is the volume of the solution.

The equilibrium sorption data were modeled using linearized Langmuir and Freundlich isotherm equations shown in Table 3.2 and the isotherm parameters calculated.

Table 3.2: The linearized isotherm equations and parameters

Isotherm Model	**Equation**	**Parameters**	**Reference**
Langmuir	$\frac{1}{q_e} = \frac{1}{Q_o} + \frac{1}{Q_o K_L C_e}$	Q_o (mg/g), K_L (L/g)	Langmuir, 1918
Freundlich	$\log q_e = \log K_f + \frac{1}{n} \log C_e$	K_f, n	Freundlich, 1906

Where; Q_o-Monolayer adsorption capacity (mg/g), K_L and K_f-Langmuir and freundlich constants, Ce is the equilibrium concentration, q_e is the solute uptake, 1/n is related to adsorption affinity and surface heterogeneity.

3.13 Effect of pH

The effect of pH on the extent of CBZ removal was investigated over a pH range of 2-10. Here, 50 mL (1 mg L^{-1}) of CBZ solution and 0.1 g of each adsorbent, separately, were placed in glass conical flasks and 1 M HCl and 1 M NaOH solutions were used for initial pH adjustment. The solutions were then agitated at 120 rpm at 298 K until equilibration. The pH was measured using a pH meter (MrC 86505, scientific instrument).

3.14 Determination of point of zero charge (pHpzc)

A 0.1 g of each adsorbent composite was dispersed into 50 mL of de-ionized water at 25 °C. The initial pH (pH_i) was adjusted to 2, 4, 6, 8 and 10, respectively in different 250 mL conical flasks. The conical flasks were then placed in an orbital shaker and shaken for 10 hours at 120 rpm. Thereafter, filtration was carried out and the final pH values (pH_f) were determined. The difference between pH_i and pH_f values ($\Delta pH = pH_f - pH_i$) was plotted against the initial pH (pH_i). The pHpzc of the adsorbent was obtained from the point of intersection of the resulting curve at which $\Delta pH=0$.

3.15 Thermodynamic **Studies**

The effect of temperature changes on adsorption was studied in the range 293 to 338 K. The method by Moussavi *et al.,* (2013) was adopted with slight modification. Briefly, 0.1 g of each of the three adsorbents were separately dispersed into 50 mL of 50 mg L^{-1} of CBZ and stirred at 200 rpm at 293, 303, 313 and 323 K, all in triplicate. After equilibration, 1.0 mL aliquots were withdrawn from the flask and transferred into sealed glass vials for residual PHC analysis by HPLC. The effect of temperature was studied in the temperature range (298-338K), to determine the thermodynamic feasibility of the adsorption process in practical applications. The values of Gibbs free energy change (ΔG, J mol^{-1}), enthalpy change (ΔH, kJ mol^{-1}), and entropy change (ΔS, $JK^{-1}mol^{-1}$) were calculated using equations 3.19 and 3.20;

$$\ln K = \frac{\Delta S}{R} - \frac{\Delta H}{RT} \qquad \text{(Eq. 3.19)}$$

$$\Delta G = \Delta H - T\Delta S \qquad \text{(Eq. 3.20)}$$

Where K, equal to (q_e/C_e), is adsorption affinity, R is the gas constant (8.314 J $mol^{-1}K^{-1}$) and T is the temperature in Kelvin. The values of ΔH and ΔS were obtained from the slope and the intercept of the plot of the Van't Hoff equation (3.19) , respectively. The values of ΔG were calculated from Eq. (3.20).

3.16 Statistical analysis

Statistical analysis was carried out using SPSS version 18.0 packages. Analysis of variance (ANOVA) was used to evaluate the difference in PHC concentrations in different matrices namely; water, sludge and sediment. Comparison was performed by paired t-test at 95 % confidence level (Bermudez-Couzo *et al*, 2011).

CHAPTER FOUR

4.0 RESULTS AND DISCUSSION

4.1 Overview

This chapter presents the results and discussions of the following areas: quality control parameters and levels of selected pharmaceuticals in various wastewater treatment plants and hospitals within Lake Victoria. The properties of engineered magneto responsive adsorbents for removal of carbamazepine, a model PHC, are also presented. The kinetics, isothermal and thermodynamic studies are discussed.

4.2 Quality Control Parameters

The selectivity of the method refers to the extent to which a particular analyte can be determined in a complex mixture without interference from other matrix components. This was verified by comparison of the chromatograms obtained from samples spiked with known concentrations of the standard and those samples free from the PHC standards. Blank samples did not present any peak at the retention time of the analyte. Moreover, the chromatograms of the pharmaceutical standards and sample extracts presented satisfactory chromatographic resolution as shown in Figure 4.1. The analyte retention times (t_R) were 9.94, 17.33, 19.02, 21.84, 23.15, 25.11 and 27.50 minutes for ampicillin (AMP), chloramphenicol (CAP), sulfamethoxazole (SMX), lamivudine (LMV), carbamazepine (CBZ), diclofenac (DCF) and aspirin (ASA), respectively. Sample HPLC and UPLC-MS/MS chromatograms are presented in appendices 6-9.

The linearity of detector response was evaluated by injecting solutions of each standard over a wide range of concentrations. The analytical calibration curves and the related linear regression data displayed good linearity of the detector response within the specified range.

The correlation coefficients obtained was greater than 0.99 ($r^2 > 0.99$) making the calibration curve useful for quantification (Figure 4.2).

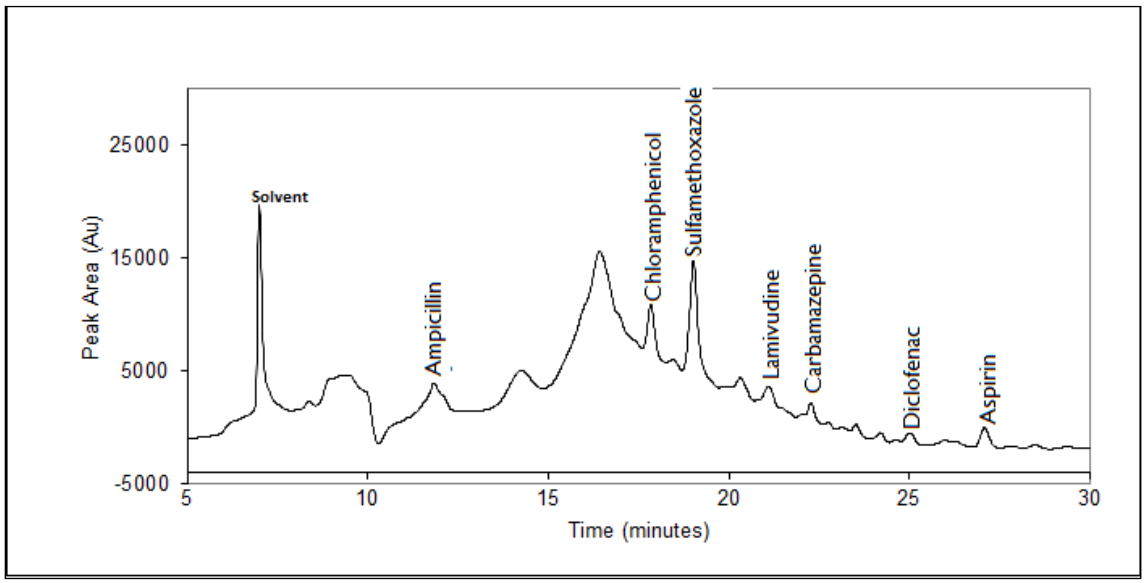

Figure 4.1: HPLC chromatogram showing separation of analytes in samples

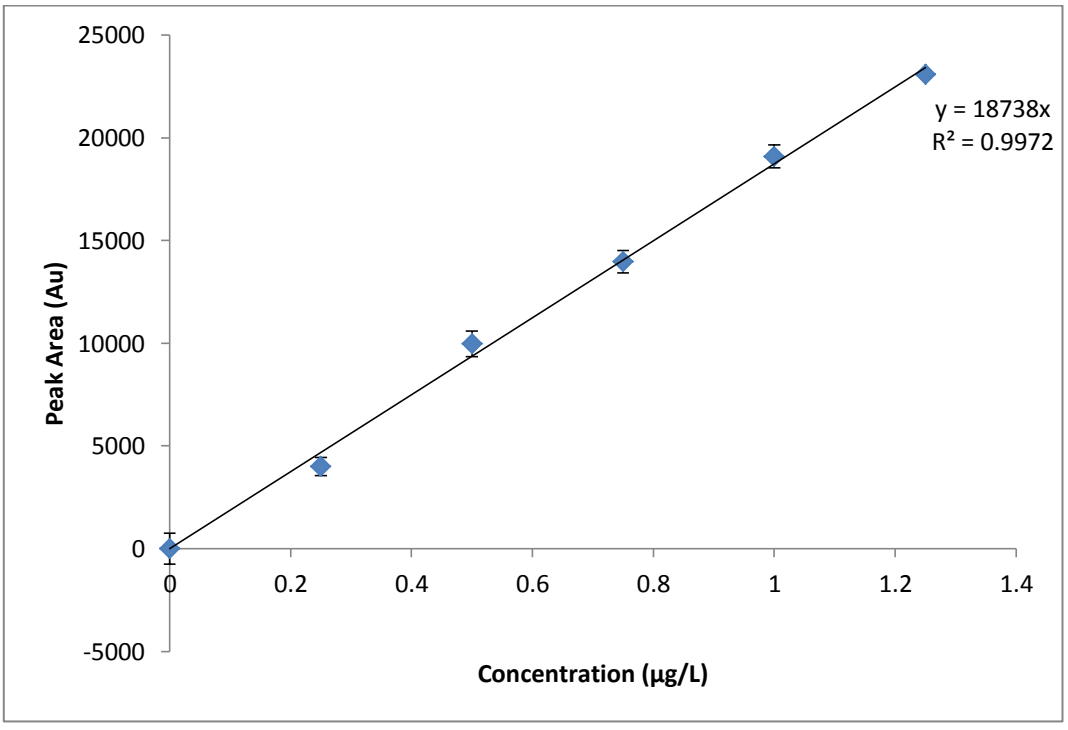

Figure 4.2: A calibration curve of Sulfamethoxazole standard

4.3 The levels of selected parmaceuticals in sludge and sediment samples from hospitals, WWTPs, rivers and streams within LVB, Kenya

All sludge samples contained quantifiable levels of the selected PHCs. The mean concentrations in sediment and sludge samples from ten WWTPs and two hospitals, rivers and streams within LVB are presented in Table 4.1, 4.2 and Figure 4.3, respectively.

Table 4.1: The distribution of selected PHCs in sediment samples (ng/g) from rivers and streams within Lake Victoria Basin, Kenya

Study Site	DCF	AMP	CBZ	SMX	CAP	ASA	LMV
MMUST stream (Upstream)	<50±2	<50±2	<50±2	<50±2	<50±2	57±3	55±4
MMUST stream (Downstream)	51±6	<50±2	<50±2	65±5	<50±2	70±5	62±3
Auji River	62±7	74±5	<50±2	61±6	54±8	71±2	61±4
Kisat River (Upstream)	<50±2	52±9	<50±2	63±3	59±7	63±3	56±3
Kisat River (Downstream)	62±5	66±6	<50±2	85±8	69±4	65±8	74±8
Sosiani River (Uptream)	<50±2	54±4	<50±2	51±5	54±7	81±5	52±2
Sosiani River (Downstream)	72±7	94±3	<50±2	81±5	94±2	74±3	80±7

Limit of quantification, LOQ=50±2 ng/g, n=3, DCF-Diclofenac, AMP-Ampicillin, CBZ-Carbamazepine, SMX-Sulfamethoxazole, CAP-chloramphenicol, LMV-Lamivudine, ASA-Aspirin

Table 4.2: The distribution of selected PCHs in sludge samples (ng/g) from WWTPs and hospital lagoons within Lake Victoria Basin, Kenya

Study Site	DCF	AMP	CBZ	SMX	CAP	LMV	ASA
Bungoma WWTP	145±9	143±15	<50±2	103±7	106±6	96±3	86±4
Bungoma Hospital	95±6	231±21	79±10	205±9	113±8	102±5	98±8
Busia WWTP	94±4	53±6	<50±2	154±9	96±8	92±3	98±6
Shirere WWTP	82±6	<50±2	<50±2	105±6	79±7	99±9	68±6
Mumias Hospital	165±8	151±10	55±5	276±12	<50±2	89±3	236±3
Homabay WWTP	82±7	74±3	<50±2	121±5	54±3	78±6	<50±2
Nabongo WWTP	98±7	57±8	<50±2	94±4	66±11	55±6	<50±2
MMUST WWTP	56±2	<50±2	<50±2	89±7	<50±2	<50±2	51±9
Kisat WWTP	92±3	74±5	<50±2	101±5	65±9	59±9	60±3
Eldoret WWTP	67±6	112±6	<50±2	84±3	102±7	65±7	76±7
Kisii WWTP	106±5	108±11	<50±2	103±2	<50±2	52±9	96±9
Nyalenda WWTP	86±7	98±3	54±5	101±7	97±3	115±3	98±6

Limit of quantification, LOQ=50±2 ng/g, n=3, DCF-Diclofenac, AMP-Ampicillin, CBZ-Carbamazepine, SMX-Sulfamethoxazole, CAP-Chloramphenicol, LMV-Lamivudine, ASA-Aspirin

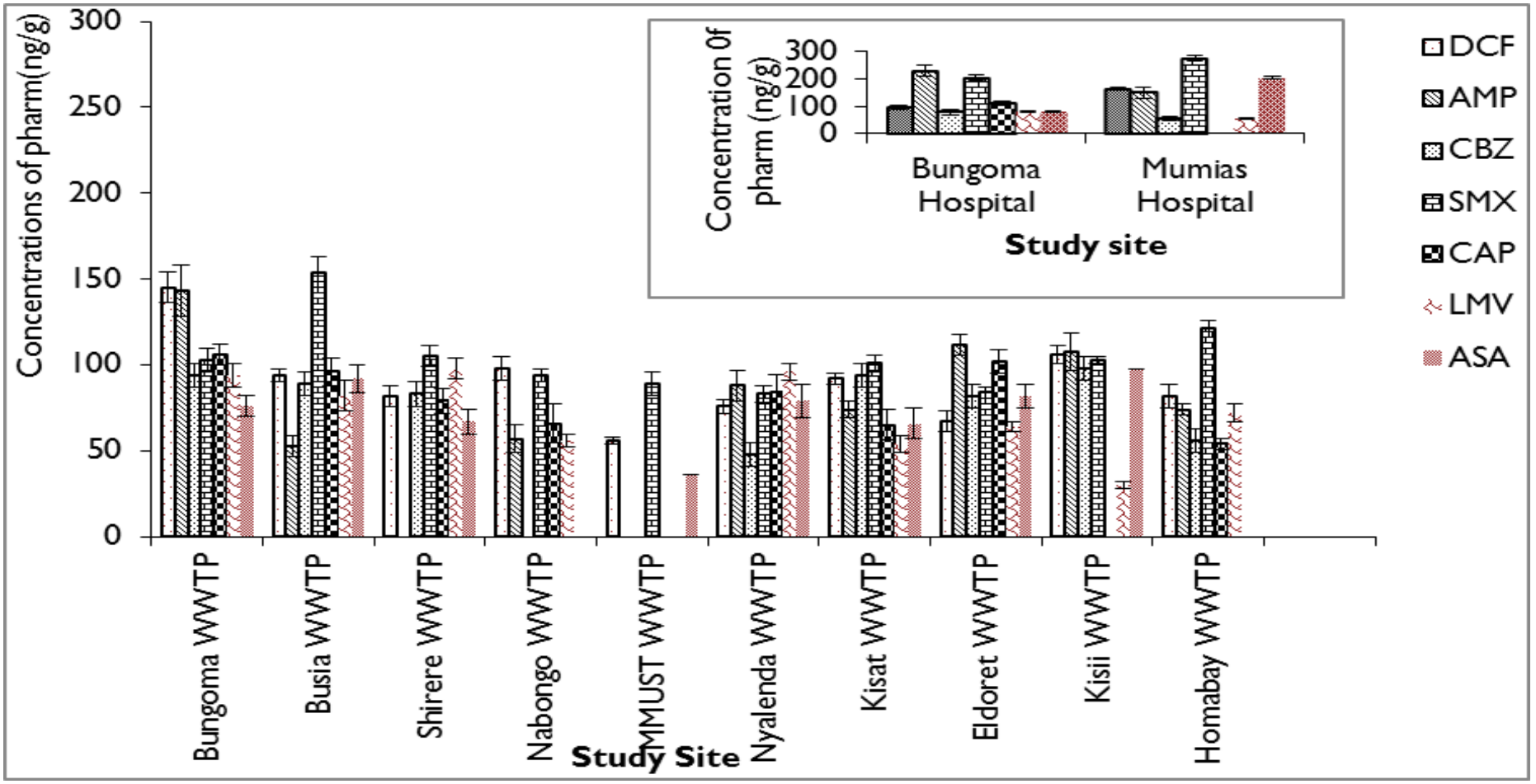

Figure 4.3: The distribution of selected pharmacueticals in sludge samples (ng/g) from WWTPs and hospitals in major urban towns within LVB, Kenya.

The average PHCs concentrations in the sludge and sediment samples varied for individual compounds and amongst samples from different sources (Table 4.1 and Table 4.2). The mean residue levels for all the seven PHCs in sludge was found to range from <50±2 ng/g to 276±12 ng/g, while sediment samples from rivers and streams recorded lower levels ranging fom <50±2 ng/g to 94±3 ng/g (Table 4.2). This may be attributed to dilution in the river environment. The maximum amount of PHCs recorded was 276±12 ng/g sulfamethoxazole in sludge discharged from Mumias Hospital general ward (Figure 4.3). The high levels of sulfamethoxazole in sludge samples may be due to prescription patterns and the intrinsic properties of the compound. The low octanol-water partition of sulfamethoxazole (log Kow = 0.89) makes it preferrentially adsorb onto sludge (Liang *et al.,* 2013; Kihampa, 2014). During this study, the pH of the wastewater sampled ranged from 7.5-8.5. The pH of the effluent may also affect the solubility of the analyte, hence its partition in solid-liquid phases.

4.4 Pharmaceutical residues in river water and effluents from hospital lagoons and WWTPs within Lake Victoria Basin, Kenya

PHCs were widely detected in effluents from wastewater treatment plants within the study region as shown in Table 4.3. From literature, this kind of survey on pharmaceutical residues within the Lake Victoria Basin of Kenya is the first one to be done. The levels of PHCs in hospital effluents were high ranging from <0.05±2 to 0.79±0.07 µg/L. Eldoret hospital recorded the highest concentrations (ampicillin of 0.79±0.07 µg/L). This shows that hospitals are hot spots for PHCs discharge into WWTPs. The mean concentrations of PHCs in effluents from the ten WWTPs studied ranged between <0.05±2 to 0.36±0.04 µg/L.

The highest levels in WWTPs was recorded in Nyalenda (Kisumu) with ampicillin levels of 0.36±0.04 µg/L. Kisumu is the largest among the towns within the region with the highest population as shown in Table 3.1.

Table 4.3: Concentration of selected pharmaceuticals in effluents (µg/L) from hospitals and WWTPs within LVB, Kenya

Study Site	**Diclofenac**	**Ampicillin**	**Carbamazepine**	**Sulfamethoxazole**	**Chloramphenicol**	**Aspirin**	**Lamivudine**
Kakamega Hospital	0.42±0.05	0.61±0.08	0.12±0.02	0.59±0.06	0.07±0.01	0.10±0.02	<0.05±0.02
Shirere Domestic	0.08±0.02	0.13±0.05	0.08±0.03	<0.05±0.02	<0.05±0.02	0.14±0.03	0.07±0.02
Nabongo WWTP	<0.05±0.02	0.06±0.01	<0.05±0.02	0.07±0.01	<0.05±0.02	<0.05±0.02	0.02±0.01
MMUST WWTP	0.06±0.01	0.07±0.02	0.06±0.01	<0.05±0.02	<0.05±0.02	0.09±0.02	0.07±0.03
Mumias Hospital	0.09±0.3	0.16±0.05	0.06±0.01	0.07±0.01	0.07±0.01	0.14±0.01	0.10±0.06
Bungoma Hospital	0.54±0.02	0.17±0.01	0.07±0.02	<0.05±0.02	0.08±0.02	0.14±0.04	0.19±0.04
Bungoma WWTP	0.08±0.02	0.35±0.06	0.07±0.02	0.08±0.03	0.06±0.01	0.07±0.02	0.16±0.05
Homabay WWTP	<0.05±0.02	0.07±0.03	<0.05±0.02	<0.05±0.02	0.06±0.01	<0.05±0.02	0.12±0.02
Busia WWTP	0.07±0.02	0.08±0.03	<0.05±0.02	<0.05±0.02	<0.05±0.02	<0.05±0.02	0.08±0.03
Kisat WWTP	0.02±0.01	0.20±0.02	0.07±0.02	<0.05±0.02	<0.05±0.02	0.06±0.02	<0.05±0.02
Nyalenda WWTP	0.07±0.03	0.36±0.04	0.07±0.02	<0.05±0.02	<0.05±0.02	0.07±0.02	0.06±0.01
Kisii WWTP	0.10±0.06	0.12±0.05	<0.05±0.02	<0.05±0.02	<0.05±0.02	0.11±0.02	0.06±0.01
Eldoret Hospital	0.19±0.04	0.79±0.07	0.08±0.03	0.06±0.01	0.08±0.02	0.08±0.03	0.07±0.02
Eldoret WWTP	0.16±0.05	0.34±0.08	0.06±0.01	<0.05±0.02	<0.05±0.02	0.08±0.03	0.07±0.02

Limit of quantification, LOQ=0.05±2 µg/L, n=3

The mean concentrations of PHCs in water from rivers and streams within the region ranged from <0.05±0.02 to 0.29±0.02 µg/L (Table 4.4). Although the PHC residues were lower in rivers and streams compared to WWTPs, they may pose long term effects on aquatic ecosystem. The presence of higher levels of pharmaceutical residues downstream of the WWTPs indicate the transfer of these compounds from WWTP effluents to rivers (Table 4.4). During sampling, it was observed that effluents from these WWTPs are discharged directly into rivers and streams which discharge into the Lake Vitoria (Kimosop *et al.*, 2016). This poses great health concerns due to the possible ecotoxicological effects of these compounds on aquatic ecosystem and human health (Matozzo, 2014).

Table 4.4: Concentration of PHCs in water samples (µg/L) from streams and rivers within Lake Victoria Basin, Kenya

Study site	**DCF**	**AMP**	**CBZ**	**SMX**	**CAP**
MMUST river (U.S)	<0.05±0.02	0.05±0.04	<0.05±0.02	<0.05±0.02	<0.05±0.02
MMUST river (D.S)	0.06±0.02	0.07±0.05	0.05±0.03	<0.05±0.02	<0.05±0.02
Kisat river (U.S)	<0.05±0.02	0.13±0.07	<0.05±0.02	<0.05±0.02	0.05±0.02
Kisat river (D.S)	0.06±0.05	0.17±0.06	0.06±0.01	<0.05±0.02	0.06±0.08
Auji River	0.05±0.02	0.29±0.02	0.05±0.01	<0.05±0.02	0.06±0.02
Sosiani river (U.S)	0.10±0.04	0.09±0.07	<0.05±0.02	<0.05±0.02	0.05±0.02
Sosiani river (D.S)	0.12±0.07	0.24±0.06	<0.05±0.02	<0.05±0.02	0.05±0.02

U.S- Upstream, D.S- Downstream, limit of quantification, LOQ=0.05±0.02µg/L, n=3, DCF-Diclofenc, AMP-Ampicillin, CBZ-Carbamazepine, SMX- Sulfamethoxazole, CAP-Chloramphenicol

4.5 Discharge loads of selected pharmaceuticals from WWTPs

The daily discharge loads of selected PHCs from WWTPs was estimated based on the assumption that the concentration of selected pharmaceuticals in wastewater and sludge recorded were constant throughout the day (Chirikona *et al.,* 2015). This was done using Eq.1 below;

$$Dd = C_w * C_{WWTP} * 1000 * 10^{-3} (mg\ day^{-1}) \quad \text{Eq. 1}$$

Where;

Dd = daily discharge of selected pharmaceuticals (mg day^{-1}),

C_w = concentration of individual PHC in wastewater (µg L^{-1}) (obtained from Table 4.2),

C_{WWTP} = capacity of WWTP ($M^3 day^{-1}$) (obtained from Table 3.1),

1000 = conversion factor from cubic meters to litres,

10^{-3} = conversion from nanogram to milligram

Selected pharmaceuticals discharge loads from the various WWTPs are shown in Table 4.5. The discharge loads were calculated only for WWTPs whose daily capacities are known. An estimated total amount of selected pharmaceuticals discharged from the nine WWTPs was calculated using Eq. 2

$$Dd_{Total} = \sum Dd_{WWTPs} \quad \text{Eq. 2}$$

Where;

Dd_{Total} = Total amount of the five selected pharmaceuticals discharged from the nine WWTPs studied, $\sum Dd_{WWTPs}$ = sum of the daily discharge loads of selected pharmaceuticals in the WWTPs (mg day^{-1}).

Table 4.5: Daily discharge loads (Dd) of selected pharmaceuticals (mgL^{-1}) from WWTPs within LVB, Kenya

Study Site (WWTP)	Diclofenac	Ampicillin	Carbamazepine	Sulfamethoxazole	Chloramphenicol	Aspirin	Lamivudine	∑Dd
Kakamega	64.1±0.6	104.6±0.2	64.0±0.5	Nd	nd	nd	nd	**232.7±0.5**
MMUST	25.0±0.5	29.7±0.3	26.1±0.2	Nd	nd	nd	42.5±0.4	**123.3±0.3**
Bungoma	120.1±0.2	525.2±0.7	105.0±0.4	120.4±0.9	90.1±0.4	120.1±0.2	nd	**1080.7±0.7**
Homabay	Nd	50.4±0.6	nd	Nd	43.2±0.3	nd	96.3±0.4	**189.9±0.1**
Busia	42.3±0.1	48.4±0.2	nd	Nd	nd	nd	64.2	**154.9±0.2**
Kisat	49.0±0.5	490.1±0.9	171.5±0.3	Nd	nd	nd	25.5	**736.1±0.7**
Nyalenda	423.5±0.3	2178.0±0.1	423.5±0.4	Nd	nd	nd	105.0	**3130.0±0.7**
Kisii	140.4±0.1	168.1±0.5	Nd	Nd	nd	nd	nd	**308.5±0.4**
Eldoret	256.6±0.3	544.3±0.7	96.2±0.4	Nd	nd	27.2±0.2	120.6±0.4	**1042.5±0.5**
							Total daily discharge	**7001.6±0.6**

nd-not determined

The daily discharge loads from the nine WWTPs ranged between 123.3±0.3 mg/L day^{-1} to 3130.0±0.7 mg/L day^{-1} (Table 4.5). Nyalenda WWTP in Kisumu recorded the highest amounts of PHCs discharge of 3130 mg/L day^{-1}. This could be attributed to the high population in Kisumu city which is the largest among the other towns studied (Table 3.1). The total Discharge loads from the nine WWTPs was 7001.6±0.6 mg/L day^{-1}.

4.6 Comparison of results with data from other parts of the world

Results from this study were compared with data from other countries worldwide. The concentrations of selected pharmaceuticals obtained in effluents from WWTPs in this study ranged between <0.05 to 0.36±0.04 µg/L. Hospital effluents recorded levels ranging from <0.05 to 0.79±0.07 µg/L. These results are comparable to results from other studies elsewhere. A study by Li and Zhang, (2011) reported selected pharmacueticals ranging from 0.01 to 0.233 µg/L in WWTPs in China. Another study by Giger *et al.*, (2003) reported individual antibiotic levels ranging from 0.057 to 0.330 µg/L. However, a study by Kihampa, (2014) recorded higher levels of up to 37 µg/L in WWTP effluent from Dar es Salaam City in Tanzania. This may be attributed to the high population in the capital city of Tanzania (Kihampa, 2014). PHCs residues in sludge samples from WWTPs in the present study ranged between <50 to 154±9 ng/g. Sludge from hospital lagoons recorded PHCs residues between <50 to 276±12 ng/g. Similar levels ranging between 299- 455 ng/g were detected in sludge samples from Spain (Radjenović *et al.*, 2009).

The daily discharge loads of selected pharmaceuticals from the nine WWTPs studied ranged between 123.3 mg day^{-1} to 3130 mg day^{-1} which are comparable to other data elsewhere. For example; results obtained from China had daily discharge loads between 3000-5200 mg/L/day for each WWTP (Li and Zhang, 2011), while in Michigan (USA) 4800 mg/L day^{-1} was reported (Nakata *et al.*, 2005). The difference in discharge loads is largely dependent on

the capacity of WWTP, population served and the method of treatment employed (Li and Zhang, 2011).

4.7 Dissipation of Selected pharmaceuticals in WWTPs within LVB

The results from dissipation studies showed the average loss for the selected pharmaceuticals ranging between 19.47±0.84 % for SMX and 54.29±0.63 % for CAP, respectively (Table 4.6). This indicates the inefficiency of WWTPs in removal of PHCs in wastewater. For individual treatment plants, Bungoma WWTP was the most inefficient in removal of PHCs with a mean of 18.74±0.59 % for the seven PHCs while Nabongo WWTP in Kakamega recorded the highest removal efficiency of 62.89±0.94 %. It was noted during sampling that the Nabongo WWTP was invested by plants such as water hyacinth and could have contributed to the high removal efficiencies. Carbamazepine was among the lowest removed compounds from the WWTPs (26.73±1.02 %), hence it was chosen as a model compound for remediation studies through adsorption processes.

Table 4.6: The percent dissipation of the selected pharmaceuticals in ten WWTPs within LVB, Kenya.

PHCs	Percent Dissipation										
	Eldoret	Bungoma	Busia	Kakamega			Kisumu		Homabay	Kisii	Mean
				Shirere	Nabongo	MMUST	Nyalenda	Kisat			
AMP	42.74±0.35	24.57±0.65	55.56±1.05	27.69±0.37	57.45±2.05	36.36±0.47	18.92±2.01	49.40±0.94	53.57±0.69	37.5±2.01	**36.73±1.02**
LMV	58.43±0.40	5.47±0.23	73.08±2.17	35.31±0.45	83.33±0.66	13.29±0.71	84.74±1.03	nd	68.08±0.78	66.67±0.86	**45.97±0.56**
SMX	Nd	Nd	Nd	Nd	16.00±0.59	nd	nd	25.34±0.44	nd	16.67±1.05	**19.47±0.84**
ASA	16.67±0.18	72.62±0.45	Nd	49.97±1.34	13.29±0.71	35.31±0.45	25.34±0.44	nd	32.43±0.37	nd	**29.34±0.44**
DCF	24.62±1.05	25.39±0.52	50.00±1.00	69.83±1.10	81.25±1.02	nd	72.62±0.45	30.84±0.95	49.97±1.34	62.5±2.10	**45.89±0.92**
CBZ	7.83±0.86	50.00±0.98	25.34±0.44	16.67±0.56	36.67±1.05	17.77±0.95	nd	41.12±0.86	30.00±0.59	17.77±0.95	**26.73±1.02**
CAP	Nd	20.48±0.55	Nd	Nd	32.43±0.37	18.92±2.01	nd	41.00±0.84	60.14±0.89	60±0.45	**54.29±0.63**
Mean	**49.72±0.78**	**18.74±0.59**	**60.49±1.51**	**61.77±0.61**	**62.89±0.94**	**24.83±0.82**	**58.59±0.99**	**37.56±0.71**	**60.48±0.88**	**58.67±1.11**	**36.92±0.78**

Nd-not determined

4.8 Adsorbent Characterization

Characterization was carried out in order to understand the properties of the iron-modified adsorbent composites. This was done using various techniques such as X-ray fluorescence (XRF) technique, scanning electron microscopy (SEM), X-ray diffraction (XRD) method Fourier Transform Infra-red (FTIR) spectroscopy, Brunauer Emmet and Teller (BET) surface area and magnetic measurement.

4.8.1 Elemental Composition by XRF

The elemental composition of the unmodified diatomaceous earth (DTE), carbonized bagasse (CBG) and maize cob (CMC) and the iron-modified adsorbents obtained from XRF indicate successful impregnation of iron into the adsorbents (Table 4.7). Elemental analysis showed that iron modification drastically increased the adsorbents' iron content from 53 to 73 % in maize cob biochar (CMC), 18 to 78 % in carbonized bagasse (CBG) and 15 to 71 % in diatomaceous earth (DTE) (Appendices 10-21). Of the untreated materials, DTE had the least iron content. The percentage increase in iron content after treatment was in the order CBG>DTE>CMC which is consistent with literature (Wu *et al*., 2014). There was also increase in chloride content in iron modified CMC from 19.43 to 22.00 % while chloride was introduced in the iron modified bagasse (19.20 %). This may have resulted from iron exchange during impregnation of the adsorbents with ferric chloride salt solution. Furthermore, the percentage potassium in all the iron modified composites was lower than the pristine adsorbents. A similar trend was also observed for calcium and silicon (Table 4.7). The relative variation of the percent content of certain elements after chemical treatment suggests that iron inclusion possibly involved cation

exchange or iron was precipitated on the biochar surface thus replacing or shielding other elements previously observed or not observed (Shikuku *et al.*, 2015).

Table 4.7: Elemental Composition of the three adsorbents and their iron modified composites.

Adsorbent	**Percent composition (mass %)**								
	Fe	**K**	**Ca**	**Cl**	**Si**	**Mn**	**Ti**	**Zn**	**Cu**
DTE	15.27	3.20	6.74	Nd	73.45	nd	1.34	nd	nd
α-Fe_2O_3-DTE	71.11	1.42	0.76	Nd	26.44	0.28	nd	nd	nd
CBG	18.53	29.52	37.52	Nd	5.29	5.50	2.21	0.82	0.62
α-Fe_2O_3-CBG	78.80	0.87	0.71	19.20.	nd	nd	nd	nd	nd
CMC	53.94	26.24	Nd	19.43	nd	nd	nd	0.40	nd
β-FeO(OH)-CMC	74.88	3.13	Nd	22.00	nd	nd	nd	nd	nd

nd- not detected, n=3

4.8.2 SEM analysis

SEM imaging of the unmodified and the iron modified magneto responsive adsorbent composites are illustrated in appendices 22-31. The morphology of the three adsorbents and their respective iron modified composites depicted heterogeneous surfaces with appropriate sites for adsorption of analyte.

4.8.2.1 SEM characteristics of Diatomaceous earth (DTE) and iron modified composite (α-Fe_2O_3-DTE)

SEM micrographs of diatomaceous earth (DTE) and the iron modified sample (α-Fe_2O_3-DTE) are illustrated in Figures 4.4 (a) and (b), showing a significant difference between the microstuctures of the two adsorbents with distinct micropores. The porous structure examination of the precursor DTE can be clearly seen in the SEM photograph (Fig. 4.4(a), revealing the variety of rigid shapes and open voids that give the diatomaceous earths a high ability to trap pollutant residues for separation from aqueous media (Yu *et al.,* 2015). The centric type frustules characterized by honeycomb structure was also reported by Knoerr *et al.* (2013). Chemical modification of DTE resulted in flaws and small iron oxide particle deposits as shown in Figure 4.4 (b). These iron oxide particles would possibly create more active sites for adsorption of pollutants.

Figure 4.4 (a): SEM micrograph of unmodified diatomaceous earth (DTE)

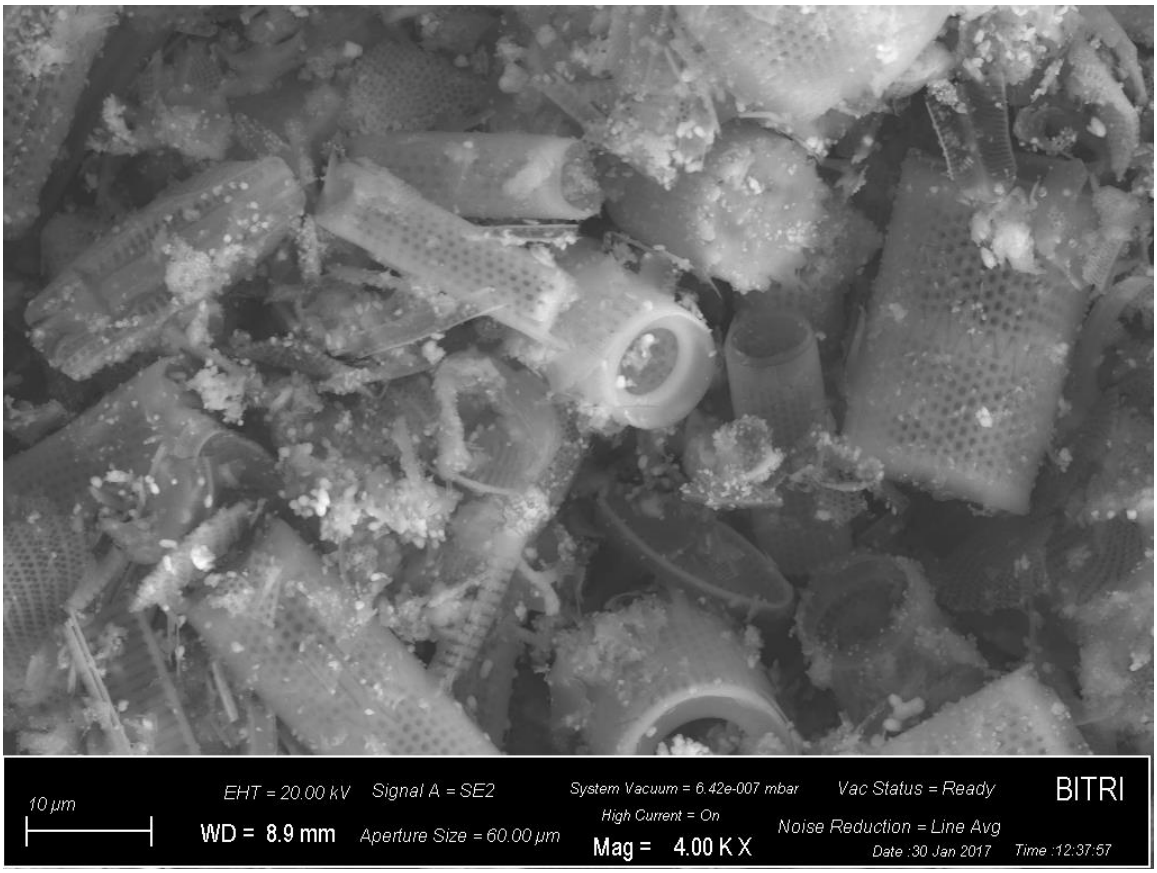

Figure 4.4 (b): SEM micrograph iron modified diatomaceous earth (α-Fe_2O_3-DTE)

The heterogeneity of the iron modified DTE adsorbent surfaces was further confirmed by EDAX analysis. Both SEM imaging and EDAX spectra showed extremely high peaks of Si (34.83 wt%), O (48.22 wt%) and Fe (13.13 wt%). The high silicon content is characteristic of diatomite feedstock while chloride and iron was incorporated during impregnation. Other elements present in the magneto responsive α-Fe_2O_3-DTE adsorbent were Cl (1.66 wt%), Al (1.57 Wt%) and K (0.58 wt%) as shown in Figure 4.5. Chloride may have been incorporated during treatment with iron salt while other elements such as aluminium and potassium may have been present in the unmodified diatomaceous earth.

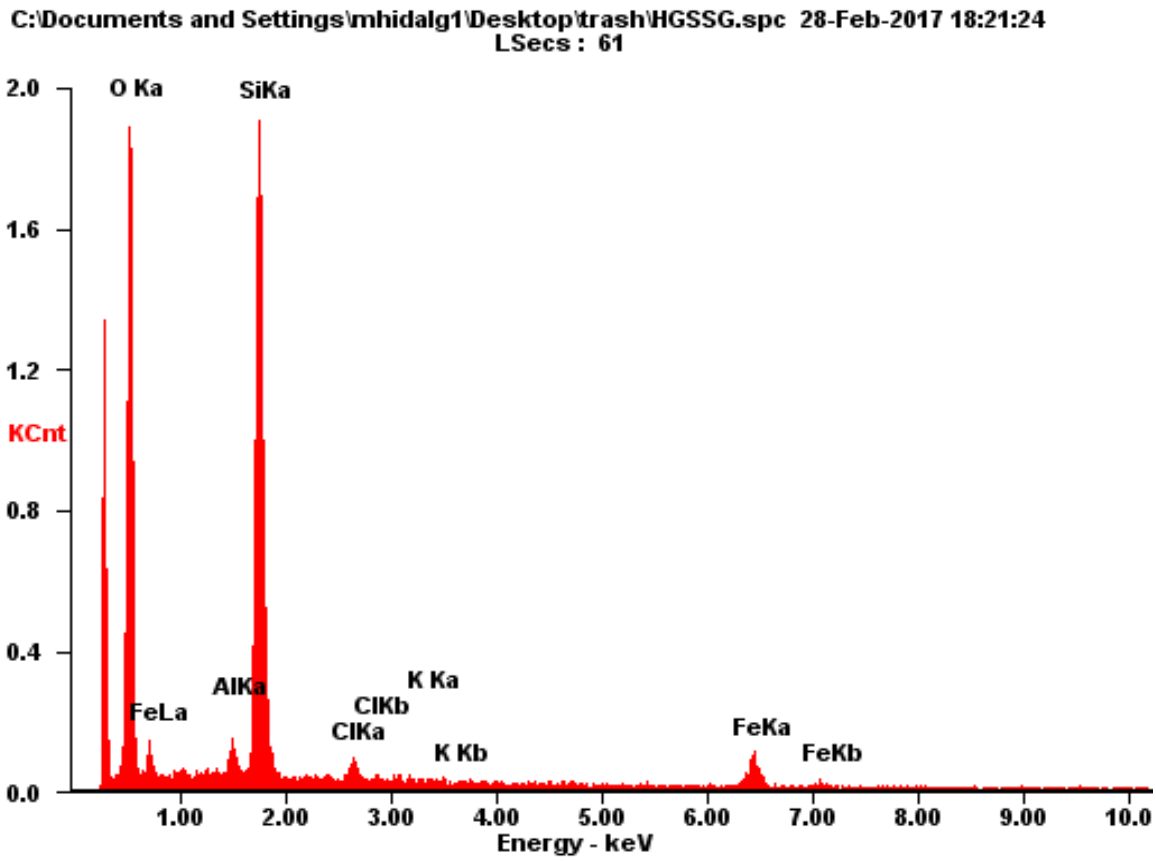

Figure 4.5: SEM-EDAX spectrum showing elemental Composition of the α-Fe_2O_3-DTE obtained from EDAX

The distribution of elements in the iron modified α-Fe_2O_3-DTE composite is presented in Figures 4.6 (a-e). The micrographs a-e represent Fe, O, Al, Si and Cl, respectively showing the major components as oxygen, silicon and iron. The elemental distribution in the composite is consistent with EDAX spectrum (Figure 4.5) and XRF results.

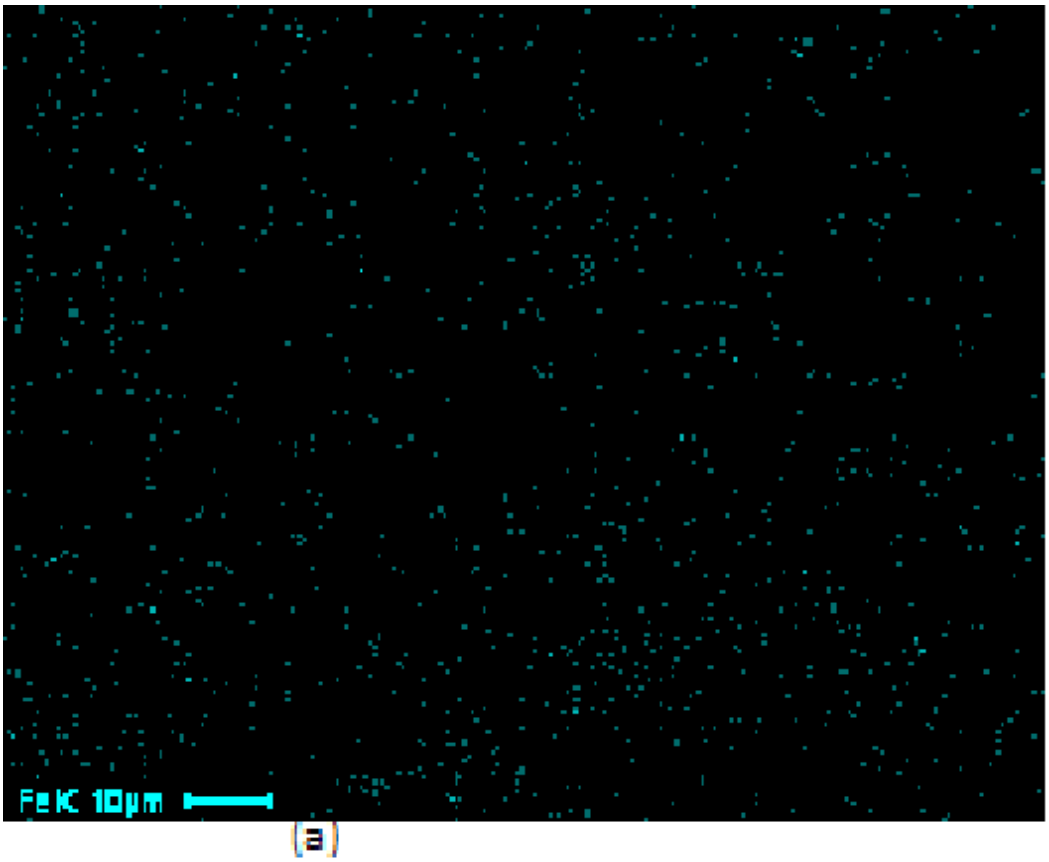

Figure 4.6 (a): The EDAX micrographs showing distribution of iron in the modified magneto responsive adsorbent composite (α-Fe_2O_3-DTE).

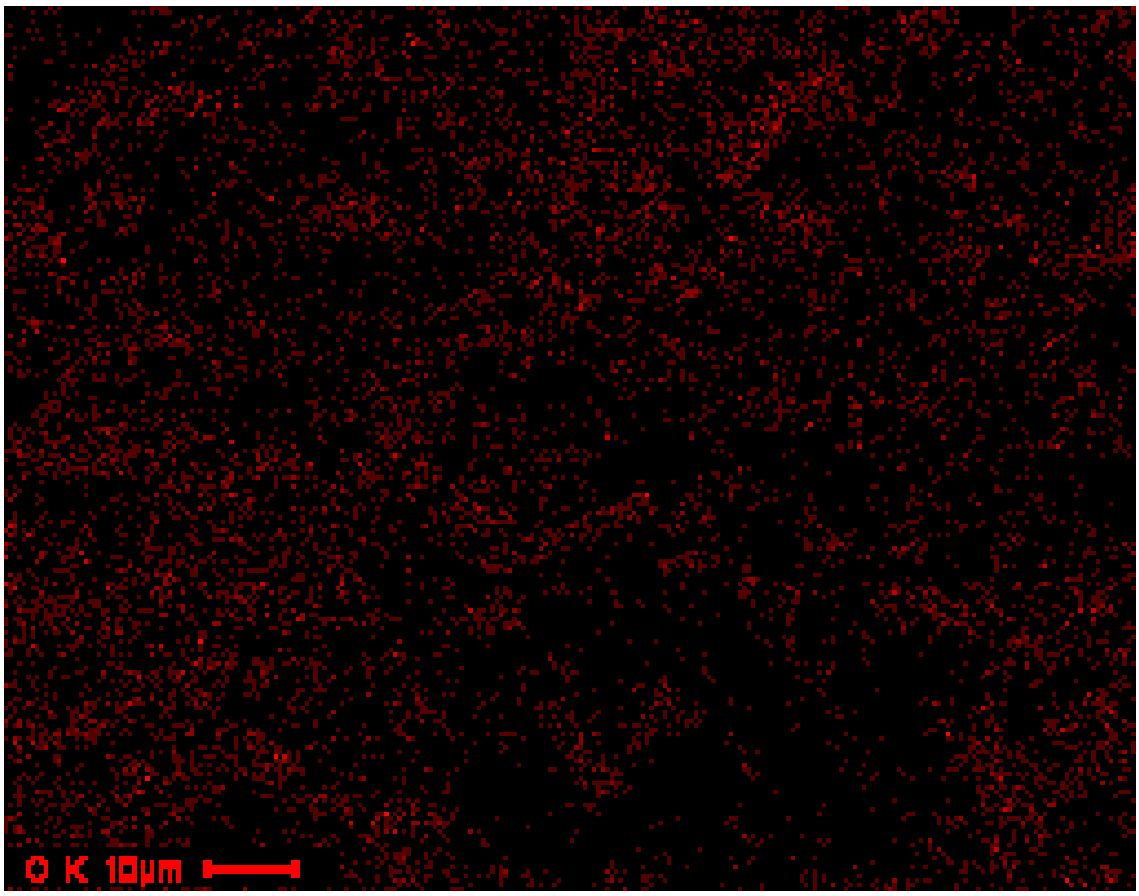

(b)

Figure 4.6 (b): The EDAX micrographs showing distribution of oxygen element in the modified magneto-responsive adsorbent composite (α-Fe_2O_3-DTE).

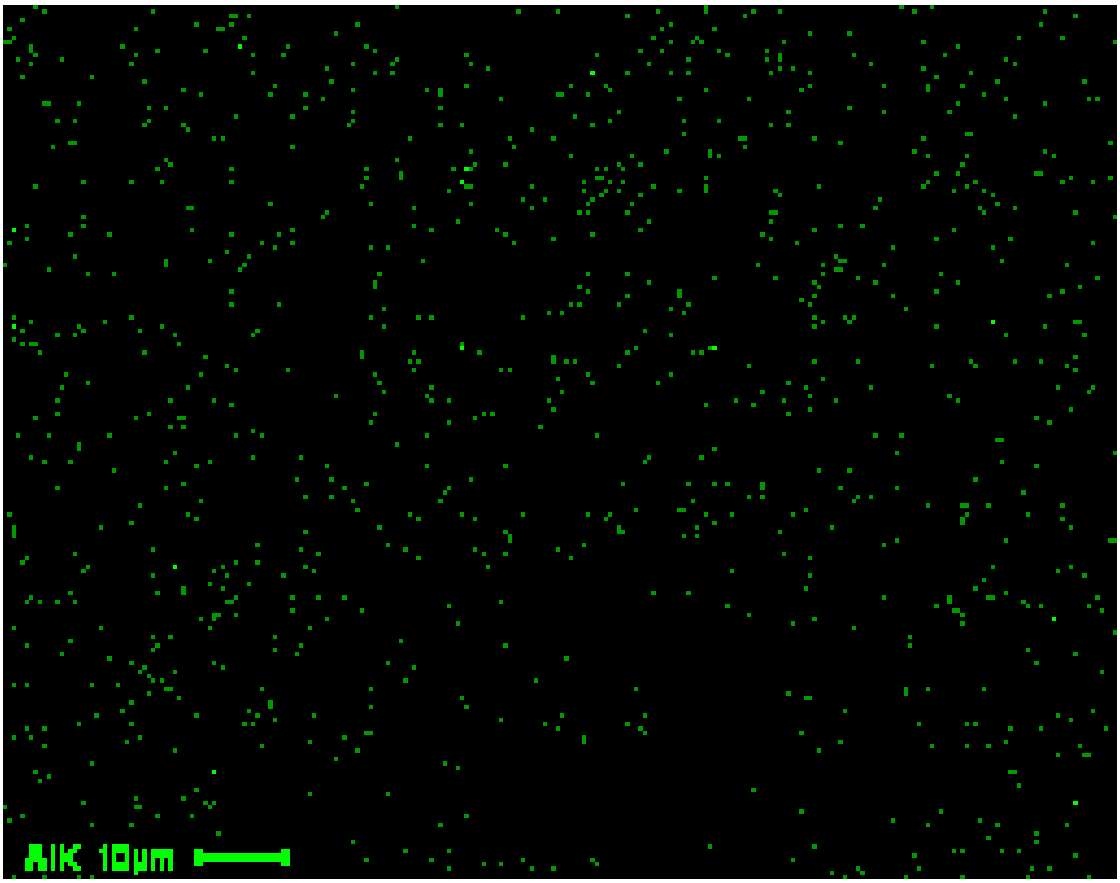

(c)

Figure 4.6 (c): EDAX micrographs showing distribution of aluminium in the modified adsorbent composite (α-Fe_2O_3-DTE).

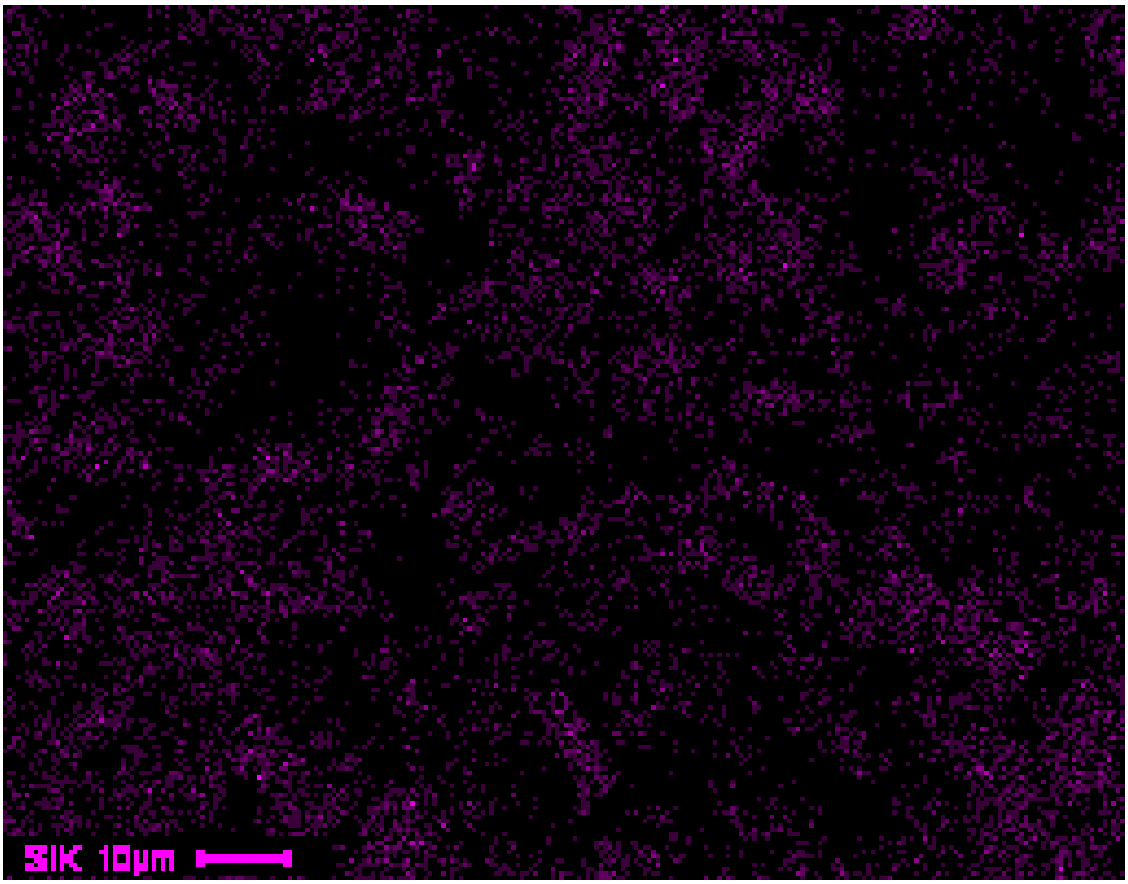

Figure 4.6 (d): EDAX micrographs showing distribution of silicon element in the modified adsorbent composite (α-Fe_2O_3-DTE).

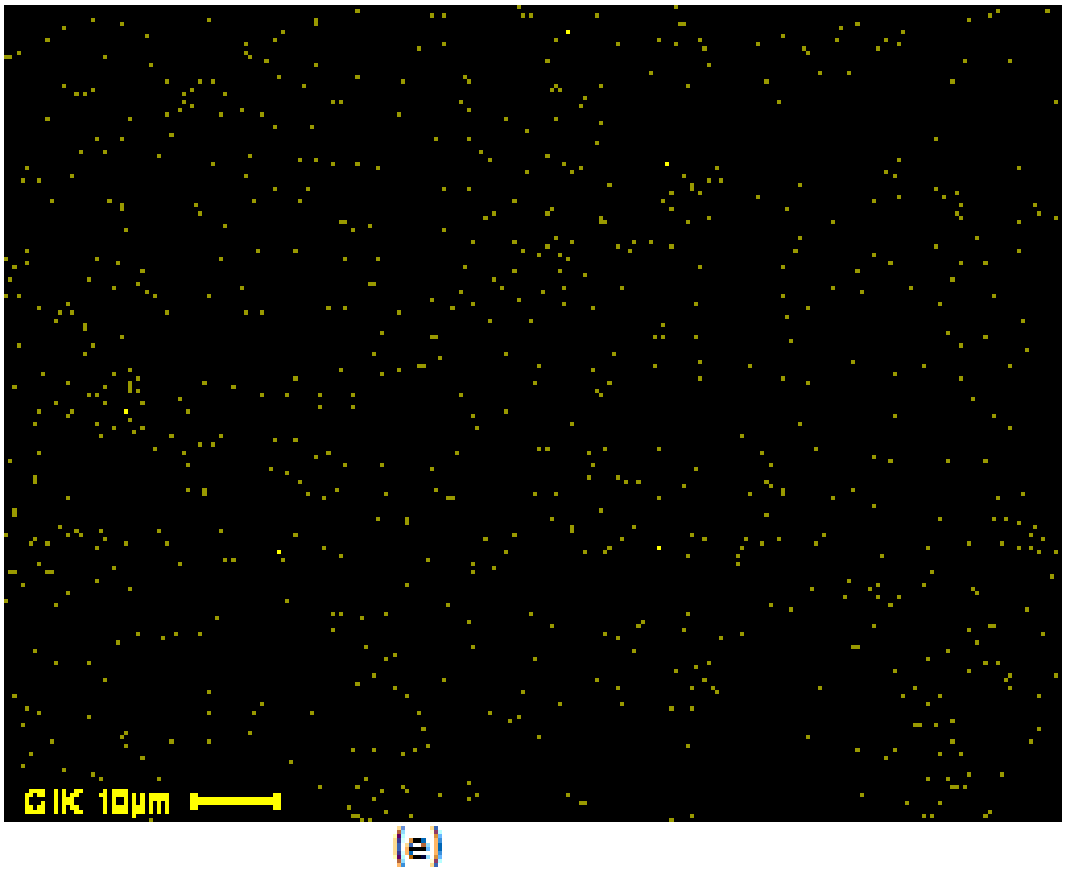

Figure 4.6 (e): The EDAX micrographs showing distribution of chloride in the modified adsorbent composite (α-Fe_2O_3-DTE).

The SEM-EDAX micrographs of iron modified diatomaceous earth indicate the main elements being oxygen, silicon and iron. This is in accordance to other studies elsewhere (Lang, *et al.*, 2017). A study by Knoerr *et al.*, (2013), reported increase in surface area of iron modified DTE due to presence of ferric oxide crystallites. Other phases reported in the diatomite frustules were fibrillar crystals of ferric oxyhydroxides. In this study, iron oxide (α-Fe_2O_3) crystals were the only form of iron present.

4.8.2.2 SEM Micrographs of carbonized maize cobs and the iron modified composite

The SEM micrographs for carbonized maize cob biochar (CMC) and iron modified β-FeO(OH)-CMC (Figures 4.7(a) and (b) showed heterogeneous surfaces, with the modified sample being rough with discontinuities and distinct micro pores (Figure 4.7(b). The layered microstructures contain vacant sites. However, the image of the modified composite shows agglomerates of the iron impregnated on the CMC adsorbent surface.

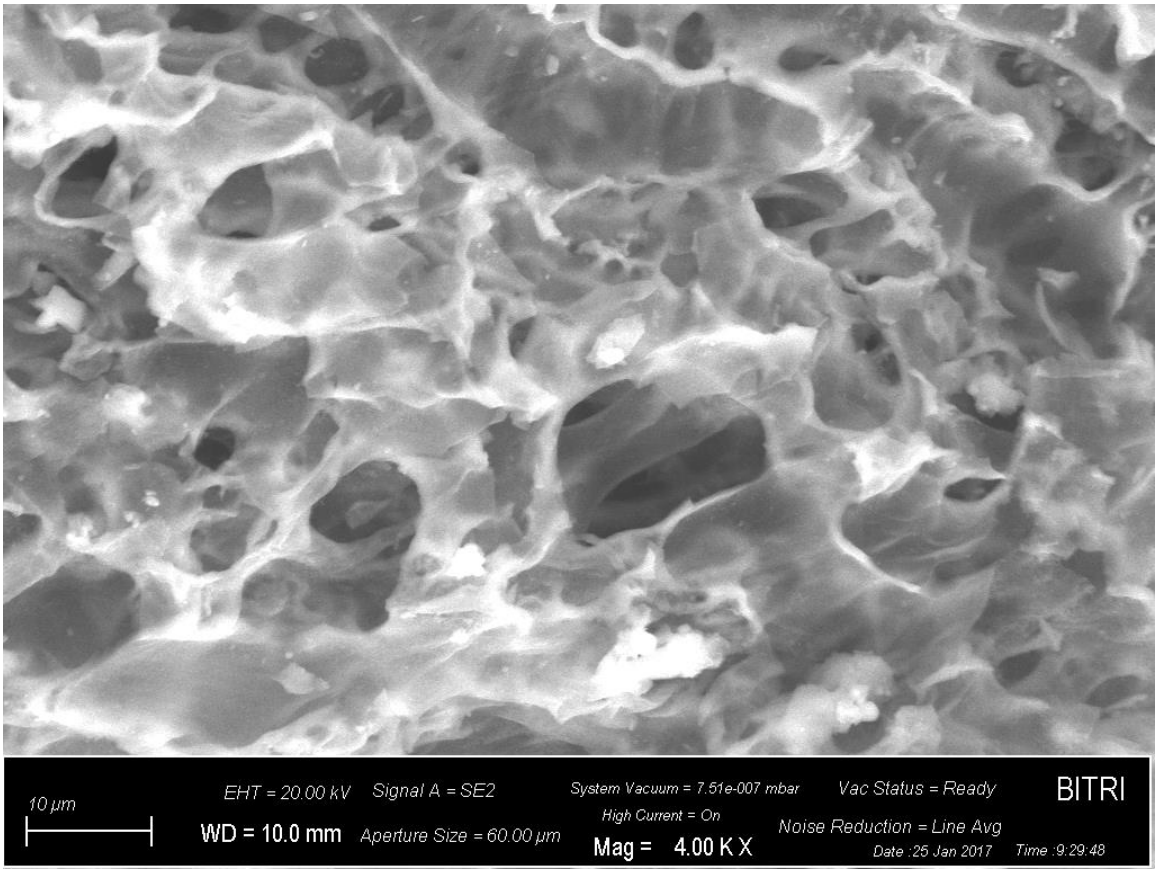

Figure 4.7(a) SEM micrographs of carbonized maize cob biochar (CMC)

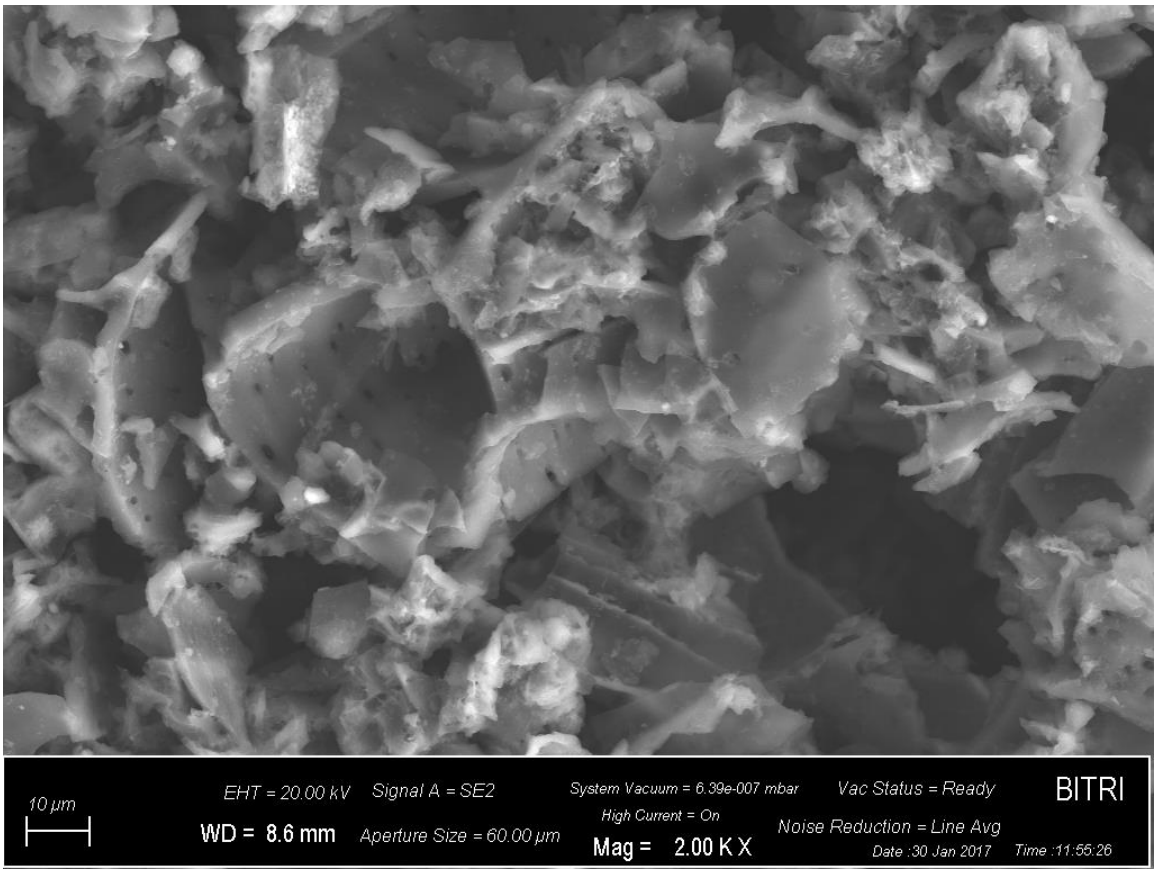

Figure 4.7 (b): SEM micrographs of iron modified carbonized maize cob composite (β-FeO(OH)-CMC).

The SEM–EDAX spectra (Figure 4.8) for β-FeO(OH)-CMC show that there is a high amount of Fe (45.39 %), which is consistent with XRF results (Table 4.6). This suggests that iron was successfully incorporated on the biochar matrix. Other elements present in the composite are O (26.68 %), Cl (23.93 %), Si (2.02 %), K (1.34 %) and Al (0.65 %). The high oxygen percentages may be due to formation of oxides during carbonization, while chloride may have been incorporated during treatment with ferric chloride. The distribution of major elements in the iron modified composite shows similar results as

shown in Figures 4.9 (a-d). The micrographs a-d represents the elements O, Al, Si and Cl, respectively.

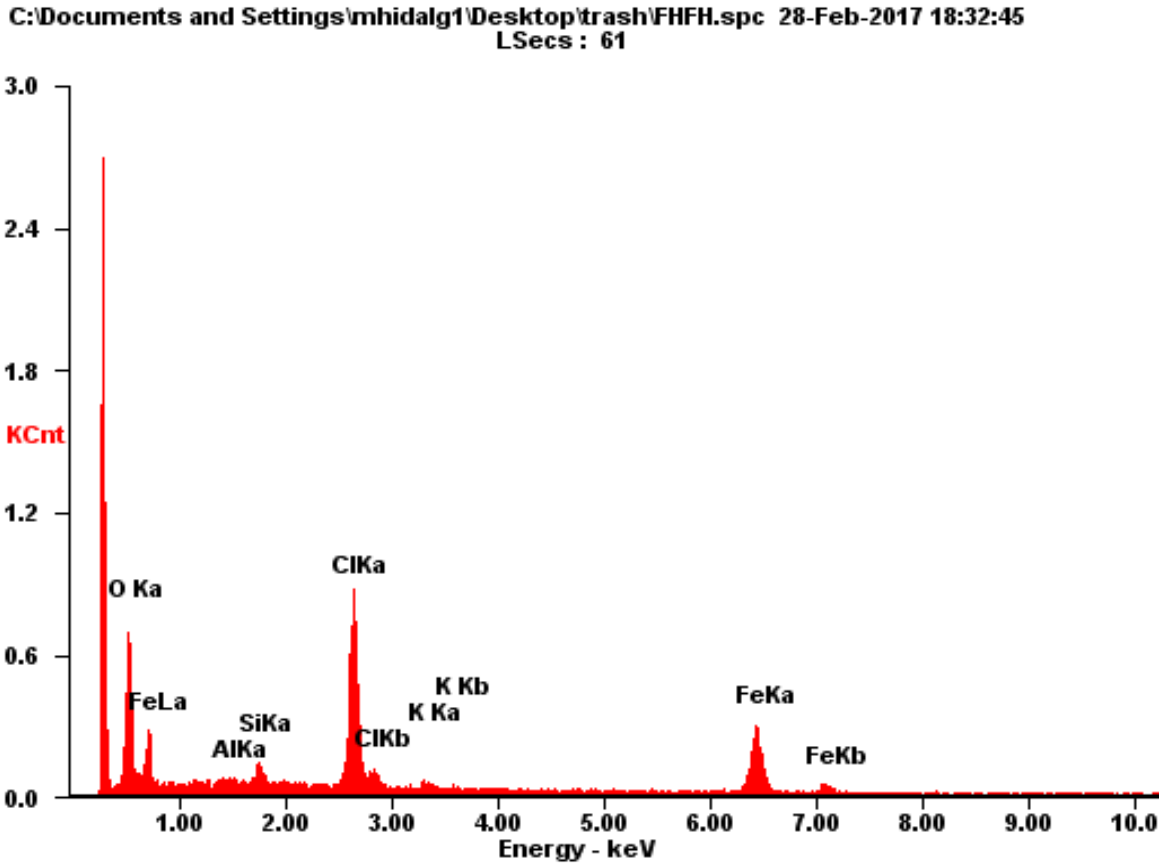

Figure 4.8: Elemental composition of iron modified maize cob biochar (β-FeO(OH)-CMC)

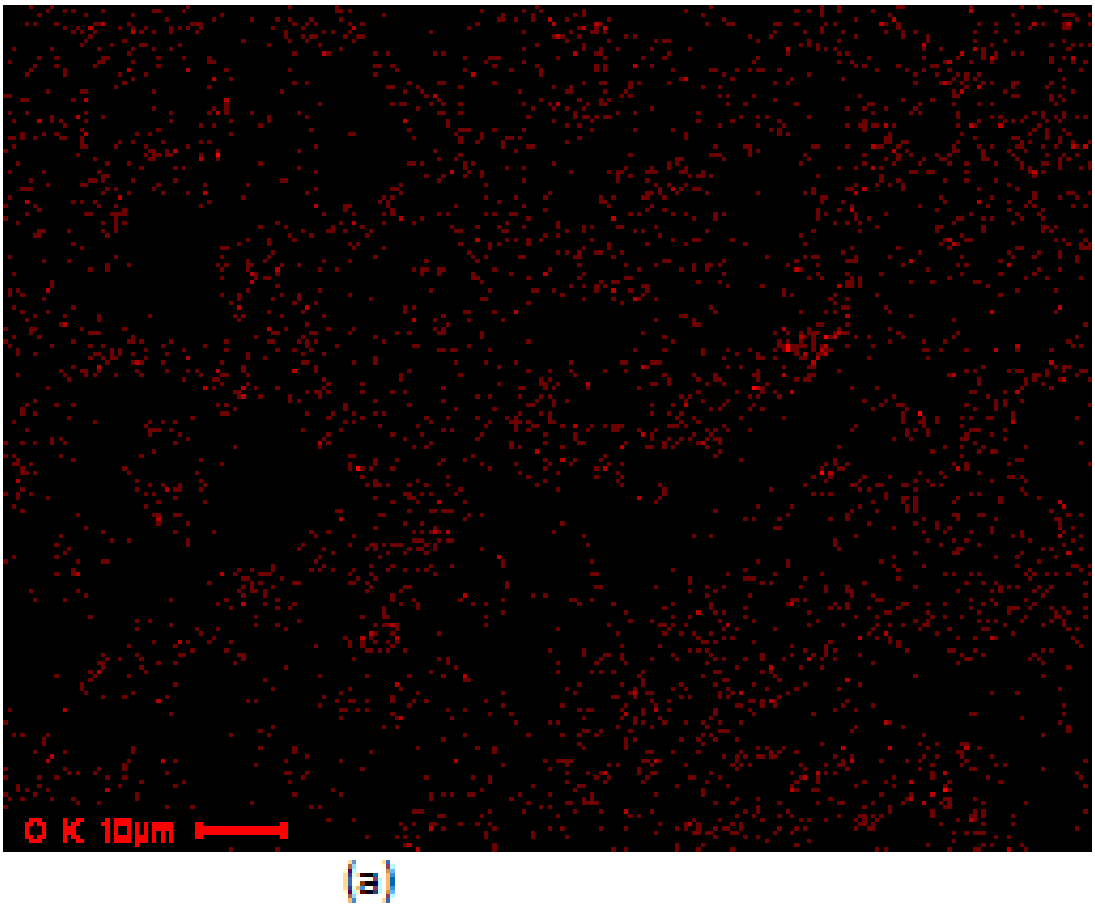

Figure 4.9(a): EDAX micrographs showing distribution of oxygen element in the modified carbonized maize cob adsorbent composite (β-FeO(OH)-CMC).

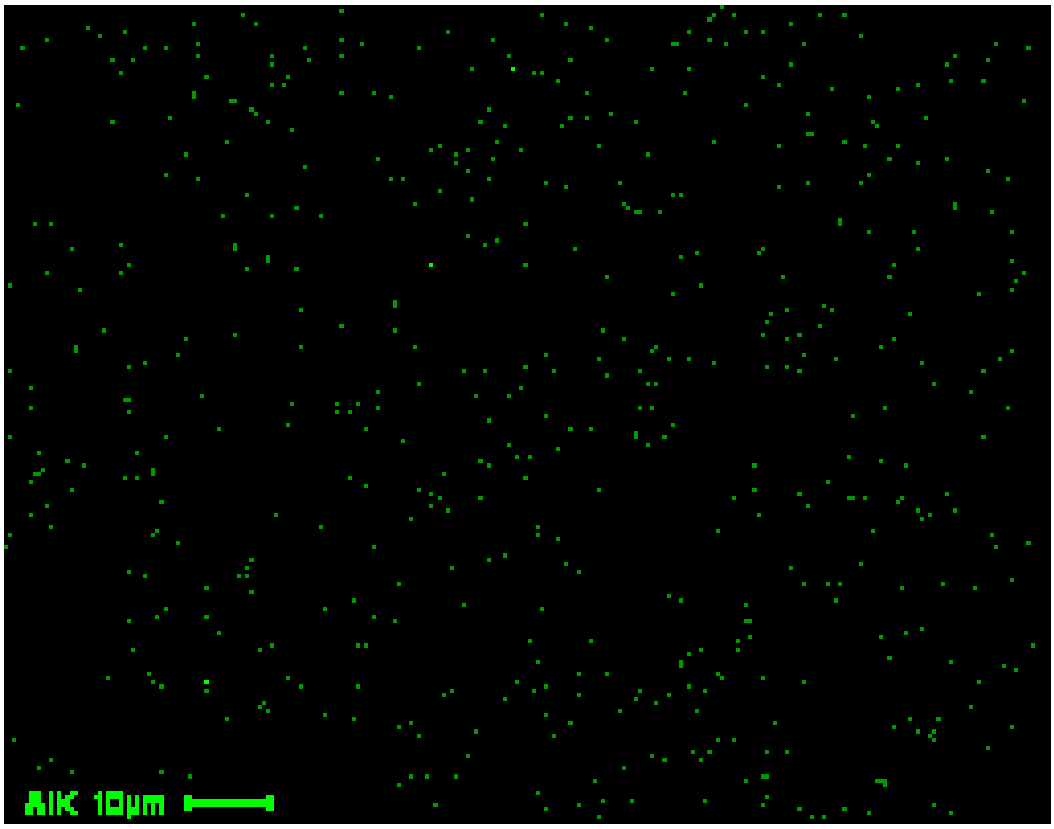

(b)

Figure 4.9(b): EDAX micrographs showing distribution of Al in the modified carbonized maize cob adsorbent composite (β-FeO(OH)-CMC).

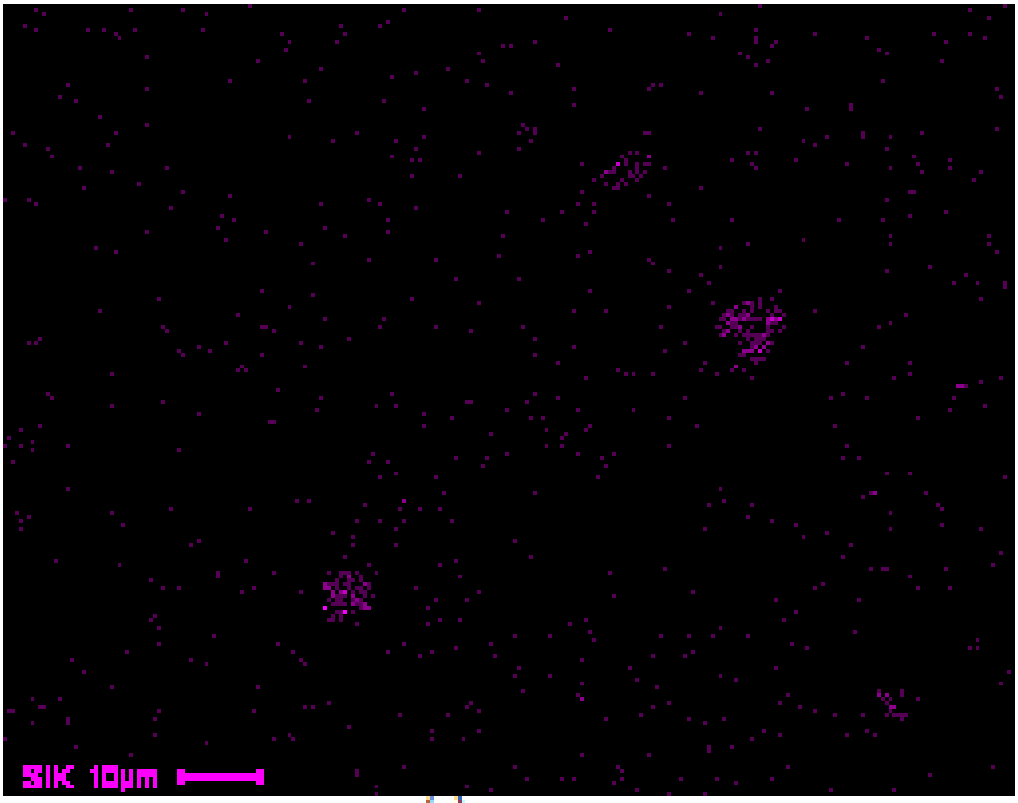

Figure 4.9(c): EDAX micrographs showing distribution of Silicon element in the modified carbonized maize cob adsorbent composite (β-FeO(OH)-CMC).

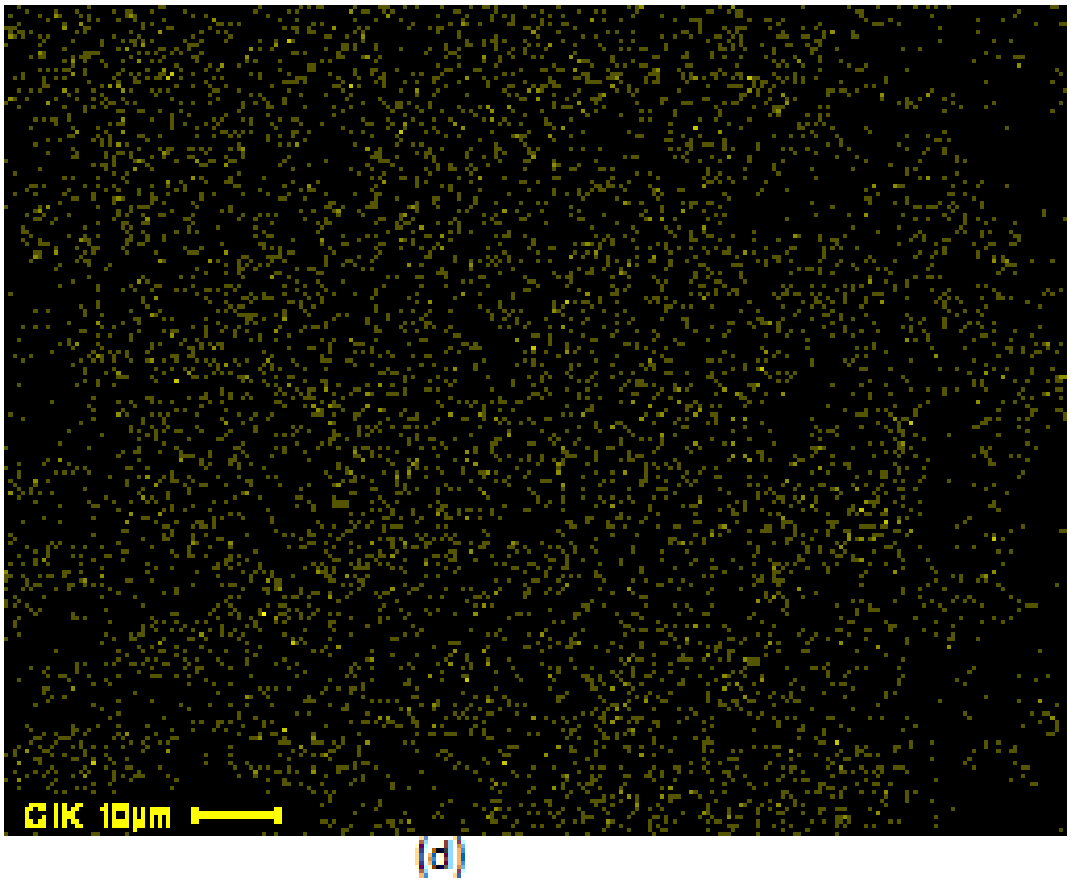

Figure 4.9 (d): EDAX micrographs showing distribution of various elements in the adsorbent composite (β-FeO(OH)-CMC).

4.8.2.3 SEM images of carbonized bagasse biochar (CBG) and the iron modified composite (α-Fe_2O_3-CBG)

The SEM images of carbonized bagasse biochar (CBG) and the iron modified composite (α-Fe_2O_3-CBG) are shown in Figures 4.10 (a) and (b), respectively. Visual inspection of the images illustrates the difference in microstructures of the two adsorbents. The unmodified CBG adsorbent has needle-like microstructure with defined phases (Figure 4.10 (a). The iron modified (α-Fe_2O_3-CBG) composite has a heterogeneous, rough and

fibrillar morphology. It has distinct phases; however, the carbon surface is covered by agglomerates of iron (Fig 4.10 (b). This is consistent with results by Song *et al.,* (2014) who reported agglomeration of iron in modified biochar sample.

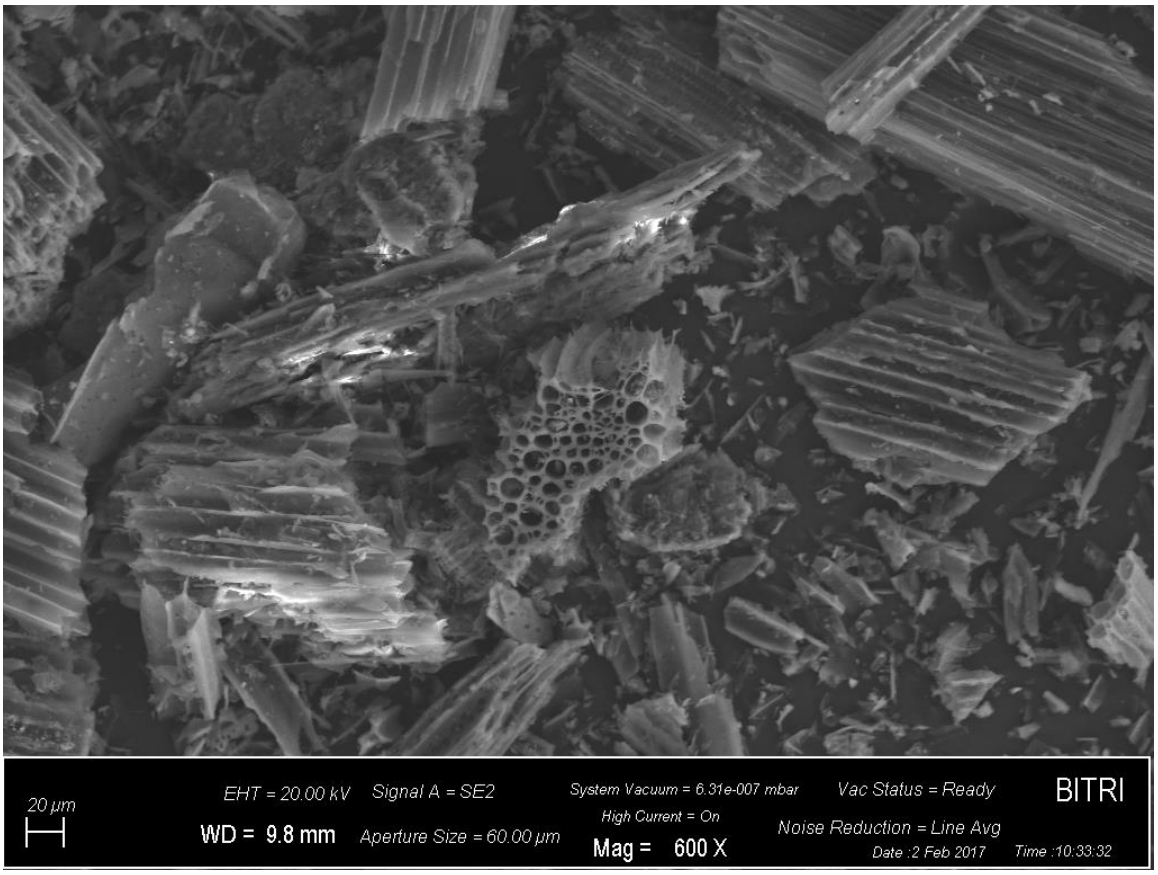

Figure 4.10 (a): SEM micrographs of carbonized bagasse biochar (CBG)

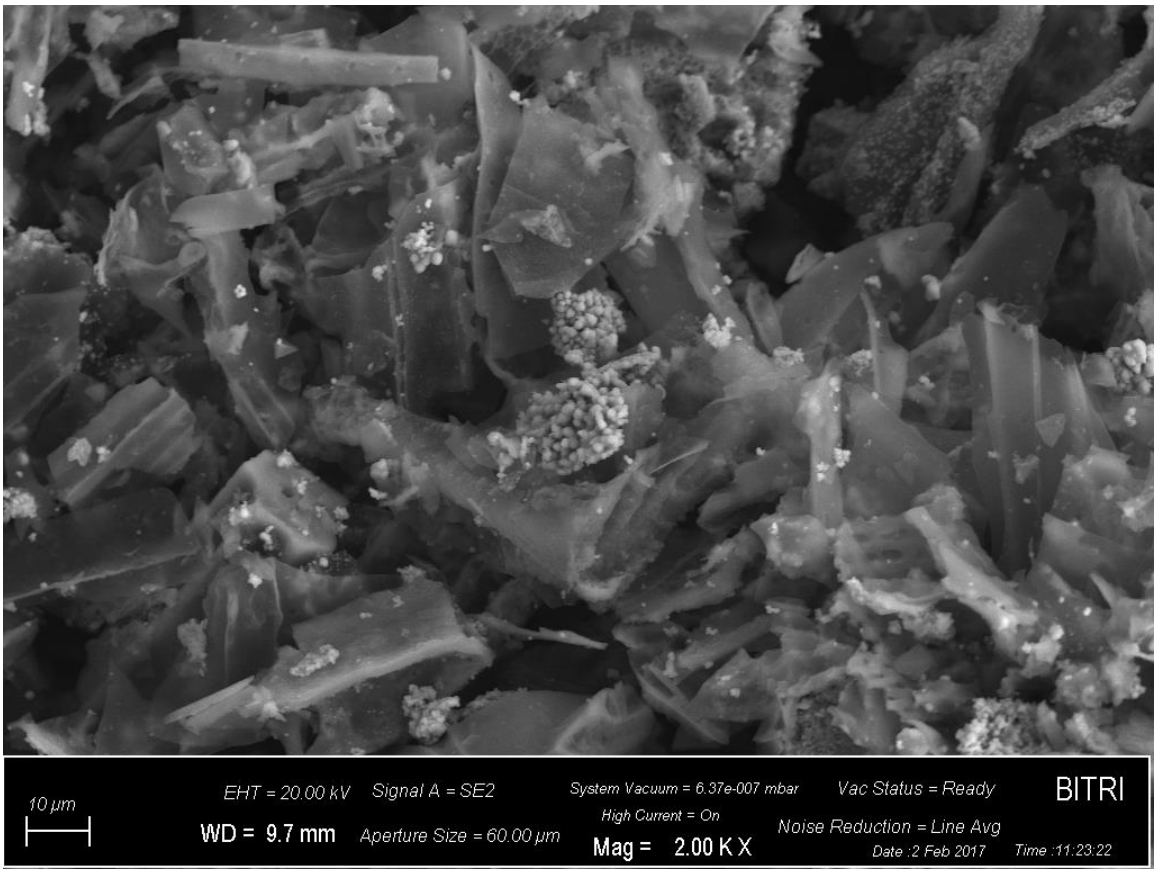

Figure 4.10 (b): SEM micrographs of iron modified bagasse (α-Fe_2O_3-CBG)

SEM-EDAX spectra illustrates the presence of intense peaks of oxygen, chloride and iron as shown in Figure 4.11, which confirms the existence of Fe_2O_3 in the modified composite. The mass percentages for each element were O (15.09 %), Al (0.67 %), Si (1.27 %), Cl (15.16 %), K (0.86 %) and Fe (66.94 %). The distribution of elements in α-Fe_2O_3-CBG is presented in the EDAX micrographs a-d in Figure 4.12. The major elements are Fe, O, Cl and Si as shown in micrographs a-d, respectively. The elevated oxygen levels may be attributed to formation of oxides during carbonization, while iron

and chloride were incorporated during modification with ferric chloride. The other elements such as silicon and aluminium may have been present in the bagasse feedstock.

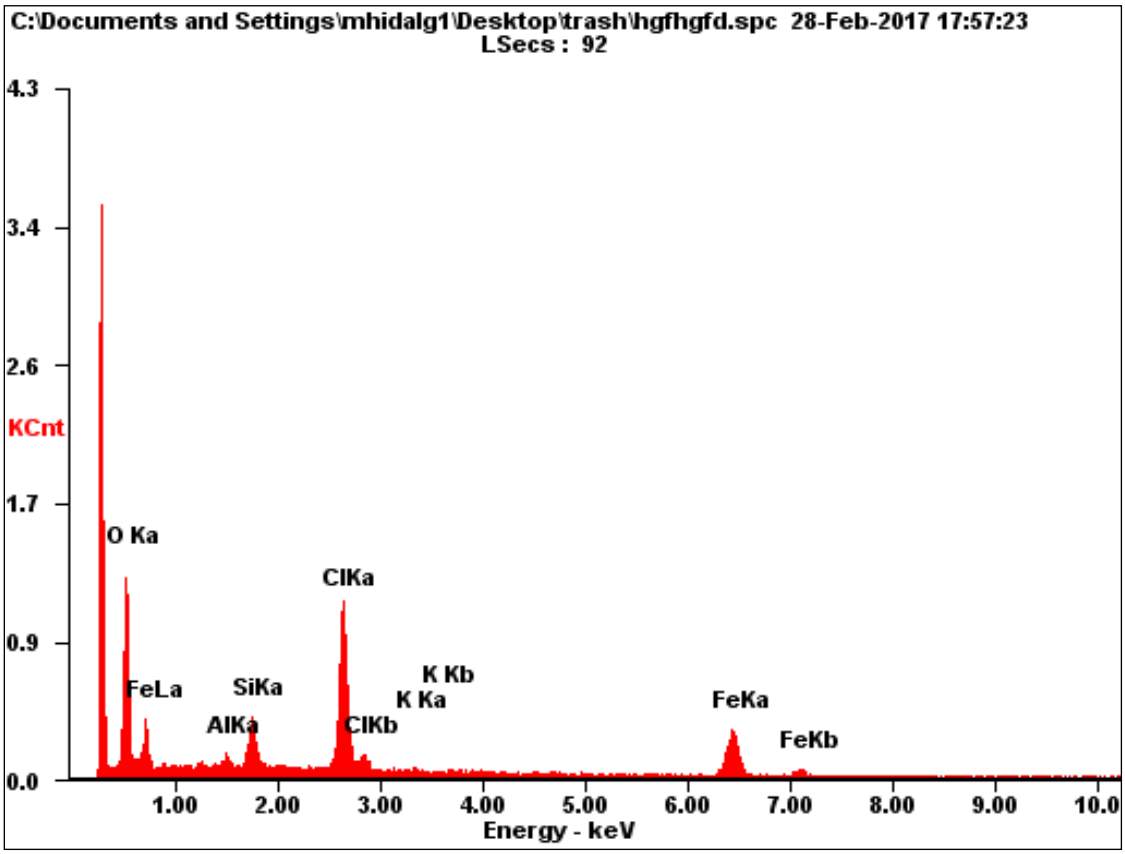

Figure 4.11: Elemental composition of modified carbonized bagasse (α-Fe_2O_3-CBG)

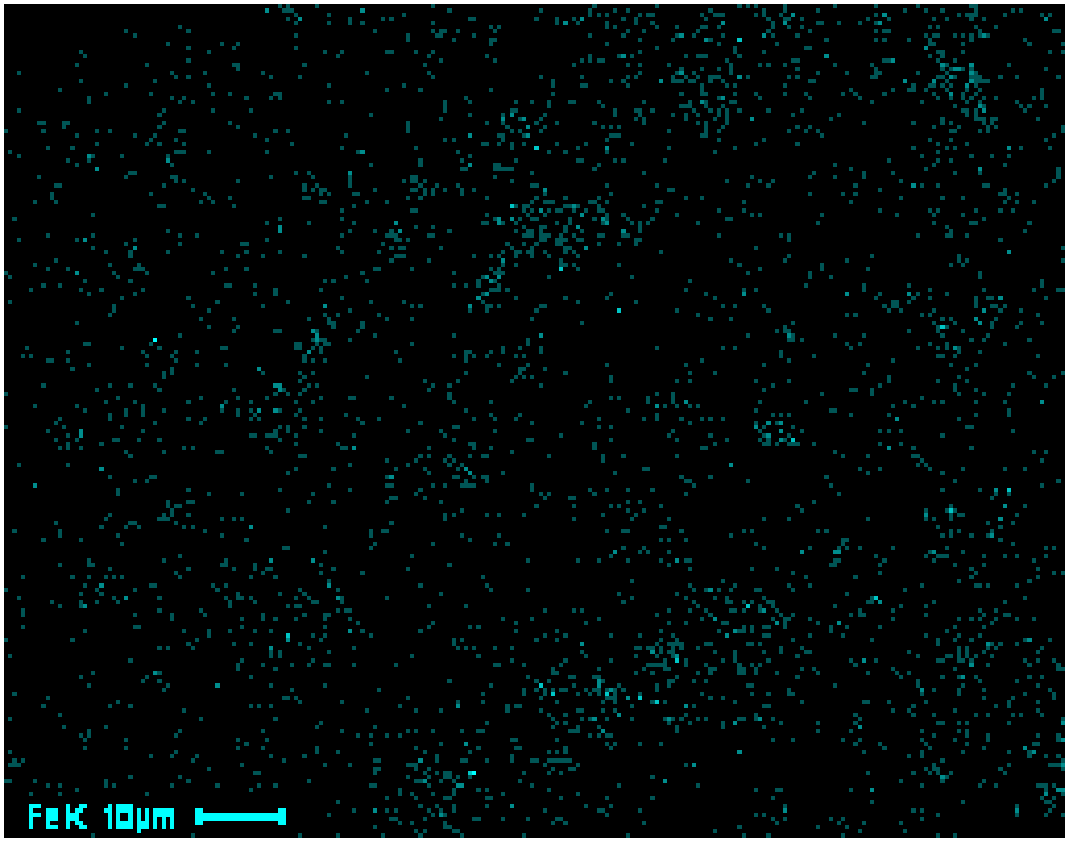

Figure 4.12 (a): The distribution of iron in modified carbonized bagasse (α-Fe_2O_3-CBG).

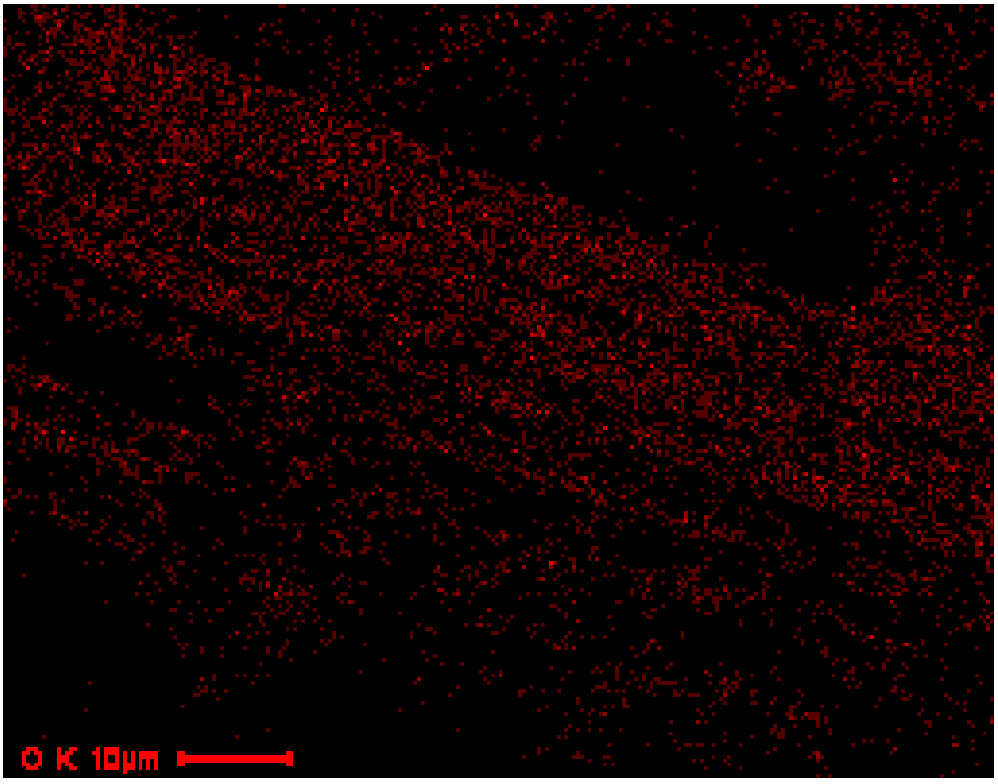

(b)

Figure 4.12 (b): The distribution of oxygen in iron modified carbonized bagasse (α-Fe_2O_3.CBG).

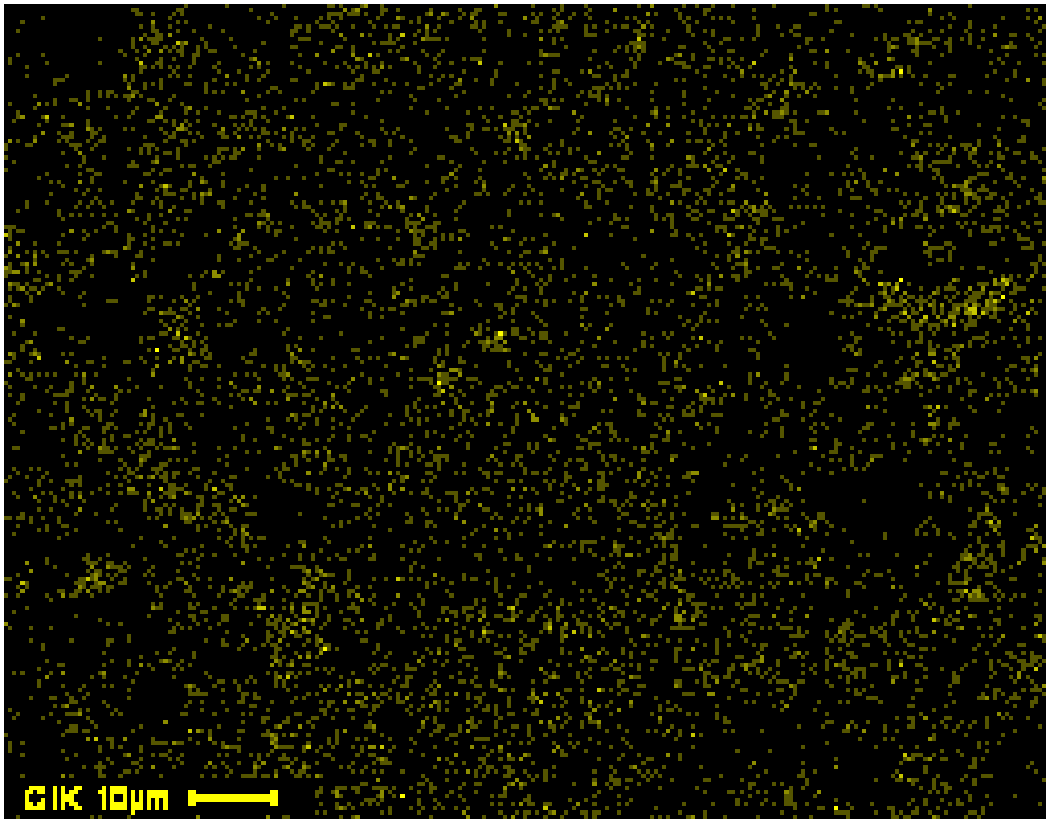

(c)

Figure 4.12 (c): The distribution of chloride in iron modified carbonized bagasse (α-Fe_2O_3-CBG).

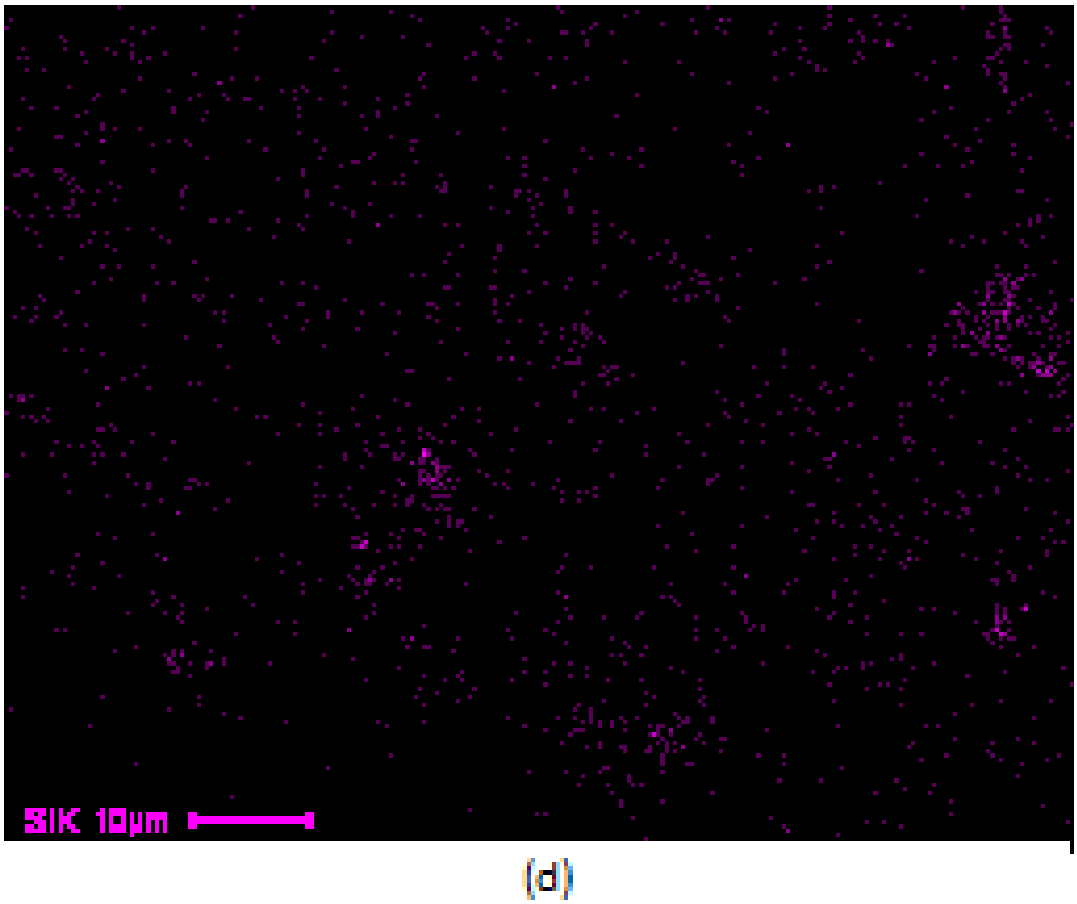

Figure 4.12 (d) The distribution of silicon in iron modified carbonized bagasse (α-Fe_2O_3-CBG)

In a nutshell, there was successful impregnation of iron in the surfaces of the modified DTE, CMC and CBG adsorbents. This is consistent with results reported by Song *et al.,* (2014) where biochar surface was covered by manganese oxide on impregnation with potassium permanganate solution. Similar studies reported successful impregnation of iron oxide onto the surface of biochar derived from paper pulp (Al-Khateeb *et al.*, 2014).

4.8.3 XRD analysis

X-Ray Diffraction is a magnificent tool for distinguishing the different magnetic iron oxides, namely magnetite (Fe_3O_4), maghemite (γ-Fe_2O_3) and haematite (α-Fe_2O_3) (Chaukura *et al*., 2016). Appendices 32-37 shows the XRD patterns of the prepared and chemically engineered magneto-responsive adsorbent composites.

4.8.3.1 The XRD Diffractograms of carbonized baggase biochar (CBG) and iron modified composite (α-Fe_2O_3-CBG)

The XRD spectra for carbonized bagasse biochar (CBG) and its iron modified composite are shown in appendices 32 and 33, respectively. The identification of crystals was based on their d spacing from the Bragg's law (Eq. 3.4). Each peak in the spectrum represents a lattice plane characterized by a miller index. The miller indices were obtained by Debye Scherrer method and the crystal structure determined using equations 3.8-3.11. Noticeably, the XRD data (appendix 33) showed haematite (α-Fe_2O_3) as the only crystallized iron phase in the modified bagasse biochar (α-Fe_2O_3-CBG), with diffraction peaks at 2θ = 24.11°(012), 33.06°(104), 35.49°(110), 40.81°(113), 49.32°(024), 53.91°(116), 62.28°(214), 63.89°(300) (Figure 4.13(a)). This is characteristic of rhombohedral iron oxide (haematite) crystal structure. The only crystalline phase in the unmodified DTE is SiO_2 with a peak at 2Θ value of 26.40°(101) (Figure 4.13(b)). Other forms of magnetic minerals possibly formed during sythesis, *viz*, magnetite (Fe_3O_4) and maghemite (γ-Fe_2O_3), were converted to haematite under thermal treatment (Shikuku *et al.,* 2017). The other prominent crystalline phase in α-Fe_2O_3-CBG composite was quartz (SiO_2) represented by peaks at 2Θ values 20.78°(100) and 26.58°(101) (Fig. 4.13(a)). This

is consistent with EDAX results indicating presence of the two oxides in the iron modified composite. On the other hand, there was absence of α-Fe_2O_3 peaks in the diffractogram for the unmodified carbonized bagasse (CBG) biochar (appendix 32). However, the quartz (SiO_2), a common mineral in biochars (Yao *et al.*, 2014), peaks were observed at 2Θ values of 26.40° in unmodified CBG adsorbent (Fig. 4.13(b)).

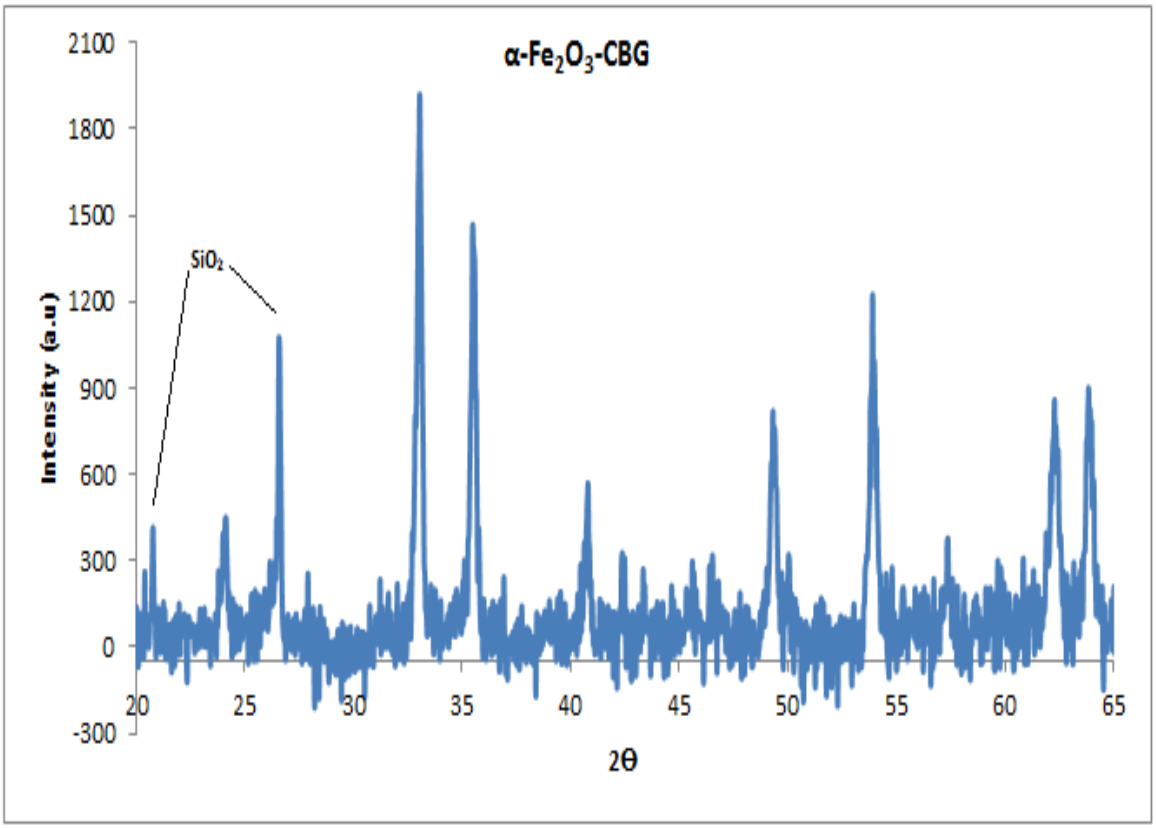

Figure 4.13 (a): Diffractogram showing the crystalline phases in α-Fe_2O_3-CBG composite

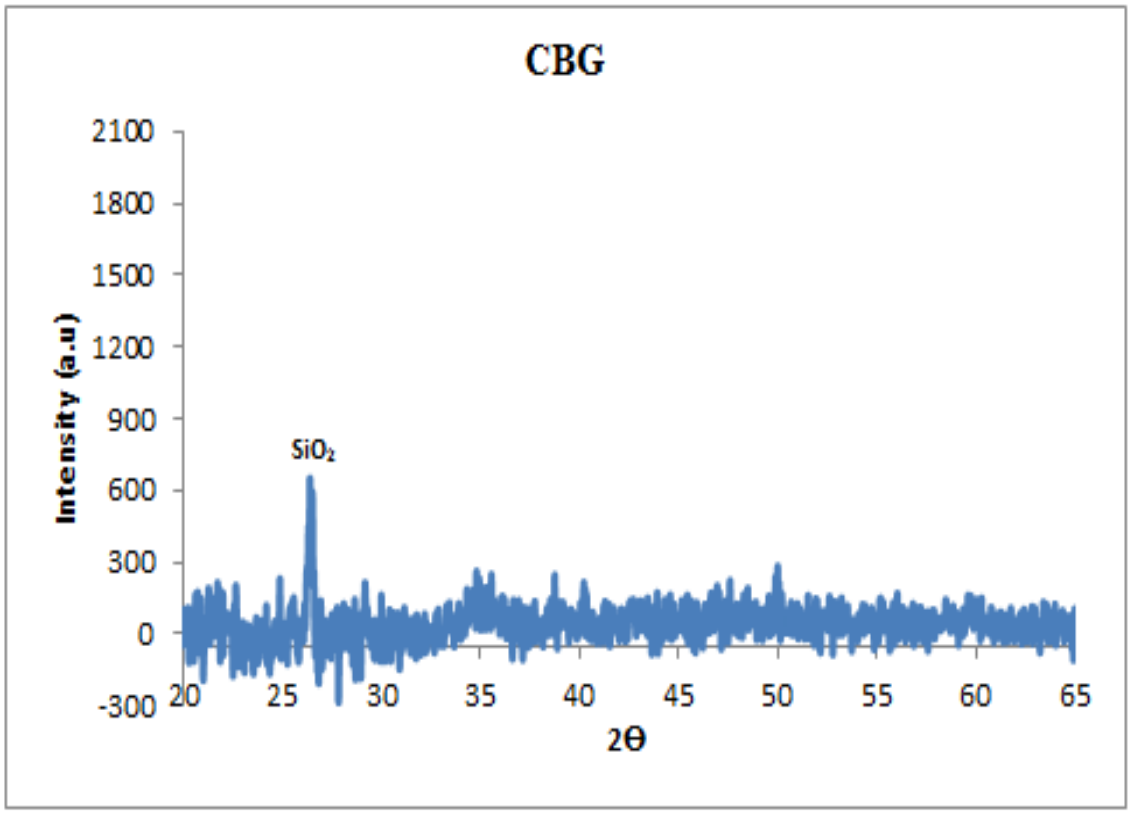

Figure 4.13 (b): Diffractogram showing the crystalline phases in unmodified CBG adsorbent

4.8.3.2 The XRD Diffractogram for carbonized maize cob (CMC) biochar and iron modified composite (β-FeO(OH)-CMC

The diffractogram for carbonized maize cob (CMC) biochar had prominent peaks characteristic of quartz (SiO_2) as shown in appendix 34. It can be observed that CMC exhibited diffraction peaks at 2Θ values of 26.40°, 34.91°, 38.99°, 55.53°, 60.98° and 77.41° typical of Sylvite, KCl (Figure 4.14(a)). Unexpectedly, after chemical treatment, the iron phase incorporated into the biochar network was characteristic of Akaganeite, β-FeO(OH), as depicted in the diffractogram in appendix 35. It can be observed that β-

FeO(OH)-CMC adsorbent revealed well resolved peaks in the region of 2Θ values from 28° to 75°. The diffraction peaks exhibited were at 28.22°(310), 34.71°(400), 40.40°(301), 49.94°(530), 55.56°(521), 58.51°(002), 66.23°(541) and 73.57° (Figure 4.14(b)) characteristic of tetragonal Akaganeite structure. In literature, Akaganeite is associated with presence of relatively high chloride content (Elizalde-gonza, 2008) which is consistent with the XRF and EDAX results.

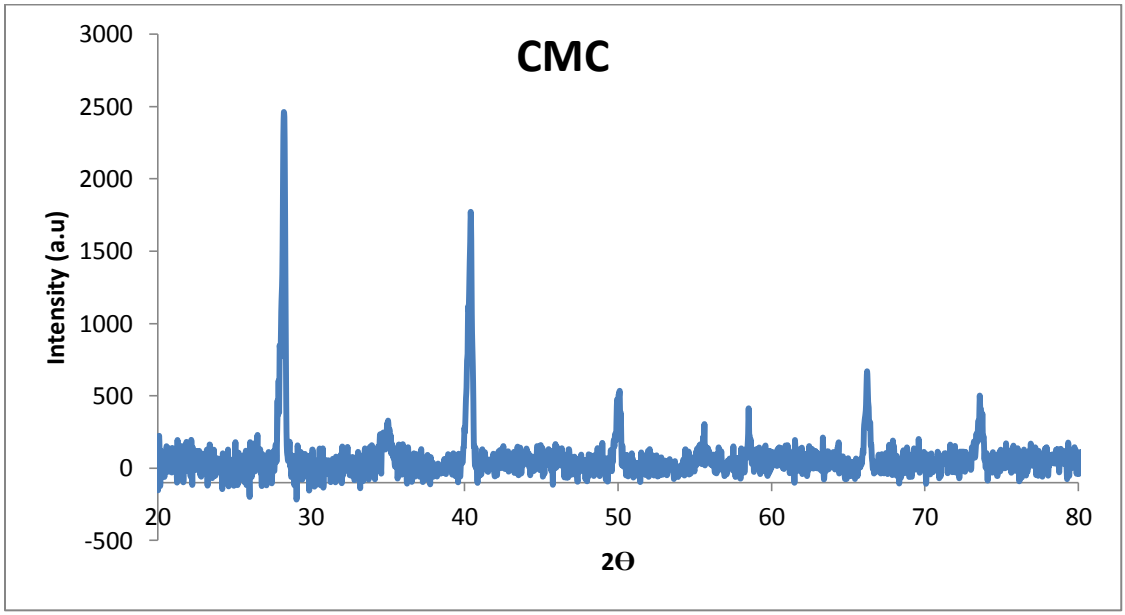

Figure 4.14(a): Diffractogram showing the crystalline phase in unmodified CMC

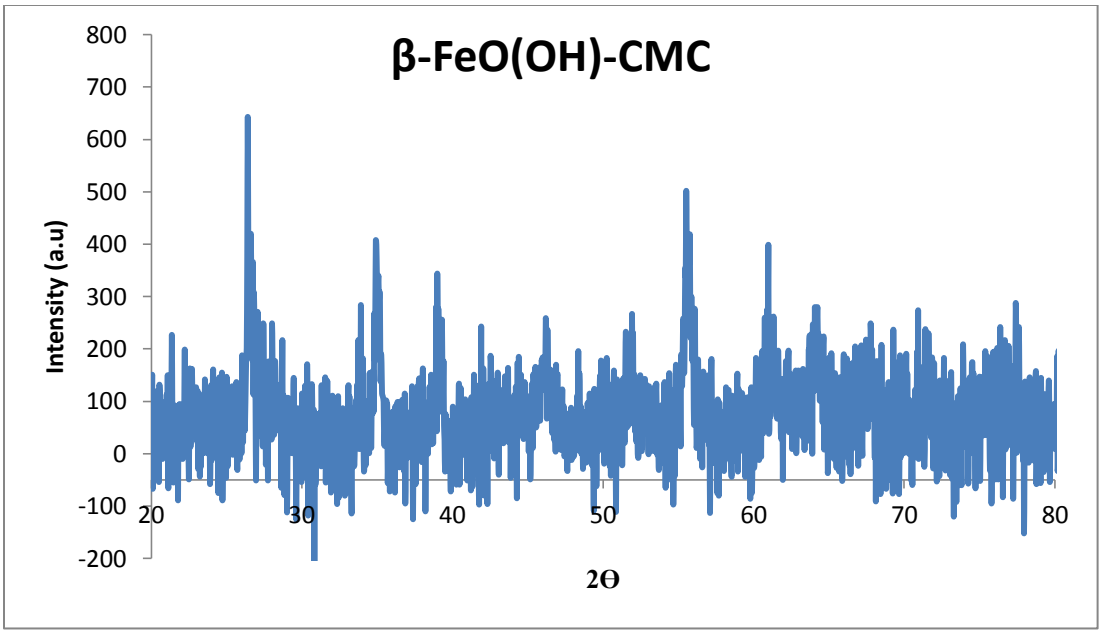

Figure 4.14 (b): Diffractogram showing the crystalline phase in iron modified β-FeO(OH)-CMC adsorbent.

4.8.3.3 The XRD Diffractogram for Diatomaceous Earth (DTE) and iron modified (α-Fe_2O_3-DTE) composite

The untreated diatomaceous earth was notably rich in silicon and largely amorphous with no significant crystalline phases noted (appendix 36). However, after chemical treatment, crystallinity was induced and the crystallized iron phase incorporated as shown in the respective diffractogram was haematite (α-Fe_2O_3) (appendix 37). The strong and sharp reflection XRD peaks were observed at 2Θ values of 24.07°(012), 33.09°(104), 35.53°(110), 40.67°(113), 49.39°(024), 53.91°(116), 57.45°(022), 62.35°(214) and 63.86°(300) (Figure 4.15(b)). This suggests that the synthesized iron modified diatomaceous earth composites are well crystallized with rhombohedral structure.

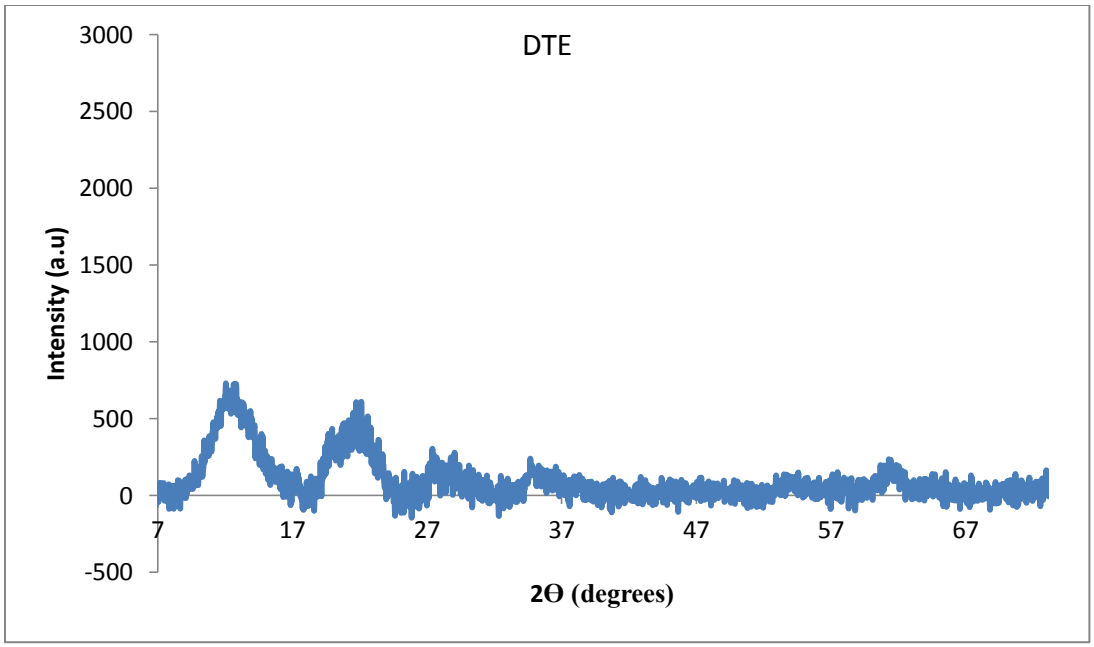

Figure 4.15 (a): The XRD pattern for unmodified ditomaceous earth (DTE) adsorbent.

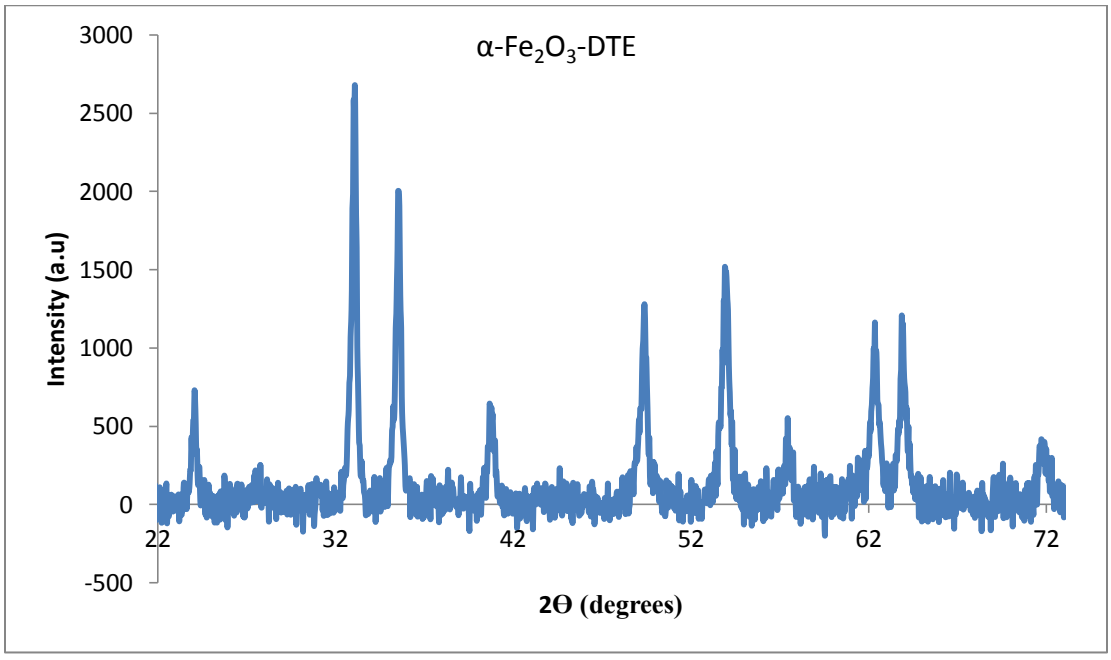

Figure 4.15 (b): The XRD pattern for iron modified (α-Fe_2O_3-DTE) composite.

Notably, the XRD pattern of unmodified DTE shows the presence of amorphaous SiO_2 forms (appendix 36). This is in tandem with data reported by Knoerr *et al.,* (2013) showing the amorphous form in the frustules of pristine DTE. On the other hand, the calcium carbonate phases; aragonite and calcite were also reported which was not found in DTE used in this study. In the iron modified DTE, α-Fe_2O_3 was found to be the only crystalline phase of iron incorporated. However, the same study reported two more allotropies of iron oxyhydroxide phases; lepidocrocite (α-FeOOH) and goethite (γ-FeOOH) together with the trivalent iron species.

4.8.4 FT-IR analysis

The structural features and functional groups present in the unmodified and chemically treated adsorbents were investigated by near IR (400-4000 cm^{-1}) analysis in transmittance mode.

4.8.4.1 The FT-IR spectra for unmodified bagasse biochar (CBG)-BB and iron modified bagasse biochar (α-Fe_2O_3-CBG)-MBB

In order to identify the reactive functional groups, FTIR analysis was carried out. The FTIR plot for the unmodified and modified bagasse derived biochar is displayed in Figure 4.16. The bands at 3600-3300 cm^{-1} were assigned to both free and hydrogen bonded –OH stretching vibrations due to phenolic functions. The peaks in the 1700-1600 cm^{-1} region were ascribed to C=O stretching vibrations resulting from ketones, carboxylic acids, anhydrides and esters (Mohan *et al.,* 2014). The peaks in the region 1500-1400 cm^{-1} were attributed to the presence of inorganic functional groups such as alumina-silicates and metal oxides (Jin *et al.,* 2014). The bands centered in the region 700- 500 cm^{-1} are

characteristic absorption bands of Fe–O bonds suggesting successful incorporation of iron oxides as testified by XRD analyses (Ercuta and Chirita, 2013).

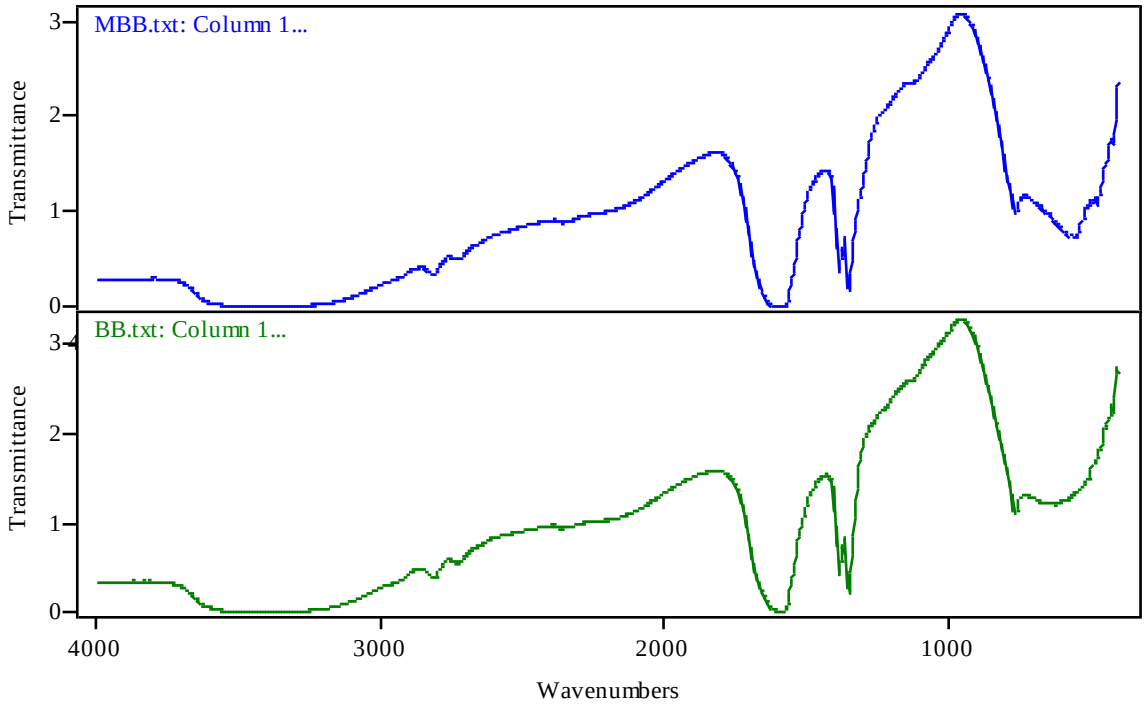

Figure 4.16: FT-IR spectrum for the iron modified baggase biochar (α-Fe_2O_3-CBG)-MBB (top) and unmodified (CBG)-BB (bottom)

Notably, there was no new peak in the modified adsorbent indicating that there was no new chemical bond introduced as a consequence of the treatment process. There was also no bond breaking. Furthermore, the analogous peaks were nearly identical suggesting minimum structural modifications of the biochar if any. Similarly, the spectrum depicting the functional groups present in the maize cob derived adsorbents as is shown in Figure 4.17. The bands were similar to those observed in the bagasse-based biochars (Norsuraya

et al., 2016). This was attributed to the presence of similar functional groups, with notable differences.

4.8.4.2 The FT-IR spectra for unmodified Maize Cob biochar (CMC)-MCC and iron Modified maize cob char (α-Fe_2O_3-CMC)-MMCC

The FT-IR spectra for unmodified maize cob biochar and the iron modified composite are presented in Figure 4.17. First, the bands at 3600-3300 cm^{-1} assigned to –OH stretching vibrations in the modified maize cob biochar were sharp and pronounced compared to the untreated biochar. This suggests increase in hydroxyl groups which serve as binding sites for organic adsorbates. This observation is expected to improve the adsorption capacity of the iron laden maize cob biochar relative to the untreated one.

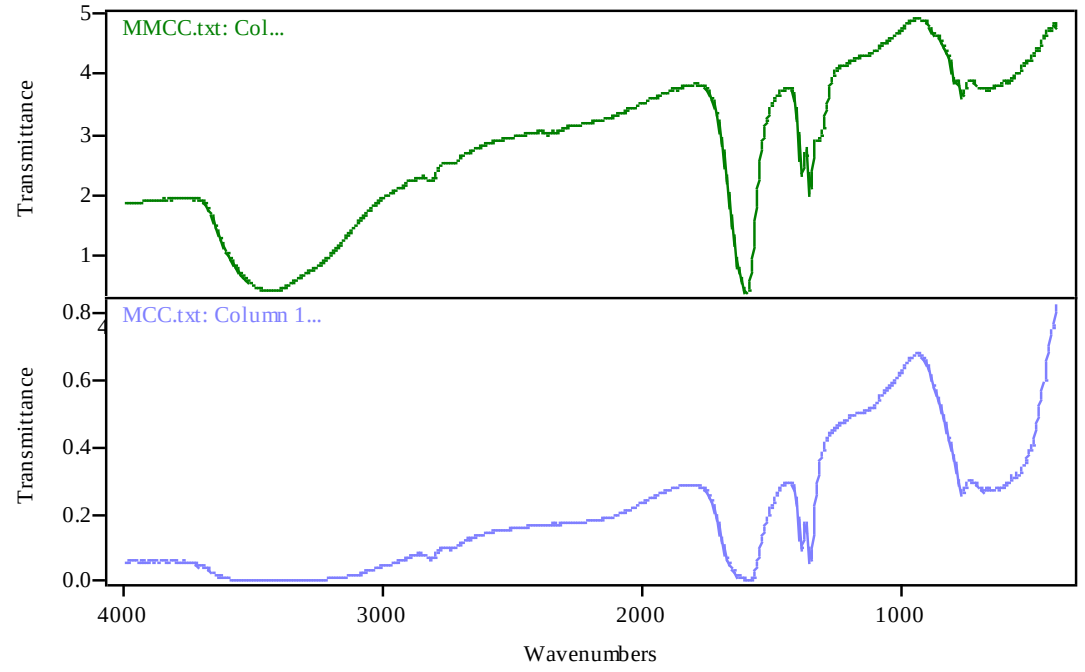

Figure 4.17: FT-IR spectrum for the iron modified maize cob biochar (β-FeO(OH)-CMC)-MMCC (top) and the unmodified (CMC)-MCC (bottom)

The absorption bands in the region between 1700-1600 cm^{-1} are assigned to carbonyl (C=O) stretch, while those at 1500-1400 cm^{-1} are attributed to metal oxide. The bands in the region 700-500 cm^{-1} can be ascribed to Fe-O vibration signals (Shikuku *et al*., 2017).

4.8.4.3 The FT-IR spectra for unmodified diatomaceous earth (DTE)-DE and iron modified diatomaceous earth (α-Fe_2O_3-DTE)-MDE

The functional groups in the diatomaceous earth and its modified counterpart are depicted in figure 4.18 below.

-

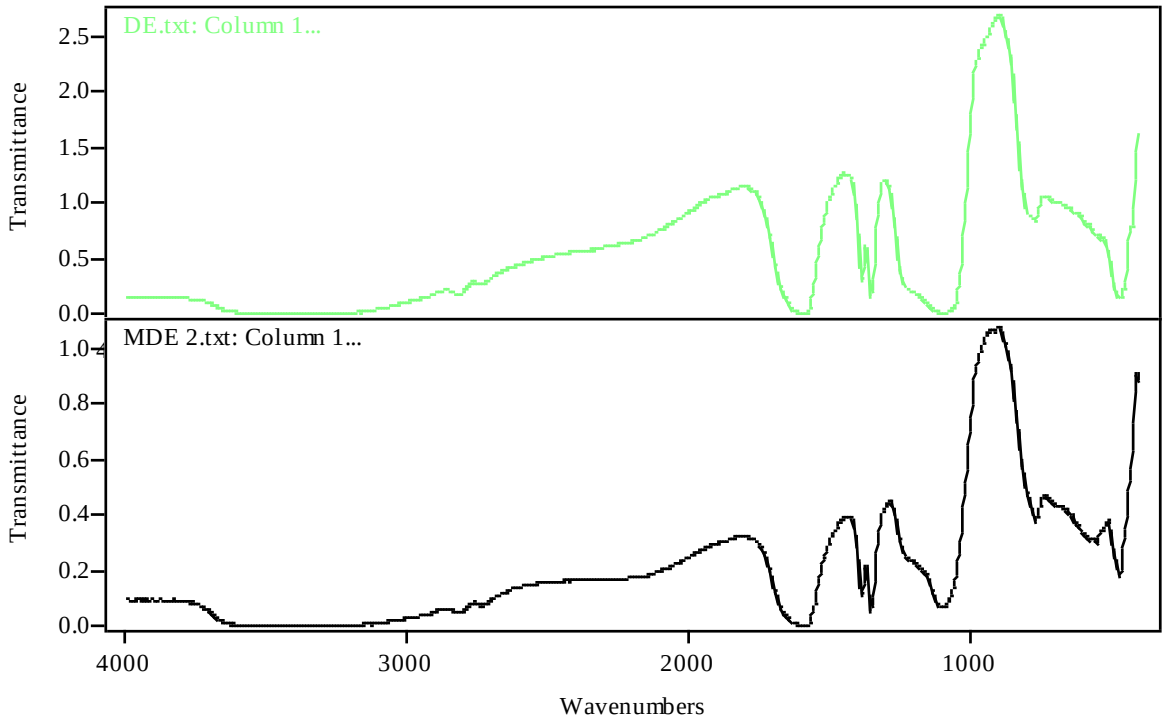

Figure 4.18: FT-IR spectrum for the unmodified (DTE)-DE (top) and iron modified diatomaceous earth (α-Fe_2O_3-DTE)-MDE (bottom)

The FTIR data confirms the presence of silica in the unmodified DTE adsorbent. The spectra of the unmodified samples (DTE) and the chemically treated adsorbent (α-Fe_2O_3-DTE) are displayed in Figure 4.18. Clearly, there were no significant differences between

characteristic bands ranging from 1400 and 400 cm^{-1} (that is 1200–1000 and 795 cm^{-1}) due to silicates structure(Fujiwara *et al.,* 2006). The wide bands centered at around 1090 cm^{-1} can be due to Si–O–Si in-plane vibration (asymmetric stretching). Similar observations can be seen at 795 cm^{-1}, which are also characteristic of silica. Again, the weak absorption peak at 616 cm^{-1} was possibly attributed to Si–O deformation and Al–O stretching (Yuan *et al*., 2013)

4.8.5 Surface Area of the Adsorbent Composites

The surface area of α-Fe_2O_3-DTE, α-Fe_2O_3-CBG and β-FeO(OH)-CMC adsorbents was determined by Brunauer–Emmet–Teller (BET) method. The total pore volume and the average pore diameter were derived from the Barrett–Joyner–Halenda (BJH) method. The BET surface areas for the three modified adsorbents were 22.0097 m^2g^{-1}, 2.0741 m^2g^{-1} and 2.58 m^2g^{-1}, respectively. The BJH desorption surface areas were 20.4619 m^2g^{-1}, 1.2504 $m^2g^{-1}$and 2.0601 m^2g^{-1}, respectively. The total pore volumes were 0.060931 cm^3g^{-1}, 0.010235 cm^3g^{-1} and 0.030614 cm^3g^{-1}, respectively. The average pore diameters for the tree adsorbents were 11.9111 nm, 32.7420 nm and 30.1452 nm, respectively.

4.8.6 Magnetic Properties of the Adsorbent Composites

To investigate the magnetic properties of the iron modified adsorbent composites, a magnetic hysteresis curve was recorded at a temperature range between 0-350 °K with a constant magnetic field of 1000 Oe. The fabricated iron modified adsorbent composites exhibited excellent ferromagnetic properties as shown in Figures 4.19, 4.20 and 4.21.

This property is essentially important for the convenient recycling of contaminant-laden composites which are easily separated using a magnet. A similar observation was reported by Zhang *et al.*, (2013). In Figure 4.19 the composite exhibited ferromagnetic behaviour at low temperature changing to paramagnetic above 25 °K as shown.

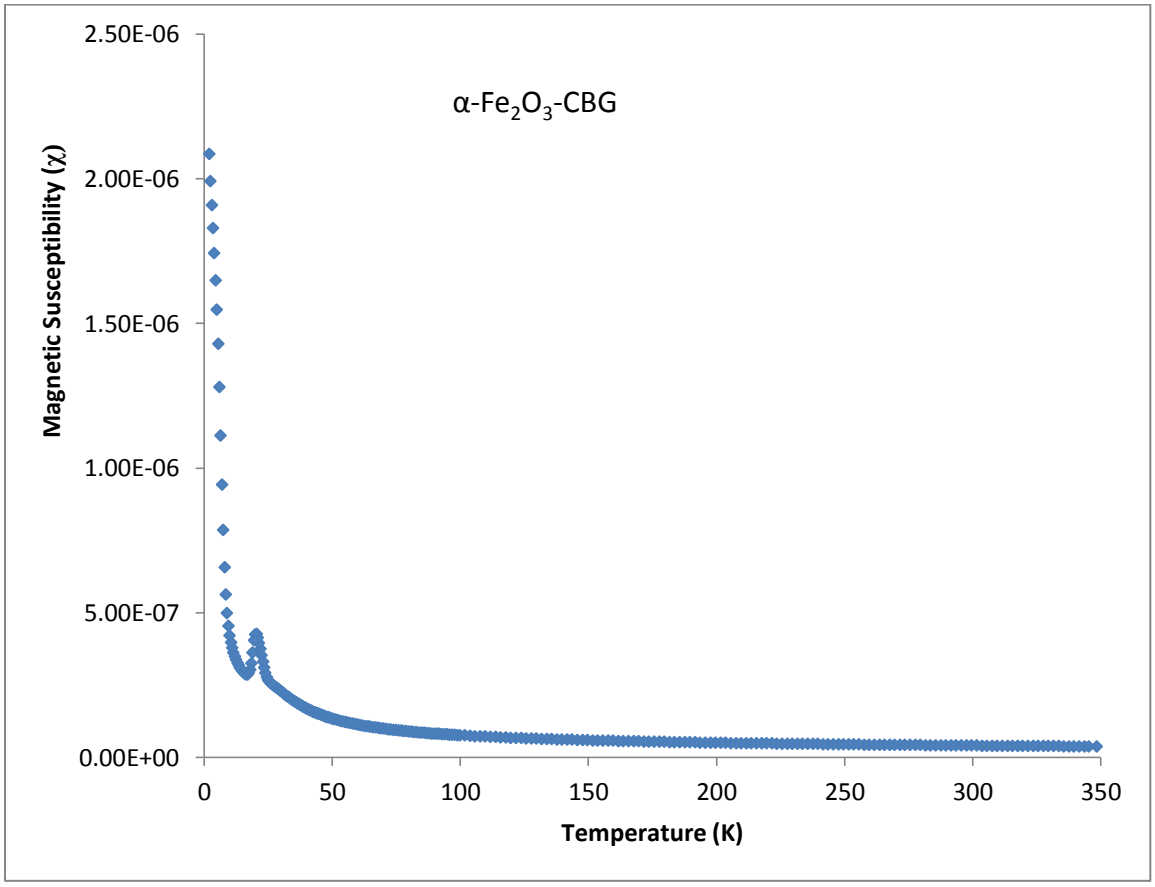

Figure 4.19: Magnetic hysterisis loop for α-Fe_2O_3-CBG composite.

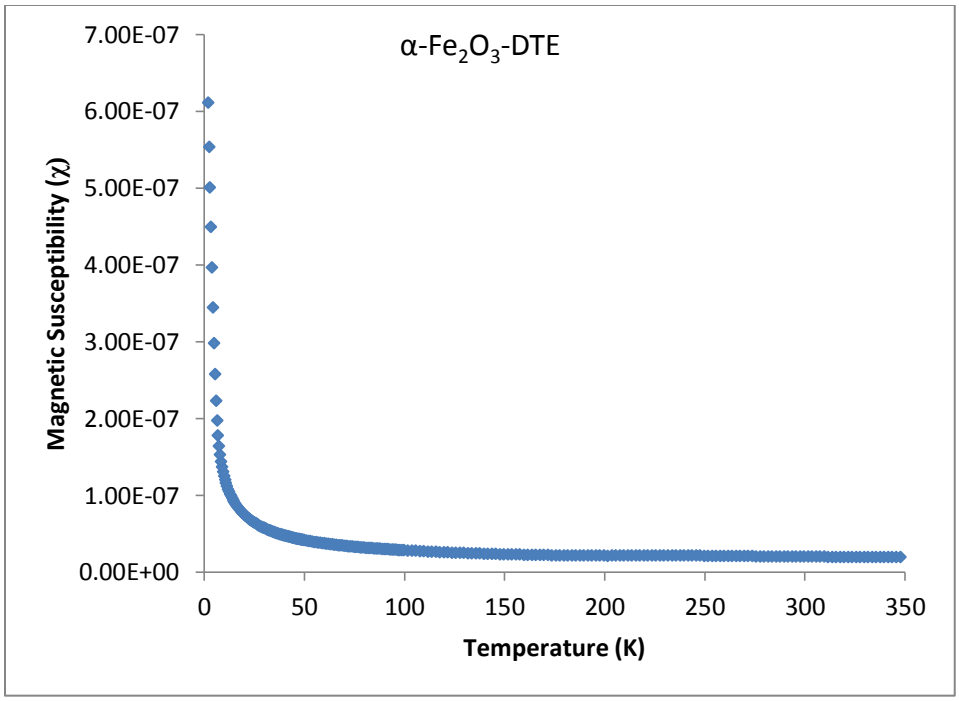

Figure 4.20: Magnetic hysterisis loop for α-Fe_2O_3-DTE adsorbent composite.

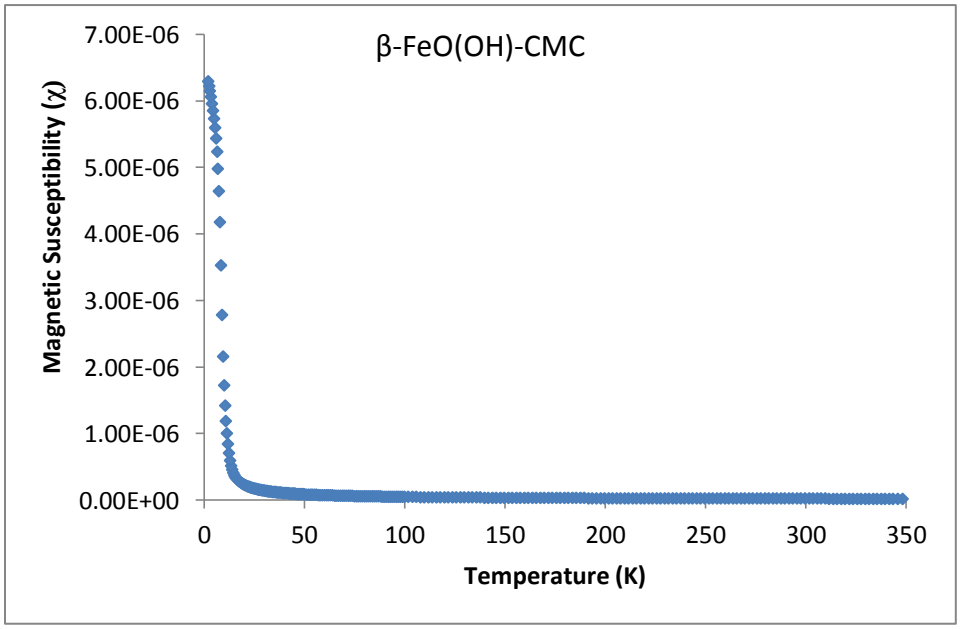

Figure 4.21: Magnetic hysterisis loop for β-FeO(OH)-CMC composite

4.9 Sorption of Carbamazepine (CBZ) onto Modified Carbonized Bagasse (α-Fe_2O_3-CBG), Carbonized Maize Cob (β-FeO(OH)-CMC) and Diatomaceous Earth (α-Fe_2O_3-DTE)

Kinetics and isotherm studies were carried out and the results fitted to a number of well-known sorption models in order to better understand the processes governing the adsorption of CBZ onto the magneto responsive adsorbent composites. Data from the kinetics experiment showed an initial rapid uptake followed by smooth increase, reaching equilibrium within 3 h (Fig. 4.22). Different mathematical models including pseudo-first-order, pseudo-second order and the intra-particle diffusion models were used to fit the kinetics data.

4.9.1 Effect of contact time

The removal of carbamazepine (CBZ) by the iron modified carbonized adsorbents, namely bagasse (α-Fe_2O_3-CBG), maize cob (β-FeO(OH)-CMC) and diatomaceous earth (α-Fe_2O_3-DTE) as a function of time depicted fast adsorption kinetics leading to saturation within 180 minutes (Fig. 4.22) followed by a slow phase with no appreciable change, implying pseudo-equilibrium conditions. This is due to availability of a large number of vacant adsorption sites at the onset. Accessibility to these sites becomes sequentially limited following occupancy by the pharmaceutical molecules thus the system achieves equilibrium. Noteworthy, adsorption capacity at equilibrium for the modified adsorbents was in the order α-Fe_2O_3-DTE> α-Fe_2O_3-CBG > β-FeO(OH)-CMC.

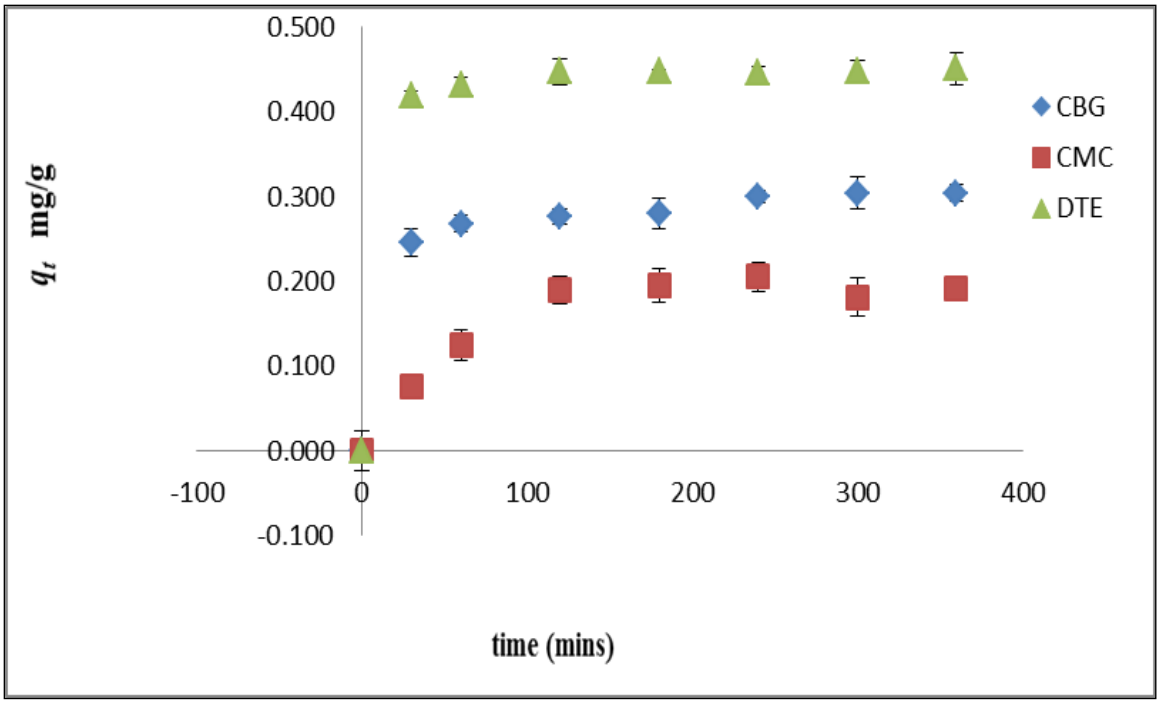

Figure 4.22: Effect of contact time for CBZ adsorption onto iron modified α-Fe_2O_3-DTE, α-Fe_2O_3-CBG and β-FeO(OH)-CMC adsorbent composites.

In order to predict the adsorption rate and nature of the rate-controlling step(s), the kinetic data were simulated using pseudo-first order and pseudo-second order kinetic models. The applicability of the model was evaluated by the linear regression coefficient (R^2) values and the closeness between experimental equilibrium adsorption capacity (q_{exp}) and the theoretical values (q_{cal}) obtained from the kinetic models. The pseudo-first order posted poor fitting to the experimental data indicating the adsorption of CBZ onto the iron modified adsorbents is not a first-order reaction. On the contrary, the pseudo-second-order kinetic model best simulated the adsorption of CBZ onto all the tested adsorbents (Figure 4.23) with high R^2 values closest to unity. This corroborated with the convergence of the calculated (q_{cal}) and experimental (q_{exp}) adsorption

capacities, implying the rate controlling step is a chemisorption process involving exchange of valence electrons (Table 4.8). The intra-particle diffusion graphs were linear (Fig. 4.24) depicting strong influence of intra-particle diffusion process with CBG posting highest linearity (R^2=0.941). Nevertheless, the plot did not pass through the origin implying that pore transport is not the only rate controlling mechanism; hence other adsorption sequences are involved (Shikuku *et al*., 2015). Relative to the pre-equilibrium adsorption, the linear plots had relatively significant intercepts (Table 4.8) suggesting significant boundary layer effects in α-Fe_2O_3-DTE> α-Fe_2O_3-CBG > β-FeO(OH)-CMC, attributable to a wide distribution of pore sizes (Ng'eno *et al*., 2016).

Table 4.8: Kinetic parameters for CBZ adsorption onto the three magneto responsive adsorbents

Adsorbent	Pseudo-second order parameters	Intra-particle diffusion parameters
α-Fe_2O_3-CBG	q_e 0.313 mg/g	*Kp* 0.004
	K_2 0.256 g mg^{-1} min^{-1}	C 0.228 mg/g
	R^2 0.998	R^2 0.941
α-Fe_2O_3-CMC	q_e 0.216 mg/g	*Kp* 0.007
	K_2 0.129 g mg^{-1} min^{-1}	C 0.064
	R^2 0.976	R^2 0.686
α-Fe_2O_3-DTE	q_e 0.453 mg/g	*Kp* 0.002
	K_2 0.913 g mg^{-1} min^{-1}	C 0.415
	R^2 1.00	R^2 0.769

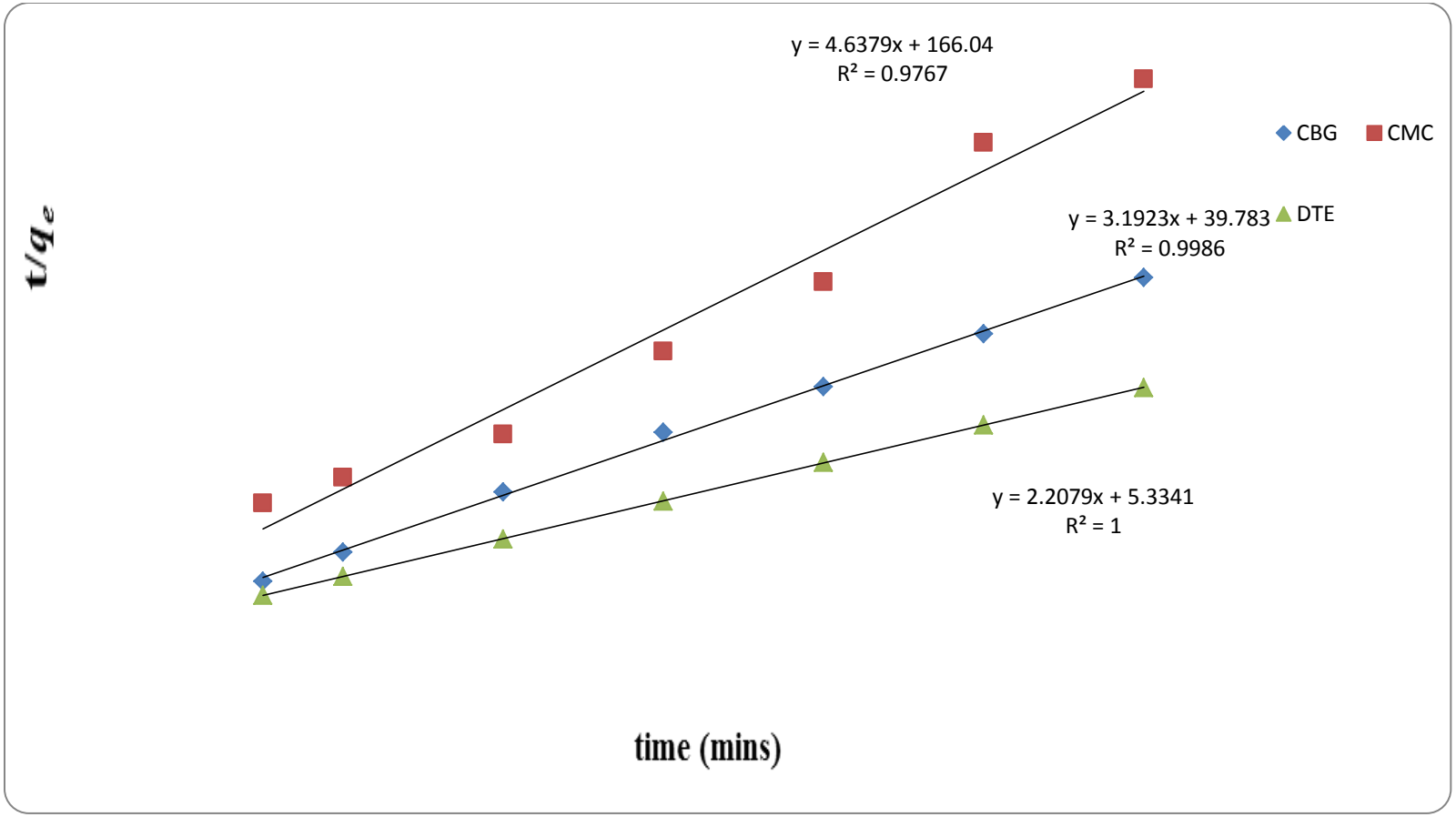

Figure 4.23: Pseudo-second order kinetic plot for CBZ adsorption onto α-Fe_2O_3-DTE, α-Fe_2O_3-CBG, β-FeO(OH)-CMC adsorbent composites

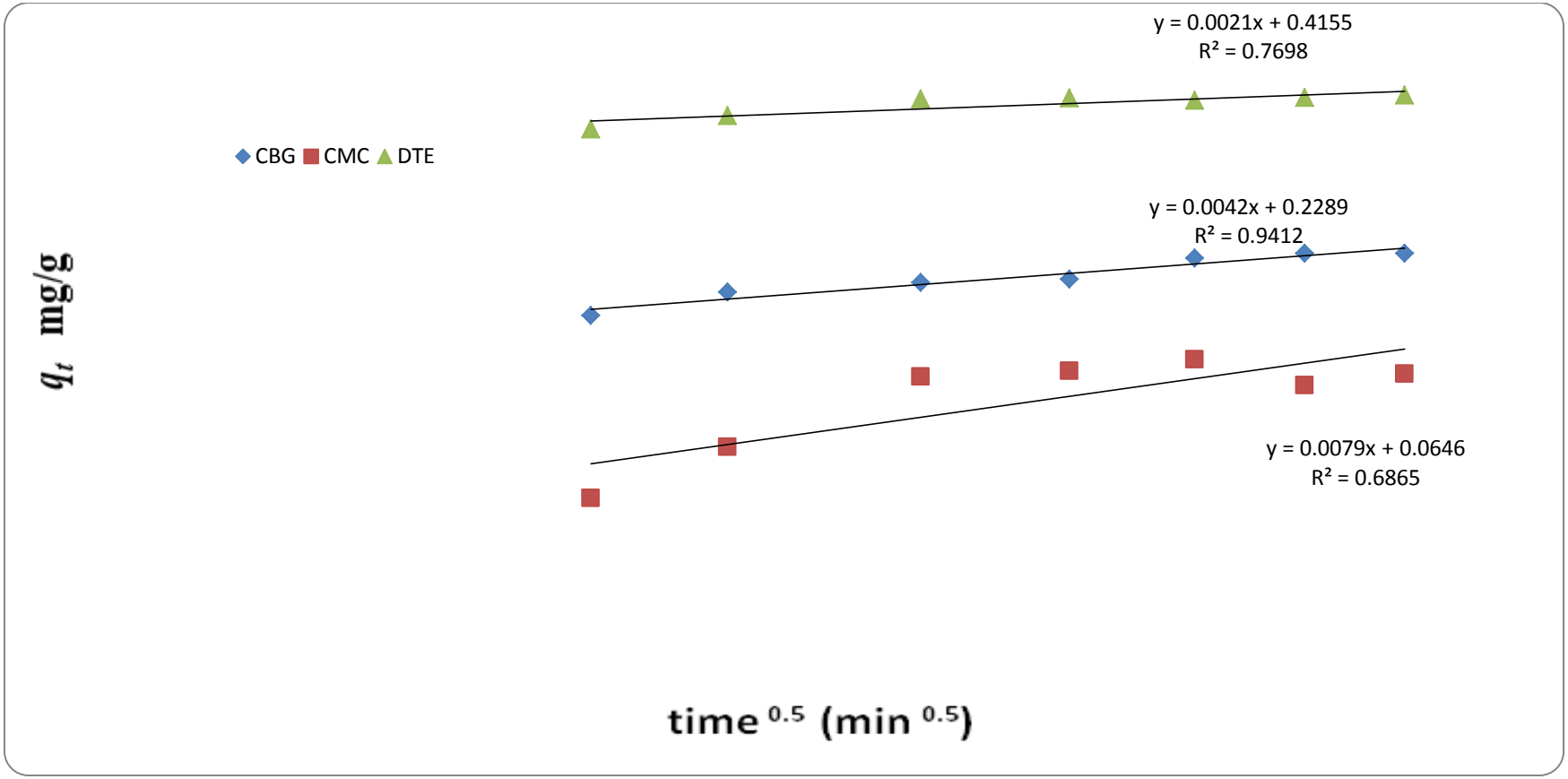

Figure 4.24: Intraparticle diffusion plot for CBZ adsorption onto α-Fe_2O_3-DTE, α-Fe_2O_3-CBG, β-FeO(OH)-CMC adsorbent composites

4.9.2 Effect of initial concentration

The removal extent in percentage was found to increase for all three adsorbents when the initial concentration was raised from 0.5 to 1.0 mg/L for adsorbent dosage of 0.1g/50 mL beyond which a decrease was noted for α-Fe_2O_3-CBG and β-FeO(OH)-CMC. The initial increase indicates that mass gradient serves as the driving force for the adsorption process. As observed in the evolution of distribution coefficient (K_d) as a function of initial concentration (Figure 4.25), the increase in K_d with increase in adsorbate concentration imply availability of more energetically favoured sites for adsorption (Shikuku *et al.*, 2014).

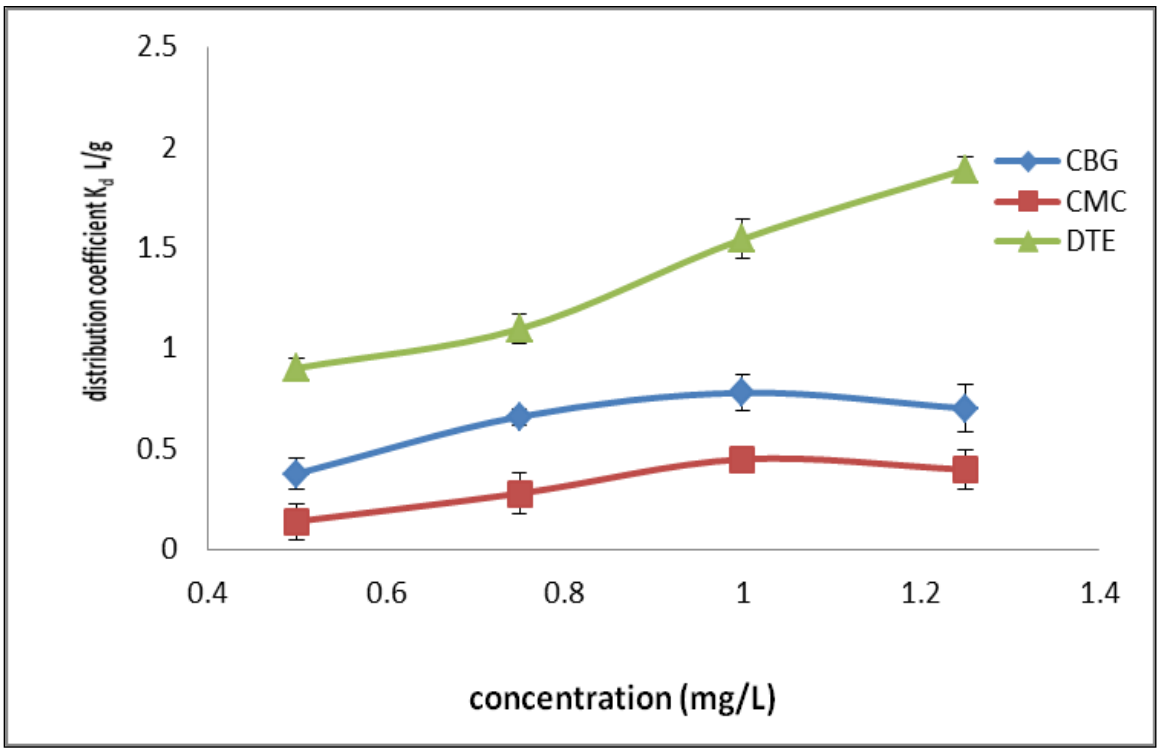

Figure 4.25: Evolution of CBZ distribution coefficient (K_d) as function of initial concentration

The gradual decrease beyond 1 mg/L, for α-Fe_2O_3-CBG and β-FeO(OH)-CMC, is due to saturation of the active binding sites with concomitant repulsion between the adsorbates at high concentration.

4.9.3 Adsorption isotherms

The distribution of CBZ between the three adsorbents and aqueous solution at equilibrium explains the capacity of the adsorbent for removal of the compounds. Adsorption was evaluated using commonly used Langmuir and Freundlich isotherm models (Sheshdeh *et al.*, 2014). Langmuir isotherm applies to monolayer adsorption on a surface with finite number of identical adsorption sites. Conversely, the Freundlich model incorporates heterogeneity of adsorbent surfaces. Data were fitted to the two models as shown in Figures 4.26 and 4.27.

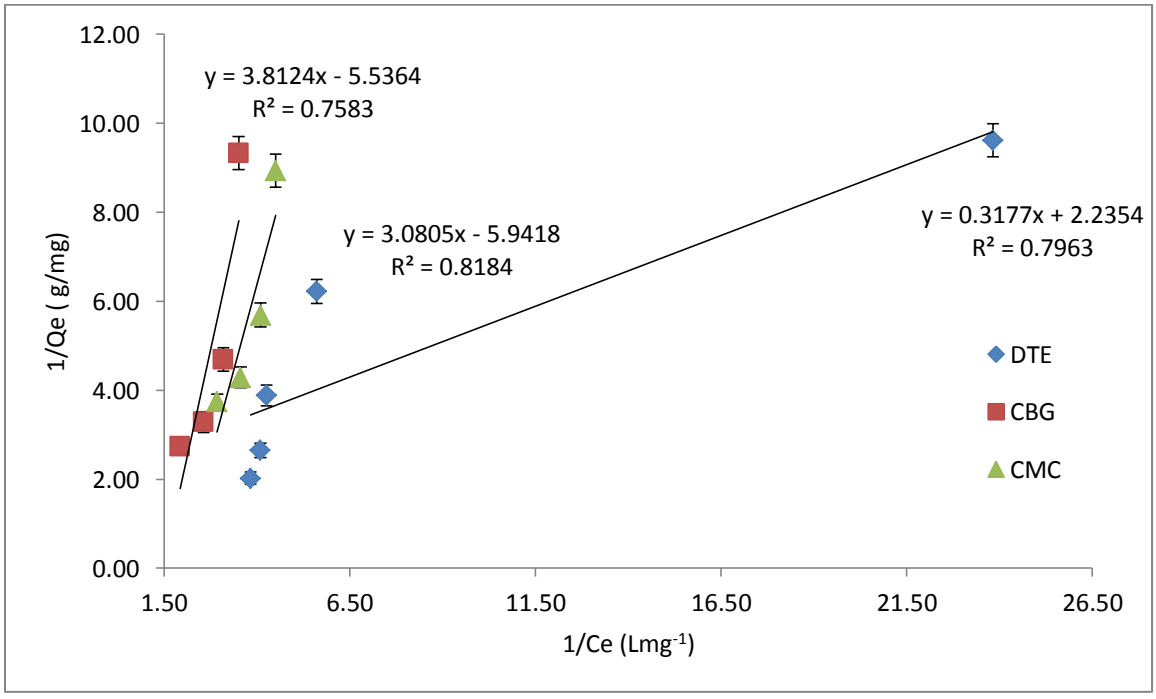

Figure 4.26: Langmuir adsorption isotherms for iron modified adsorbent composites

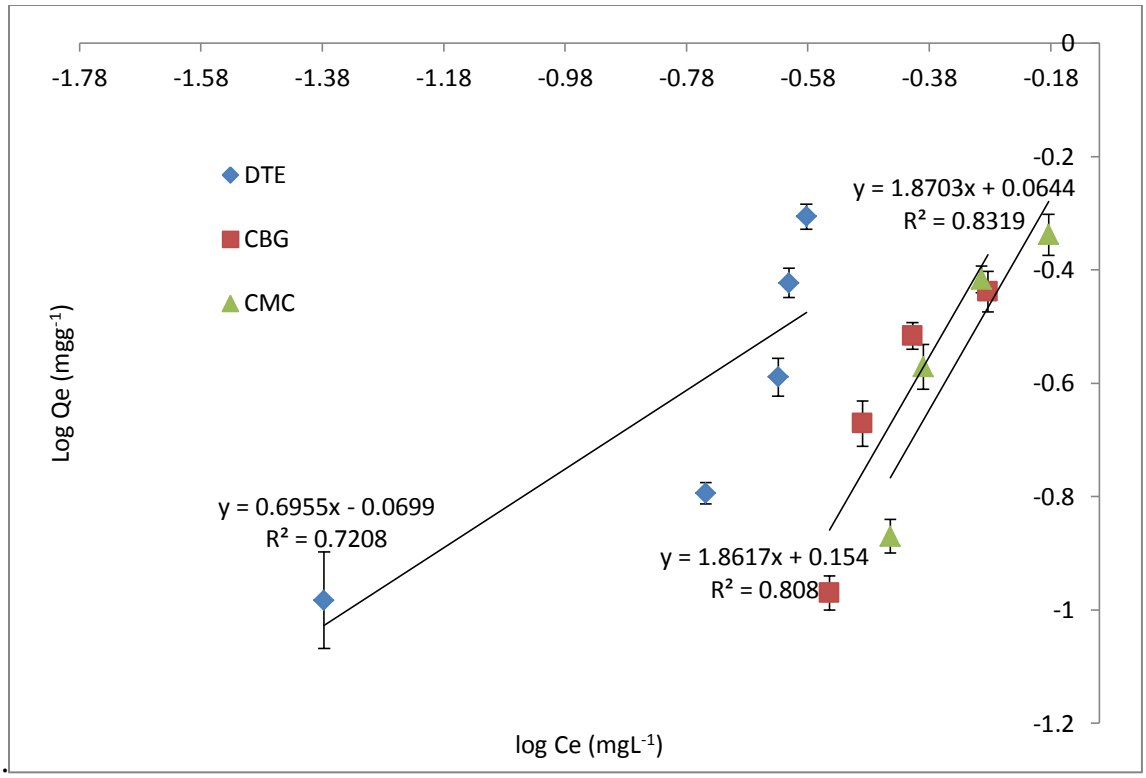

Figure 4.27: Freundlich adsorption isotherms for iron modified adsorbent composites

Table 4.9 shows the various parameters calculated after fitting data to the linearized forms of the isotherms. Both isotherm models posted relatively low linear correlation coefficients (R^2), implying each individual model could not completely describe the adsorption mechanism suggesting multi-mechanistic adsorption sequences (Jemutai-Kimosop *et al.*, 2017). However, the data tended to conform to the Freundlich model. Furthermore, besides the low R^2 values, the negative Langmuir isotherm constants (Q_o and K_L) values for α-Fe_2O_3-CBG and β-FeO(OH)-CMC were unacceptable for they bear no physical meaning. This indicates that the inherent postulates of this model cannot satisfactorily explain the adsorption mechanism of carbamazepine onto iron modified α-Fe_2O_3-CBG and β-FeO(OH)-CMC adsorbents (Shikuku *et al.*, 2015).

Table 4.9: Adsorption isotherm parameters for iron modified adsorbent composites

Isotherm Model	Calculated Parameters for α-Fe_2O_3-CBG	Calculated Parameters for β-FeO(OH)-CMC	Calculated Parameters for α-Fe_2O_3-DTE
Langmuir	Q_m(mg g^{-1}) = -0.1806 K_L (L g^{-1}) = -1.4525 R^2 = 0.758	Q_m(mg g^{-1}) = -0.547 K_L (L g^{-1}) = -1.360 R^2 = 0.818	Q_m(mg g^{-1}) = 0.447 K_L (L g^{-1}) = 7.050 R^2 = 0.796
Freundlich	K_f, =1.4256 L/mg n = 0.5373 R^2 = 0.808	K_f, (L/mg) = 0.957 n = 0.356 R^2 = 0.832	K_f (L/mg)= 0.853 n = 1.439 R^2 = 0.720

Therefore, rationally, despite the relatively low R^2 values, the adsorption of CBZ onto the two adsorbents could be explained in terms of Freundlich isotherm model. In these cases, the magnitude of Freundlich constant *n* was less than unity indicating poor adsorptive character while 1/n is above unity corroborating the aforementioned cooperative adsorption constituting several mechanisms (Saleh, 2015; Treybal, 1981). On the contrary, adsorption of CBZ onto modified diatomaceous earth (α-Fe_2O_3-DTE) followed the Langmuir model with a theoretical maximum monolayer adsorption capacity of 0.447 mg/g.

4.9.4 Effect of pH and adsorption mechanism

The pH dependence was studied in the range 2.0 to 12.0. The adsorption of CBZ onto CBG and CMC modified adsorbents were strongly pH dependent while CBZ adsorption

onto iron modified DTE seemed independent of pH changes with insignificant variation in percent removal (Fig. 4.28). The points of zero charge for the three adsorbents were 6.0, 5.8 and 5.6, respectively for the corresponding modified DTE, CBG and CMC. This means that at pH values lower than the pHpzc, the adsorption sites on the adsorbents are positively charged, but at pH values higher than pHpzc, the sample surfaces are negatively charged, which could adsorb anions by electrostatic attraction.

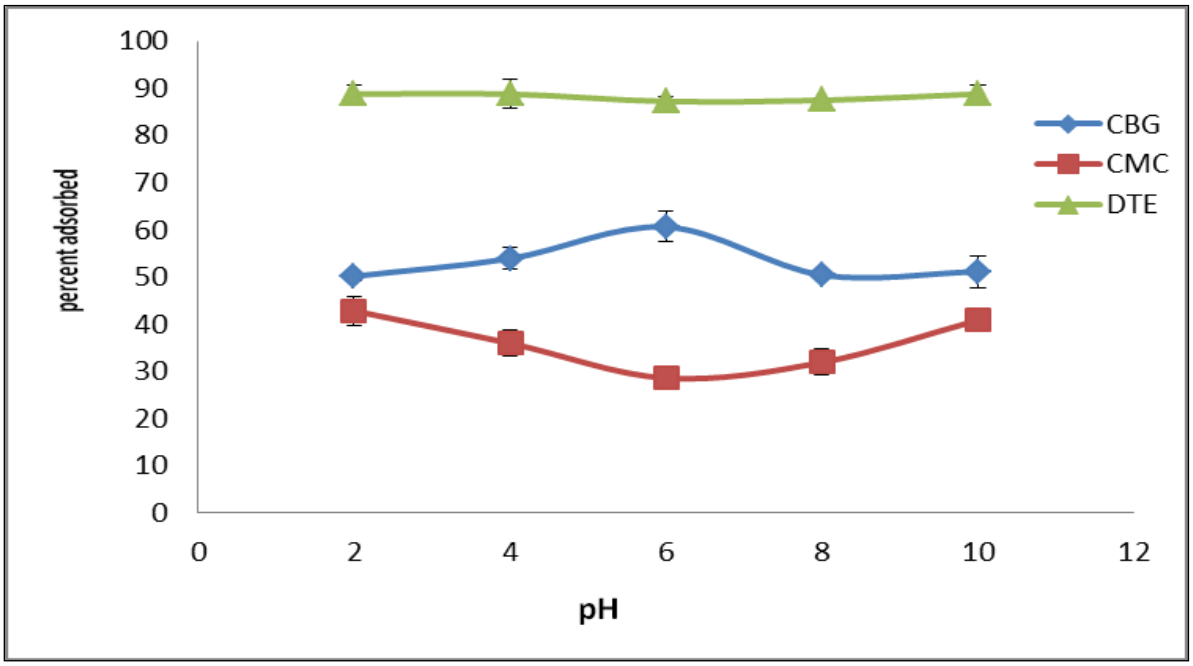

Figure 4.28: pH dependence plot for CBZ adsorption onto α-Fe_2O_3-CBG, β-FeO(OH)-CMC and α-Fe_2O_3-DTE adsorbent composites

The variation of adsorption capacities with pH gives insight on the possible interaction mechanisms involved. CBZ has two pK_a values because it dissociates at two different functional groups depending on the pH. These are pK_a at 2.30 (ketone group) and 13.90 (amine group) for CBZ (Punyapalakul and Sitthisorn, 2010). Therefore, below pH 2.3,

CBZ was a positively charged species (CBZ^{+}) and electrostatic repulsion became significant and accounted for the decreased adsorption capacity observed.

However, throughout the pH range, CBZ were neutrally charged species (CBZ^{0}) and the effect of electrostatic interactions was negligible and can be neglected and hence other adsorption mechanisms besides electrostatic interactions such as hydrophobic interactions play a key role. On the contrary, at pH 2 CBZ existed predominantly in cationic form (CBZ^{+}) hence electrostatic repulsion is expected to be significant yet the amount adsorbed onto β-FeO(OH)-CMC was maximum and decreased as pH tended towards neutral (Kim *et al*., 2014). Further increase in pH, above pH 6, CBZ was electrically neutral (CBZ^{0}) and at higher pH values the adsorbent surface acquired a net negative charge and electrostatic interactions would be insignificant to account for the increased adsorption observed. These results indicate that the pH-dependent speciation of the compounds largely control their adsorption extent. Also, the retention mechanism seems to involve, in part, non-electrostatic driven interactions.

4.9.5 Thermodynamics Studies

The influence of temperature variation was studied in the range 25 to 65 °C. The thermodynamic parameters were calculated by fitting the data into the Vant' Hoff plot at 25 °C (Figure 4.29). The calculated parameters are summarized in Table 4.10. Sorption efficiency for CBZ decreased with increase in temperature indicating an exothermic sorption process as shown by negative value of ΔH (Table 4.10). The percentage decrease in removal efficiency could be attributed to concomitant weakening of binding forces between the framework of the adsorbent composite and the CBZ molecules. As a result,

there was increase in CBZ solubility in water at elevated temperatures thus lowering the molecule's affinity for the adsorbent surfaces (Daneshvar *et al.*, 2012). This confirms that adsorption process is not only controlled by the intra-particle transport-pore diffusion.

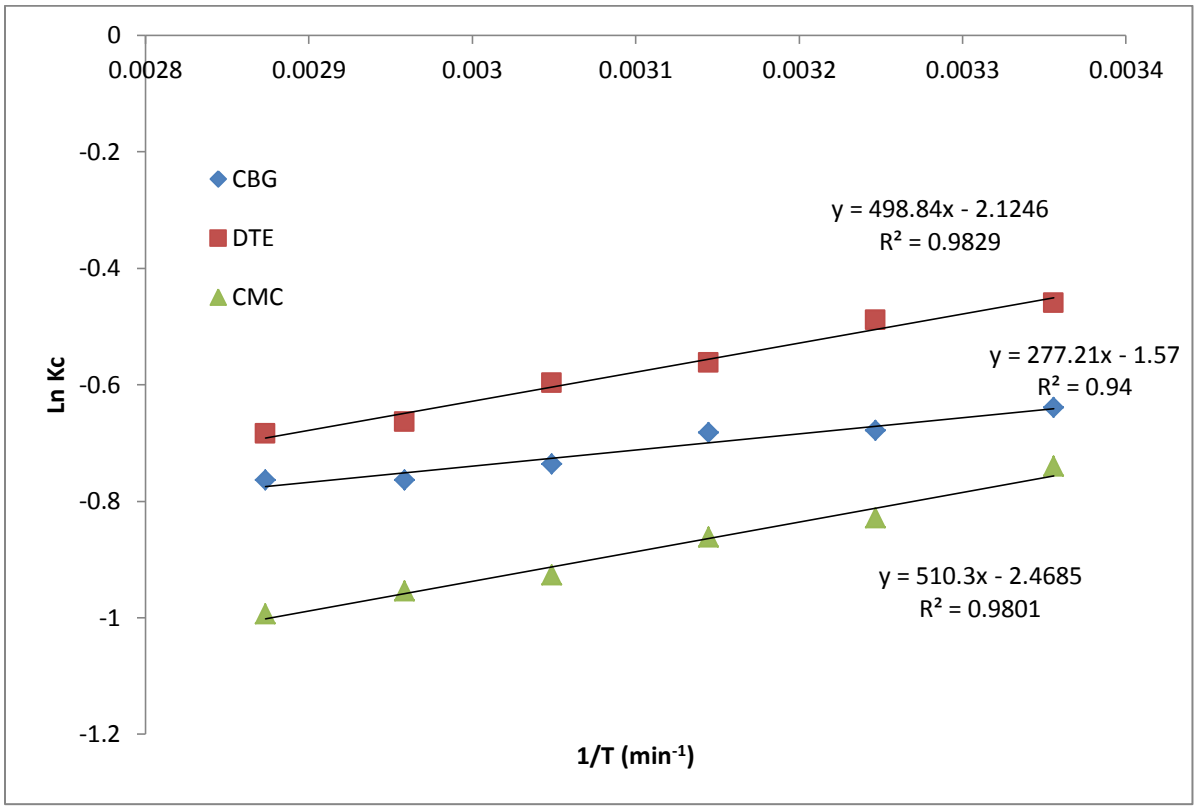

Figure 4.29: The Vant' Hoff plot of iron modified adsorbent composites at 25 °C

Thermodynamically, spontaneous and non-spontaneous processes are indicated by negative and positive ΔG values, respectively. The reaction involving sorption of CBZ onto α-Fe_2O_3-DTE is spontaneous. However, the overall sorption reaction involving α-Fe_2O_3-CBG and β-FeO(OH)-CMC with positive ΔG values (Table 4.10) may be driven by enthalpy and the system may draw energy from its surroundings as observed by Latifu *et al*. (2014).

Table 4.10: Thermodynamic parameters for the adsorption of CBZ onto α-Fe_2O_3-DTE, α-Fe_2O_3-CBG and β-FeO(OH)-CMC composites

Adsorbent	TEMP (K)	% Removal	ΔG ($Jmol^{-1}$)	ΔH ($kJmol^{-1}$)	ΔS ($Jmol^{-1}$)
α-Fe_2O_3-Diatomaceous Earth	298	90.15	-2220	-26.40	-34.04
	308	88.90	-1304		
	318	74.52	-1290		
	328	67.45	-1071		
	338	55.40	-873		
α-Fe_2O_3-Carbonized Baggasse	298	60.94	1584	-2.31	-13.05
	308	55.66	1739		
	318	52.18	1803		
	328	50.890	2009		
	338	48.94	2147		
β-FeO(OH)-Carbonized Maize Cobs	298	43.00	1441	-24.72	-90.04
	308	41.08	3626		
	318	39.56	4683		
	328	37.55	4450		
	338	34.98	5411		

All the sorption processes were exothermic for the three adsorbent composites. However, the magnitudes of ΔH and ΔS (Table 4.10) indicate that the adsorption of CBZ onto α-Fe_2O_3-CBG and β-FeO(OH)-CMC composites is entropically driven and that the system, therefore, draws energy from its surrounding as observed by Shikuku *et al.*, (2017) and Laifu *et al.*, (2014). Generally, the magnitude of ΔH value ranges from 40–120 kJ mol^{-1} for chemisorption mechanisms (Sapawe *et al.*, 2013; Shikuku *et al.*, 2017). In the present study, the ΔH values indicate physisorption (–26.40, -2.31 and -24.72 kJ mol^{-1}) processes for the three adsorbent composites, respectively. The reaction is exothermic in nature and the magnitude of ΔH implies a physical process corroborating with the values obtained for ΔG (Punyapalakul and Sitthisorn, 2010). The decrease in amount adsorbed with increase in temperature implies the exothermic nature of the process exceeds the effect of increasing the diffusion rate of the molecules with increased thermal energy (Blasioli *et al.*, 2014). The negative ΔS implies decrease in randomness at the solid/liquid interphase (Table 4.10).

4.10 The percentage removal of selected PHC's and applications of the prepared adsorbents in wastewater treatment

The adsorption of carbamazepine on the modified composites show that the percentage removal decreased with increase in temperature (Table 4.10). At room temperature, adsorption of carbamazepine was found to be 90.15 %, 60.94 % and 43.00 % for α-Fe_2O_3-DTE, α-Fe_2O_3-CBG and β-FeO(OH)-CMC, respectively. It was found that α-Fe_2O_3-DTE recorded the highest removal capacity followed by α-Fe_2O_3-CBG and finally β-FeO(OH)-CMC. The α-Fe_2O_3-DTE composite consists of a variety of rigid shapes and

open voids characterized by honeycomb structure with large surface area (22.0097 m^2g^{-1}). These properties as well as various types of interactions between adsorbent and adsorbate make the composite ideal for trapping carbamazepine in water. The lower adsorption of capacities of α-Fe_2O_3-CBG and β-FeO(OH)-CMC may be attributed to the low surface areas of 2.0741 m^2g^{-1} and 2.58 m^2g^{-1}, respectively. In this study, synthetic wastewater was used and thus the potential of fouling was not tested. A real environmental wastewater sample containing various matrices may result in fouling of the adsorbent as described by Shimabuku *et al*., 2016. The high natural organic matter present in real wastewater may cause scaling and would reduce the efficiency of the adsorbents (Liu and Balasubramanian, 2013).

Similar results have been reported for pentachlorophenol removal by nanoscale zero valent iron modified paper mill sludge biochar. The respective removal efficiencies were 100 % and 73 % for synthetic and real effluent samples (Devi and Saroha, 2014). Similar results have been reported for the removal of methyl orange from aqueous solution by the functional supported bimetallic nanoscale zero valent iron/palladium adsorbent (Wang *et al*., 2013).

CHAPTER FIVE

5.0 CONCLUSIONS AND RECOMMENDATIONS

5.1 Conclusions

In this study, the concentrations of individual pharmaceuticals varied for different wastewater sources. Residue levels of individual PHC's analyzec in this study from Wastewater Treatment Plant (WWTP) effluents ranged from <0.05±0.02 to 0.36±0.04 µg/L. Hospital effluents recorded levels between <0.05±0.02 to 0.79±0.07 µg/L. Sludge samples from WWTPs recorded PHCs between <50±2 to 154±9 ng/g, while hospital lagoons recorded residues between <50±2 to 276±12 ng/g. The daily discharge loads of selected PHCs from the nine WWTPs studied ranged between 123.3±0.3 mg/L day^{-1} to 3130.0±0.7 mg/L day^{-1}. The percentage removal from the WWTPs ranged between 19.47±0.84 % for sulfamethoxazole and 54.29±0.63 % for chloramphenicol.

The synthesized magneto responsive adsorbents were characterized and the XRD results indicated successful incorporation of iron into the adsorbents with the crystalline structures identified as α-Fe_2O_3 for CBG and DTE while β-FeO(OH) was the crystalline form in CMC. Silicon dioxide (SiO_2) was also found to be a major component of the composites. This was also confirmed by XRF and SEM-EDAX results depicting successful impregnation. Fourier transform infrared (FTIR) spectroscopy revealed the presence of hydroxyl, carbonyl and iron oxide groups on the modified sorbents. The BET surface areas for the three modified adsorbents were 22.0097 m^2g^{-1}, 2.0741 m^2g^{-1} and 2.58 m^2g^{-1} for α-Fe_2O_3-DTE, α-Fe_2O_3-CBG and β-FeO(OH)-CMC, respectively.

The BJH desorption surface area were 20.4619 m^2g^{-1}, 1.2504 $m^2g^{-1}$and 2.0601 m^2g^{-1}. The total pore volume were 0.060931 cm^3g^{-1}, 0.010235 m^2g^{-1} and 0.030614 m^2g^{-1}. The average pore diameter for the three adsorbents were 11.9111 nm, 32.7420 nm and 30.1452 nm, respectively.

The thermodynamic data indicated that the adsorption process is feasible, spontaneous for α-Fe_2O_3-DTE and non-spontaneous for α-Fe_2O_3-CBG and β-FeO(OH)-CMC adsorbent composites. Both adsorption processes were exothermic and physical in nature

The equilibrium sorption data for carbamazepine showed multi-mechanistic adsorption mechanisms with the data tending to conform with the Freundlich model for α-Fe_2O_3-CBG and β-FeO(OH)-CMC adsorbents. However, adsorption of carbamazepine onto α-Fe_2O_3-DTE was best described by the Langmuir model with a maximum monolayer adsorption of 0.447 mg/g. The adsorption processes were found to follow pseudo-second-order kinetics with a pseudo-equilibrium time of 180 minutes achieving respective removal capacities of 60.9 %, 43 % and 90.15 % for the three sorbents. The adsorption process was pH dependent for α-Fe_2O_3-CBG and β-FeO(OH)-CMC adsorbents with corresponding optimum pH of 6 and 10 for the two adsorbents. However, adsorption onto α-Fe_2O_3-DTE was not affected by variation of solution pH. This study shows that α-Fe_2O_3-CBG and α-Fe_2O_3-DTE can provide an efficient and cost-effective alternative method for removal of CBZ from aquatic ecosystems. The contaminant-laden adsorbent composites are easily recycled using a magnet.

5.2 Recommendations

Results from this study revealed a gap in the conventional treatment methods using aerated lagoons, indicating their inefficiency in removing pharmaceuticals. It is therefore recommended that emerging pollutants such as pharmaceuticals be included in environmental regulation and standards for water monitoring. This will be able to alert the wastewater regulatory bodies to adopt methodologies which will enable reduction of these compounds in wastewater hence minimize their release to the environment.

The surface properties of an adsorbent are critical in an absorption process. It is therefore imperative to characterize adsorbents as prepared with diverse high technology methods to enhance modifications that will improve their sorption capacities. There is need for modification of the structure, surface functional groups and chemistry of biochar, at scales ranging down to nanoscale (nm) structures. This allows certain biochar properties altered in order to target specific environmental contaminants.

Adsorption, being one of the green remediation technologies requires more research especially on locally available adsorbents and also modifications to improve their efficiency and versatility. The use of other magnetic minerals for impregnation also needs to be explored. Furthermore, there is need to explore on the possibility of competing interest for adsorption sites in presence of other organic and inorganic compounds.

Application of these adsorbents in the field and their use in removal of other pollutants needs to be tested. Testing with real environmental samples is important in understanding fouling by organic matter. This will enable a clear understanding of its applicability in remediation of pollutants.

REFERENCES

Adebayo, G. I., Wereiams, J., Healy, S. (2007). Aspirin esterase activity—Evidence for skewed distribution in healthy volunteers. *European Journal of Internal Medicine,* 18.4: 299-303.

Aga, D.S. (2008). Fate of Pharmaceuticals in the Environment and in Water Treatment Systems (CRC Press, Boca Raton, FL, 2008).

Ali, I., Asim, M., Khan, A. (2012). Low cost adsorbents for the removal of organic pollutants from wastewater. *J. Environ. Management*, 113: 170-183.

Al-Khateeb, L.A., Almotiry, S., Salam, M.A. (2014). Adsorption of pharmaceutical pollutants onto graphene nanoplatelets. *Chemical Engineering Journal*, 248: 191–199.

Al-Othman, Z.A., Ali, R., Naushad, Mu. (2012). Hexavalent chromium removal from aqueous medium by activated carbon prepared from peanut shell: Adsorption kinetics, equilibrium and thermodynamic studies. *Chem. Eng. J*., 184: 238– 247.

Al-Rifai, J.H., Khabbaz, H., Schäfer, A.I. (2011). Removal of pharmaceuticals and endocrine isrupting compounds in a water recycling process using reverse osmosis systems. *Separation and Purification Technology*, 77: 60-67.

Anumol, T., Merel, S., Clarke, B.O., Snyder, S.A. (2013). Ultra high performance liquid chromatography tandem mass spectrometry for rapid analysis of trace organic contaminants in water. *Chemistry Central Journal* 7(1): 104. DOI: 10.1186/1752-153X-7-104.

Arun, P.R., Azeez, P.A. (2004). Vulture population decline, diclofenac and avian

gout. *Current Science*, 87: 565-568.

Attia, T.M.S., Hu, X.L., Qiang, Y.D. (2013). Synthesized magnetic nanoparticles coated zeolite for the adsorption of pharmaceutical compounds from aqueous solution using batch and column studies. *Chemosphere*, 93: 2076-2085.

Barrett, E.P., Joyner, L.C., Halenda, P.H., (1951). The determination of pore volume and area distribution in porous substances, *J. Am. Chem. Soc.* 73: 373–380.

Basile, T., Petrella, A., Petrella, M., Boghetich, G., Petruzzelli, V., Colasuonno, S., Petruzzelli, D. (2011). Review of endocrine-disrupting-compound removal technologies in water and wastewater treatment plants: An EU Perspective. *Industrial & Engineering Chemistry Research*, 50(14): 8389-8401.

Beier, S., Cramer, C., Koester, S., Mauer, C., Palmowski, L., Schroeder, H.F., Pinnekamp, J. (2011). Full scale membrane bioreactor treatment of hospital wastewater as forerunner for hot-spot wastewater treatment solutions in high density urban areas. *Water Science and Technology*, 63(1): 66-71

Belessi, V., Romanos, G., Boukos, N., Lambropoulou, D., Trapalis, C. (2009). Removal of Reactive Red 195 from aqueous solutions by adsorption on the surface of TiO2 nanoparticles. *Journal of Hazardous Materials*,170: 836–844.

Ben, W., Qiang, Z., Adams, C., Zhang, H., Chen, L. (2008). Simultaneous determination of sulfonamides, tetracyclines and tiamulin in swine wastewater by solid-phase extraction and liquid chromatography-mass spectrometry. *J. Chromatogr. A*, 1202: 173–180.

Bendz, D., Paxeus, N.A., Ginn, T.R., Loge, F.J. (2005). Occurrence and fate of pharmaceutically active compounds in the environment, a case study: Hoje River in Sweden. *Journal of Hazardous Materials*, 123(3): 195—204.

Blasioli, S., Martucci, A., Geo, P., Lara, G., Maurizio, C., Cliff, T., Marchese, L., Braschi, I. (2014). Removal of sulfamethoxazole sulfonamide antibiotic from water by high silica zeolites: A study of the involved host–guest interactions by a combined structural, spectroscopic, and computational approach. *Journal of Colloid and Interface Science* 419: 148–159.

Boelsterli, U. A. (2003). Diclofenac-induced liver injury: a paradigm of idiosyncratic drug toxicity. *Toxicology and Applied Pharmacology*, 192(3): 307-322.

Bond, T., Huang, J., Templeton, M. R., Graham, N. (2011). Occurrence and control of nitrogenous disinfection by-products in drinking water - A review. *Water Research*, 45(15): 4341-4354.

Bottoni, P., Caroli, S., Caracciolo, A. B. (2010). Pharmaceuticals as priority water contaminants. *Toxicological & Environmental Chemistry*, 92(3): 549-565.

Brown, A.R., Riddle, A.M., Cunningham, N.L., Kedwards, T.J., Shillabeer, N., Hutchinson, T.H. (2003)**.** Predicting the effects of endocrine disrupting chemicals on fish populations. *Hum. Ecol. Risk Assess.* 9: 761–788.

Bruce, G.M., Pleus, R.C., Snyder, S.A. (2010). Toxicological relevance of pharmaceuticals in drinking water. *Environ Sci Technol* , 44: 5619-26.

Burchall, J.J. (1973). Mechanism of action of trimethoprim-sulfamethoxazole. *J. Infect. Dis*. 128: S437–S441.

Cai, M. Q., Wang, R., Feng, L., & Zhang, L. Q. (2014). Determination of selected

pharmaceuticals in tap water and drinking water treatment plant by high-performance liquid chromatography-triple quadrupole mass spectrometer in Beijing, China. *Environmental Science and Pollution Research*, 35: 1-14.

Calisto, V., Esteves, V.I. (2009). Psychiatric pharmaceuticals in the environment. *Chemosphere*, 77 (10): 1257–1274.

Cambria-Kiely, J.A, Gandhi, P.J. (2002). Aspirin resistance and genetic polymorphisms. *Journal of thrombosis and thrombolysis*, 14(1): 51-58.

Caracciolo, A.B., Grenni, P., Sacca, M.L. (2010). Effect of the antiviral drug Oseltamivir (Tamiflu) on the bacterial community structure of a surface water ecosystem analyzed using fluorescence in situ hybridization. *Bulletin of Environmental Contamination and Toxicology*, 85(5): 443-446.

Chang, B.V., Hsub, F.Y., Liao, H.Y. (2014). Biodegradation of three tetracyclines in swine wastewater. *Journal of Environmental Science and Health, Part B: Pesticides, Food Contaminants, and Agricultural Wastes,* 49(6): 449-455.

Chaukura, N., Murimba, E. C., & Gwenzi, W. (2016). Synthesis , characterisation and methyl orange adsorption capacity of ferric oxide – biochar nano-composites derived from pulp and paper sludge. *Applied Water Science*. http://doi.org/10.1007/s13201-016-0392-5.

Chen, H., Bin, G., Hui, Li., Lena, Ma, Q. (2011). Effects of pH and ionic strength on sulfamethoxazole and ciprofloxacin transport in saturated porous media. Journal *of Contaminant Hydrology* 126: 29–36.

Chen, J., Zhang, D., Zhang, H., Ghosh, S., & Pan, B. (2016). Science of the Total Environment Fast and slow adsorption of carbamazepine on biochar as affected

by carbon structure and mineral composition. *Science of the Total Environment*. http://doi.org/10.1016/j.scitotenv.2016.11.052.

Chenxi, W., Spongberg, A.L., Witter, J.D. (2008). Determination of the persistence of pharmaceuticals in biosolids using liquid-chromatography tandem mass spectrometry. *Chemosphere,* 73: 511-518.

Chirikona, F., Filipovic, M., Ooko, S., Orata, F. (2015). Perfluoroalkyl acids in selected wastewater treatment plants and their discharge load within the Lake Victoria basin in Kenya. *Environ Monit Assess,* 187: 238.

Choina, J., Bagabas, A., Fischer, C., Flechsig, G.U., Kosslick, H., Alshammari, A., Schulz, A. (2014). The influence of the textural properties of ZnO nanoparticles on adsorption and photocatalytic remediation of water from pharmaceuticals *Catalysis Today* http://dx.doi.org/10.1016/j.cattod.2014.05.014.

Christen, V., Hickmann, S., Rechenberg, B., Fent, K. (2010). Highly active human pharmaceuticals in aquatic systems: A concept for their identification based on their mode of action. *Journal of Aquatic Toxicology,* 96: 167–181.

Clara, M., Strenn, B., Gans, O., Martinez, E., Kreuzinger, N., Kroiss, H. (2005). Removal of selected pharmaceuticals, fragrances and endocrine disrupting compounds in a membrane bioreactor and conventional WWTPs. *Water Res,* 39: 4797–807.

Crane, M., Watts, C., Boucard, T. (2006). Chronic aquatic environmental risks from exposure to human pharmaceuticals. *Science of the Total Environment*, 367: 23-41.

Daneshvar, A., Aboulfadl, K., Viglino, L., Broséus, R., Sauvé, S., Madoux-Humery, A., Weyhenmeyer, A., Prévost, M. (2012). Evaluating pharmaceuticals and caffeine

as indicators of fecal contamination in drinking water sources of the Greater Montreal region. *Chemosphere,* 88: 131-139.

Danil, A. F., Namor, D., El, A., Frangie, S., Martinez, V., Valiente, L., & Webb, O. A. (2012). Turning the volume down on heavy metals using tuned diatomite . A review of diatomite and modified diatomite for the extraction of heavy metals from water. *Journal of Hazardous Materials*, 241-242: 14–31. http://doi.org/10.1016/j.jhazmat.2012.09.030

de García, S. O., Pinto, G. P., García-Encina, P. A., & Mata, R. I. (2013). Ranking of concern, based on environmental indexes, for pharmaceutical : an application to the Spanish case. *Journal of environmental management*, 129: 384-397.

Devi, P., Saroha, A.K. 2014. Synthesis of the magnetic biochar composites for use as an adsorbent for removal of pentachlorophenol from effluent. *Journal of Bioresource Technology*, 169: 525-531.

Dinsdale, R.M., Kasprzyk-Hordern, B., Guwy, A.J. (2009). The removal of pharmaceuticals, personal care products, endocrine disruptors and illicit drugs during wastewater treatment and its impact on the quality of receiving water. *Water Res*. 43: 363.

Elizalde-gonza, P. (2008). Chemically modified maize cobs waste with enhanced adsorption properties upon methyl orange and arsenic. *Bio resource and technology* 99: 5134–5139. http://doi.org/10.1016/j.biortech.2007.09.023.

Ellis, J.B. (2010). Antiviral pandemic risk assessment for urban receiving waters. *Water Science and Technology*, 61(4): 879-884.

Enick, O.V., Moore, M.M. (2007). Assessing the assessments: pharmaceuticals in the environment. *Environmental Impact Assessment Review*, 27: 707-729.

Ercuta, A., Chirita, M. (2013). Highly crystalline porous magnetite and vacancy-ordered maghemite microcrystals of rhombohedral habit. *J. Crystal Growth*, 380: 182–186.

Escher, B. I., Bramaz, N., Lienert, J., Neuwoehner, J., Straub, J. O. (2010). Mixture toxicity of the antiviral drug Tamiflu (R) (oseltamivir ethylester) and its active metabolite oseltamivir acid. *Aquatic Toxicology*, 96(3): 194-202.

Farré, M., Ferrer, I., Ginebreda, A., Figueras, M., Olivella, L., Tirapu, L., Vilanova, M., Barceló, D. (2001). Determination of drugs in surface water and wastewater samples by liquid chromatography-mass spectrometry: Methods and preliminary results including toxicity studies with Vibrio fischeri. *J. Chromatogr. A*, 938: 187–197.

Freundlich, H.M.F. (1906). U¨ ber die adsorption in lo¨sungen, Z. *Phys. Chem*. 57: 385–470.

Fujiwara, M., Shiokawa, K., Sakakura, I., & Nakahara, Y. (2006). Silica Hollow Spheres with Nano-Macroholes Like Diatomaceous Earth, *Chemosphere*, 33: 3–6.

Gao, Y., Zhang, Y.L.L., Huang, H., Hu, J., Shah, S.M., Su, X. (2012a). Adsorption and removal of tetracycline antibiotics from aqueous solution by graphene oxide. *J Colloid Interface Sci*, 368: 540–546.

Gao, P., Munir, M., Xagoraraki, I. (2012b), Correlation of tetracycline and sulfonamide antibiotics with corresponding resistance genes and resistant bacteria in a conventional municipal wastewater treatment plant. *Sci. Total Environ.* 421:

173–183.

Gathe, J.J., Badaro, R., Grimwood, A., Abrams, L., Klesczewski, K., Cross, A., (2002). Antiviral activity of enteric-coated didanosine, stavudine, and nelfinavir versus zidovudine plus lamivudine and nelfinavir. *J Acquir Immune Defic Syndr*.,31(4): 399–403.

Genc, N., Dogan, C. E. (2015). Adsorption kinetics of the antibiotic ciprofloxacin on bentonite, activated carbon, zeolite, and pumice. *J. Desalination and Water Treatment*, 53(3): 785-793.

Getenga, Z.M., Keng'ara, F.O., Wandiga, S.O. (2004). Determination of organochlorine pesticide residues in soil and water from river Nyando drainage system within lake Victoria basin, Kenya. *Bullettin of Environmental Contamination and Toxicology*, 72: 335-343.

Giger, W., Alder, A. C., Golet, E. M., Kohler, H. P. E., McArdell, C. S., Molnar, E., ... & Suter, M. J. F. (2003). Occurrence and fate of antibiotics as trace contaminants in wastewaters, sewage sludges, and surface waters. *CHIMIA Int. J. Chem.* 57(9), 485-491.

Glassmeyer, S.T., Furlong, E.T., Kolpin, D.W., Cahill, J.D., Zaugg, S.D., Werner, S.L. (2005). Transport of chemical and microbial contaminants from known wastewater discharge: potential for use as indicators of human fecal contamination. *Environmental Science and Technology*, 36: 5157–69.

Golovko, O., Kumar, V., Fedorova, G., Randak, T., Grabic, R. (2014). Seasonal changes in antibiotics, antidepressants/psychiatric drugs, antihistamines and lipid regulators in a wastewater treatment plant. *Chemosphere*, 111: 418-426.

González-Naranjo, V., Boltes, K., Biel, M. (2013). Mobility of ibuprofen, a persistent active drug, in soils irrigated with reclaimed water. *Plant Soil Environ*., 59 (2): 68–73.

Graham, J.P., Polizzotto, M.L. (2013). Pit latrines and their impacts on groundwater quality: a systematic review. *Environ. Health Perspect*. 121: 521-530.

Gregg, S.J., Sing, K.S.W. (1982). Adsorption, surface area and porosity, Ac. Press, New York.

Guler, U.A., Sarioglu, M. (2014). Removal of tetracycline from wastewater using pumice stone: equilibrium, kinetic and thermodynamic studies. *Journal of Environmental Health Science and Engineering*, 12:79.

Han, Y., Cao, X., Ouyang, X., Sohi, S. P., & Chen, J. (2016). Chemosphere Adsorption kinetics of magnetic biochar derived from peanut hull on removal of Cr (VI) from aqueous solution : Effects of production conditions and particle size. *Chemosphere*, 145: 336–341. http://doi.org/10.1016/j.chemosphere.2015.11.050

Heberer, T. (2002). Occurrence, fate, and removal of pharmaceutical residues in the aquatic environment: A review of recent research data. *Toxicol.Lett*. 131: 5–17.

Heberer, T., Fuhrmann, B., Schmidt-Bäumler, K., Tsipi, D., Koutsouba, V., Hiskia, A. (2001). Occurrence of pharmaceutical residues in sewage, river, ground and drinking water in Greece and Germany. *Scientific and regulatory issues*. 791: 70–83

Heberer, T., Reddersen, K., Mechlinski. A. (2002). From municipal sewage to drinking water: Fate and removal of pharmaceutical residues in the aquatic environment in urban areas. *Water Sci. Technol*. 46: 81–88.

Helbling, D.E., Hollender, J., Kohler, H.P.E., Fenner, K. (2010). Structure-based interpretation of biotransformation pathways of amide-containing compounds in sludge-seeded bioreactors. *Environmental Science and Technology*, 44(17): 6628-6635.

Hicks, C., Desgranges, D., Delhommelle, J. (2014). Adsorption and diffusion of the antiparkinsonian drug amantadine in carbon nanotubes. *Molecular Simulation*, 40:7-9, 656-663, DOI: 10.1080/08927022.2013.841908

Ho, Y. S. (2006) Review of second-order models for adsorption systems. *J. Hazard. Mater.*136: 681-689.

Ho, Y.S., McKay, G. (1998). Sorption of dye from aqueous solution by peat. *Chem. Eng. J.* 70: 115–124.

Hollender, J., Zimmermann, S.G., Koepke, S., Krauss, M., McArdell, C.S., Ort, C., Singer, H., von Gunten, U., Siegrist, H. (2009). Elimination of organic micropollutants in a municipal wastewater treatment plant upgraded with a full-scale post-ozonation followed by sand filtration. *Environmental Science and Technology*, 43(20): 7862-7869.

Hornyak, G. L., Tibbals, H.F., Dutta, J. and Moore, J.J. (2008). Introduction to Nanoscience and Nanotechnology, CRC Press, ISBN 9781420047790.

Hu, X., Ding, Z., Zimmerman, A. R., Wang, S., & Gao, B. (2014). Batch and column sorption of arsenic onto iron-impregnated biochar synthesized through hydrolysis. *Water Research*, 68: 206–216.

Huang, K., Tang, J., Zhang, X., Xu, K., Ren, H. (2014). A comprehensive insight into tetracycline resistant bacteria and antibiotic resistance genes in activated sludge

using next-generation sequencing. *Int. J. Mol. Sci.* 15: 10083-10100, doi:10.3390/ijms150610083

Hughes, S.R., Kay, P., Brown, L.E., (2013). Global synthesis and critical evaluation of pharmaceutical data sets collected from river systems. *Environ. Sci. Technol.* 47: 661–677.

Hutchinson, T.H., Beesley, A., Frickers, P.E., Readman, J.W., Shaw, J.P., Straub, J.O. (2009). Extending the environmental risk assessment for oseltamivir (Tamiflu(R) under pandemic use conditions to the coastal marine compartment. *Environment International*, 35 (6): 931-936.

Jain, S., Kumar, P., Vyas, R. K., Pandit, P., Dalai, A. K. (2013). Occurrence and removal of antiviral drugs in environment: a review. *Water, Air, & Soil Pollution*, 224(2): 1-19.

Jeannot, R., Sabik, H., Sauvard, E., Dagnac, T., Dohrendorf, K. (2002). Determination of endocrine-disrupting compounds in environmental samples using gas and liquid chromatography with mass spectrometry. *J. Chrom. Anal.* 974:143-159.

Jelic, A., Gros, M., Ginebreda, A., Cespedes-Sánchez, R., Ventura, F., Petrovic, M., Barceló, D. (2011). Occurrence, partition and removal of pharmaceuticals in sewage water and sludge during wastewater treatment. *Water Res*. 45: 1165-1176.

Jemutai-Kimosop, S., Okello, V.A., Orata, F., Getenga Z.M. and Shikuku V.O. (2016). Green Remediation of Carbamazepine from Water Using Novel Magnetic Iron Modified Carbonized Baggasse: Kinetics, Equilibrium and Mechanistic Studies. *Chemical Science International Journal*. DOI: 10.9734/CSIJ/2017/32444.

Jin, H., Sergio, C., Zhizhou, C., Jun, G., Yueding, X., Jianying, Z. (2014). Biochar pyrolytically produced from municipal solid wastes for aqueous As(V) removal: Adsorption property and its improvement with KOH activation. *Bioresource Technology*, 169: 622–629

Johnson, A.C., Keller, V., Dumont, E., Sumpter, J.P. (2015). Assessing the concentrations and risks of toxicity from the antibiotics ciprofloxacin, sulfamethoxazole, trimethoprim and erythromycin in European rivers. *Science of the Total Environment*, 511:747-755.

Jones, O.A.H., Voulvoulis, N., Lester, J.N. (2002). Aquatic environmental assessment of the top 25 English prescription pharmaceuticals. *Water Res.* 36: 5013–5022.

Juhlin, T., Björkman, S., Gunnarsson, B., Fyge, Å., Roth, B., Höglund, P. (2004). Acute administration of diclofenac, but possibly not long term low dose aspirin, causes detrimental renal effects in heart failure patients treated with ACE-inhibitors. *European Journal of Heart Failure*, 6(7), 909-916.

Kaplan, S., (2013). Review: pharmacological pollution in water. *Crit. Rev. Environ. Sci.Technol.* 43:1074–1116.

Kasprzyk, H.B., Dinsdale, M.R., Guwy, J.A. (2009). The removal of pharmaceuticals, personal care products, endocrine disruptors and illicit drugs during wastewater treatment and its impact on the quality of receiving waters. *Water Research*, 43:363-380.

Kelly, C. (2000). Analysis of steroids in environmental water samples using solid phase extraction and ion-trap gas chromatography-tandem mass spectrometry. *J. Chrom. Anal*. 872: 309-314.

Kern, S., Fenner, K., Singer, H.P., Schwarzenbach, R.P., Hollender, J. (2009). Identification of transformation products of organic contaminants in natural waters by computer-aided prediction and high-resolution mass spectrometry. *Environmental Science & Technology*, 43(18): 7039-7046.

Kihampa, C. (2014). β-lactams and Fluoroquinolone Antibiotics in influents and effluents of Wastewater treatment plants, Dar es Salaam, Tanzania. Research Journal of Chemical Sciences, 4(6), 31-36.

Kim, H., Hong, Y., Park, J.E., Sharma, V.K., Cho, S.J. (2013). Sulfonamides and tetracyclines in livestock wastewater. *Chemosphere*, 91: 888–894.

Kim, S.D., Jensen, J.N., Aga, D.S., Weber, A.S. (2007). Tetracycline as a selector for resistant bacteria in activated sludge. *Chemosphere 66*, 1643–1651.

Kim, Y., Bae, J., Park, J., Suh, J., Lee, S., Park, H., Choi, E.H. (2014). Removal of 12 selected pharmaceuticals by granular mesoporous silica SBA-15 in aqueous phase. *Chemical Engineering Journal*, 256: 475–485.

Kimosop, S. J., Getenga, Z. M., Orata, F., Okello, V. A., & Cheruiyot, J. K. (2016). Residue levels and discharge loads of antibiotics in wastewater treatment plants (WWTPs), hospital lagoons and rivers. *Journal of Environmental Monitoring and Assessment*, http://doi.org/10.1007/s10661-016-5534-6.

Kloss, S., Zehetner, F., Dellantonio, A., Hamid, R., Ottner, F., Liedtke, V., Soja, G. (2012). Characterization of Slow Pyrolysis Biochars: Effects of Feedstocks and Pyrolysis Temperature on Biochar Properties. doi.org/10.2134/jeq2011.0070.

Knoerr, R., Brendlé, J., Lebeau, B., & Demais, H. (2013). Microporous and Mesoporous Materials Preparation of ferric oxide modified diatomite and its application in the

remediation of As (III) species from solution. *Microporous and Mesoporous Materials*, 169, 185–191. http://doi.org/10.1016/j.micromeso.2012.09.036.

Kolpin, D.W., Furlong, E.T., Meyer, M.T., Thurman, E.M., Zaugg, S.D., Barber, L.B., Buxton, H.T. (2002). Pharmaceuticals, hormones, and other organic wastewater contaminants in U.S. streams, 1999–2000: A national reconnaissance. *Environ. Sci. Technol*. 36:1202–1211.

Kolpin, D.W., Skopec, M., Meyer, M.T., Furlong, E.T., Zaugg, S.D. (2004). Urban contribution of pharmaceuticals and other organic wastewater contaminants to streams during differing flow conditions. *Sci. Total Environ.* 328:119–130.

K'oreje, K.O., Kristof, D., Wispelaere, P., Vergeynst, L., Dewulf, J., Langenhove, H. (2012). From multi-residue screening to target analysis of pharmaceuticals in water: Development of a new approach based on magnetic sector mass spectrometry and application in the Nairobi River basin, Kenya. *Sci. Total Environ*. 437: 153–164.

Kosjek, T., Andersen, H.R., Kompare B., Ledin, A., Heath, E. (2009a). Fate of Carbamazepine during Water Treatment. *Environ Sci Technol*, 43:6256-6261.

Kosjek, T., Heath, E., Perez, S., Petrovic, M., Barcelo, D. (2009b). Metabolism studies of diclofenac and clofibric acid in activated sludge bioreactors using liquid chromatography with quadrupole - time-of-flight mass spectrometry. *Journal of Hydrology*, 372(1-4): 109-117.

Kosma, I.C., Lambropouloub, A.D., Albanisa, A.T. (2010). Occurrence and removal of PHCs in Municipal and hospital wastewaters in Greece. *Journal of Hazardous Materials*, 179: 804-817.

Koziel, M.J., Peters, M.G. (2007). "Viral hepatitis in HIV infection". *N. Engl J Med*., 356(14): 1445–1454. doi:10.1056/NEJMra065142.

Kumar, P., Kumar, P.S.K., Kulkarni, R.M. (2014). Fate of Zidovudine through Water Treatment with Chlorine: A Kinetic Study. *Int. Res. J. Environment Sci*. 3(9): 50-55, ISSN 2319–1414.

Kummerer, K. (2001). Drugs in the environment: emission of drugs, diagnostic aids and disinfectants into wastewater by hospitals in relation to other sources - a review. *Chemosphere*, 45(6-7): 957-969.

Kummerer, K. (2008). Pharmaceuticals in the environment: Sources, fate, effects and risks. (3rd ed.), Springer, Berlin Heidelberg, Germany.

Kümmerer, K. (2009). Antibiotics in the aquatic environment—a review Part I. *Chemosphere*, 75: 417–434.

Laifu, L., Manglai, G., Zheng, G., Senfeng, Y. and Yuening, L. (2014). A comparative study and evaluation of sulfamethoxazole adsorption onto organo-montmorillonites. *J. Environ. Sci.,* 26: 2535–2545.

Lake Victoria North Water Services Board and Lake Victoria South Water Services Board Technical Reports, 2012.

Lakshmi, L., Das, N. (2013). Removal of caffeine from industrial wastewater using *Trichosporon asahii*. *Journal of Environmental Biology*, 34:701-708.

Lamm, A., Gozlan, I., Rotstein, A., Avisar, D. (2009). Detection of amoxicillin-diketopiperazine in wastewater samples. *J. Environml Sci. Health A*, 44: 1512–17.

Lang, Y., Monte, F., & Dockery, P. (2017). The Multiple Roles of Diatoms in Environmental Applications : Prospects for Sol-Gel Modi fi ed Diatoms, *Chemosphere*, 101–120. http://doi.org/10.1007/978-3-319-50144-4

Langmuir, I. (1916). The constitution and fundamental properties of solids and liquids. *J. Am. Chem. Soc.* 38: 2221–2295.

Le Roux, J., Gallard, H., Croue, J.P. (2011). Chloramination of nitrogenous contaminants (pharmaceuticals and pesticides): NDMA and halogenated DBPs formation. *Water Research*, 45(10): 3164-3174.

Lee, H. J., Lee, E., Yoon, S. H., Chang, H. R., Kim, K., Kwon, J. H. (2012). Enzymatic and microbial transformation assays for the evaluation of the environmental fate of diclofenac and its metabolites. *Chemosphere*, 87(8), 969-974.

Le-Minh, N., Khan, S.J., Drewes, J.E., Stuetz, R.M. (2010). Fate of antibiotics during municipal water recycling treatment processes. *Water research*, 44: (4296)

Li, B., & Zhang, T. (2011). Mass flows and removal of antibiotics in two municipal wastewater treatment plants. *Chemosphere*, 83(9), 1284-1289.

Li, L., Xu, B. Z., Lin, C. Y., Hu, X. M. (2011). Synergetic degradation of Zidovudine wastewater by ultrasonic and iron-carbon micro-electrolysis. *Advanced Materials Research*, 347-353: 1949-1952.

Li, W.C. (2014). Occurrence, sources, and fate of pharmaceuticals in aquatic environment and soil. A review. *Environ. Poll*., 187: 193-201.

Liang, X., Chen, B., Nie, X., Shi, Z., Huang, X., & Li, X. (2013). The distribution and partitioning of common antibiotics in water and sediment of the Pearl River Estuary, South China. *Chemosphere*, 92(11), 1410–1416.

Lienert, J., Gudel, K., Escher, B.I. (2007). Screening method for ecotoxicological hazard assessment of 42 pharmaceuticals considering human metabolism and excretory routes. *Environ. Sci. Technol*. 41: 4471–4478.

Lienert, J., Larsen, T.A. (2007). Soft paths in wastewater management - The pros and cons of urine source separation. *Gaia-Ecological Perspectives for Science and Society*, 16 (4): 280-288.

Lisouza, F.A., Owuor, P.O., Lalah, J.O. (2011). Variation in indoor levels of polycyclic aromatic hydrocarbons from burning various biomass types in the traditional grass-roofed households in Western Kenya. *Journal of Environmental Pollution,*159: 1810-1815.

Liu, C., Shi, B., Zhou, J., Tang, C. (2011). Quantification and characterization of microporosity by image processing, geometric measurement and statistical methods: application on SEM images of clay materials. *Appl. Clay Sci*.54: 97–106.

Liu, L., Liu, Y., Wang , Z., Liu, C., Huang, X., Zhu, G. (2014). Behavior of tetracycline and sulfamethazine with corresponding resistance genes from swine wastewater in pilot-scale constructed wetlands. *Journal of Hazardous Materials*, 278: 304–310.

Liu, Z. Balasubramanian, R. (2013). A comparison of thermal behaviors of raw biomass, pyrolytic biochar and their blends with lignite. *Bioresource Technology*, 146: 371-378.

Lok, A.S.F., Lai, C.L., Leung, N., Yao, G.B., Cui, Z.Y., Schiff, E.R., Dienstag, J.L., Heathcote, E.J., Little, N.R., Dorothea, R., Gardner, S.D., Griffiths, .A., Castiglia,

M. (2003). Long-term safety of lamivudine treatment in patients with chronic hepatitis B. *Gastroenterology*, 125: 61714–1722.

Luo, Y., Guo, W., Ngo, H.H., Nghiem, L.D., Hai, F.I., Zhang, J., Liang, S., Wang, X.C. (2014). A review on the occurrence of micropollutants in the aquatic environment and their fate and removal during wastewater treatment. *Sci. Total Environ.* 473: 619-641.

Magnér, J., Filipovic, M., Alsberg, T. (2010). Application of a novel solid-phase-extraction sampler and ultra-performance liquid chromatography quadrupole-time-of-flight mass spectrometry for determination of pharmaceutical residues in surface sea water. *Chemosphere*, 80: 1255-1260.

Matozzo, V (2014). Effects of pharmaceuticals on immune parameters of aquatic invertebrates. A review. Invertebrate Survival Journal,11, 163-173, 2014

Mestre, S.A., Bexiga, A.S., Proen, M., Andrade, M., Pinto, M.L., Matos, I., Fonseca, I.M., Carvalho, A.P. (2011). Activated carbons from sisal waste by chemical activation with K_2CO_3: Kinetic of paracetamol and ibuprofen removal from aqueous solution. *Bioresource Technology*, 102:8253-8260.

Michael, I., Rizzo, L., McArdell, C.S., Manaia, C.M., Merlin, C., Schwartz, T., Dagot, C., Fatta-Kassinos, D. (2013). Urban wastewater treatment plants as hotspots for the release of antibiotics in the environment: A review. *Water Res.* 47: 957–995.

Miège, C., Choubert, J.M., Ribeiro, L., Eusèbe, M., Coquery, M. (2009). Fate of pharmaceuticals in wastewater treatment plants - Conception of a database and first results. *Environmental Pollution*, 157(5): 1721-1726.

Mohan, D., Kumar, H., Sarswat, A., Alexandre-franco, M., & Pittman, C. U. (2014). Cadmium and lead remediation using magnetic oak wood and oak bark fast pyrolysis bio-chars. *Chemical Engineering Journal*, 236, 513–528. http://doi.org/10.1016/j.cej.2013.09.057

Mueller, D., Müller-Vieira, U., Biemel, K. M., Tascher, G., Nüssler, A. K., Noor, F. (2012). Biotransformation of diclofenac and effects on the metabolome of primary human hepatocytes upon repeated dose exposure. *European Journal of Pharmaceutical Sciences*, 45(5), 716-724.

Nakata, H., Kannan, K., Jones, P. D., & Giesy, J. P. (2005). Determination of fluoroquinolone antibiotics in wastewater effluents by liquid chromatography–mass spectrometry and fluorescence detection. *Chemosphere*, 58(6), 759-766.

Ng'eno, E.C., Orata, F., Baraza, D.L., Shikuku, V.O. and Jemutai-Kimosop, S. (2016). Adsorption of Caffeine and Ciprofloxacin onto Pyrolitically Derivedwater Hyacinth Biochar: Isothermal, Kinetic and Thermodynamic Studies. *J. Chem. Chem. Eng.*, 10: 185-194.

Nguyen, C., Giang, D., Sebesvari, Z., Renaud, F., & Rosendahl, I. (2015). Occurrence and Dissipation of the Antibiotics Trimethoprim , and Enrofloxacin in the Mekong Delta , Vietnam, 1–24. http://doi.org/10.1371/journal.pone.0131855.

Nikolaou, A., Meric, S., Fatta, D. (2007). Occurrence patterns of pharmaceuticals in water and wastewater environments. *Anal. Bioanal. Chem*. 387: 1225-1234.

Nizamuddin, S., Ahmed, H., Gri, G. J., Mubarak, N. M., Bhutto, W., Abro, R., Si, B. (2017). An overview of effect of process parameters on hydrothermal carbonization of biomass, 73: 1289–1299.

Norsuraya, S., Fazlena, H., & Norhasyimi, R. (2016). Sugarcane Bagasse as a Renewable Source of Silica to Synthesize Santa Barbara Amorphous-15 (SBA-15). *Procedia Engineering*, 148: 839–846.

Oaks, J.L., Gilbert, M., Virani, M.Z., Watson, R.T., Meteyer, C.U., Rideout, B.A., Shivaprasad, H.L., Ahmed, S., Chaudhry, M.I., Arshad, M. (2002). Diclofenac residues as the cause of vulture population decline in Pakistan. *Nature*, 40: 65–81.

Oetken, M., Nentwig, G., Loffler, D., Ternes. T., Oehlmann, J. (2005). Effects of pharmaceuticals on aquatic invertebrates. Part I. The antiepileptic drug carbamazepine. *Arch Environ Contam Toxicol,* 49: 353-361.

Oller, I., Malato, S., Sanchez-Perez, J. A., (2011). Combination of advanced oxidation processes and biological treatments for wastewater decontamination-A review. *Science of the Total Environment*, 409 (20): 4141-4166.

Olsen, B., Munster, V.J., Wallensten, A., Waldenstrom, J., Osterhaus, A., Fouchier, R.A.M. (2006). Global patterns of influenza A virus in wild birds. *Science*, 312(5772): 384-388.

Orata, F., Quinete, N. and Wilken, R. (2009). Long chain perfluorinated alkyl acids derivatisation and identification in biota and abiota matrices using gas chromatography. *Bulletin of Environmental Contamination and Toxicology*, 83: 630-35.

Park, H., Choung, Y. (2007). Degradation of Antibiotics (Tetracycline, Sulfathiazole, Ampicillin) using enzymes of glutathion s-transferase. *Human and ecological risk assessment: International Journal*, 13(5): 1147-55.

Peng, X., Ou, W., Wang, C., Wang, Z., Huang, Q., Jin, J., Tan, J. (2014). Occurrence

and ecological potential of pharmaceuticals and personal care products in groundwater and reservoirs in the vicinity of municipal landfills in China. *Sci. Total Environ.* 490: 889-898.

Phillips, P.J., Smith, S.G., Kolpin, D.W., Zaugg, S.D., Buxton, H.T., Furlong, E.T. (2010). Pharmaceutical formulation facilities as sources of opioids and other pharmaceuticals to wastewater treatment plant effluents. *Environ. Sci. Technol*. 44: 4910–6.

Pradeep, T., Anshup, J. (2009). Noble metal nanoparticles for water purification: A critical review. *Thin Solid Films* 517: 6441–647.

Punyapalakul, P., Sitthisorn, T. (2010). Removal of Ciprofloxazin and Carbamazepine by Adsorption on Functionalized Mesoporous Silicates. *World Academy of Science, Engineering and Technology* 69: 546-550.

Rand-Weaver, M., Margiotta-Casaluci, L., Patel, A., Panter, G.H., Owen, S.F., Sumpter, J.P. (2013). The read-across hypothesis and environmental risk assessment of pharmaceuticals. *Environ Sci Technol*, 47(20): 11384–11395.

Ribeiro, A.V.F.N., Belisário, M., Galazzi, R.M., Balthazar, D.C., Pereira, M.G., Ribeiro, J.N. (2011). Evaluation of two bioadsorbents for removing paracetamol from aqueous media. *Electronic Journal of Biotechnology*, 14(6): 8-16, DOI: 10.2225/vol14-issue6-fulltext-8.

Richardson, S.D., Plewa, M.J., Wagner, E.D., Schoeny, R., De Marini, D.M. (2007). Occurrence, genotoxicity, and carcinogenicity of regulated and emerging disinfection by-products in drinking water: A review and roadmap for research. *Mutation Research-Reviews in Mutation Research*, 636 (1-3): 178-242.

Robertson, W.D. (1994). Chemical fate and transport in a domestic septic system: Site description and attenuation of dichlorobenzene. *Environ. Toxicol. Chem.,* 13: 183–191.

Ruiz, B., Cabrita, I., Mestre, A.S., Parra, J.B., Pires, J., Carvalho, A.P., Ania, C.O. (2010). Surface heterogeneity effects of activated carbons on the kinetics of paracetamol removal from aqueous solution. *Applied Surface Science,* 256: 5171-5175.

Saleh, T.A. (2015). Isotherm, kinetic, and thermodynamics studies on Hg (II) adsorption from aqueous solution by silica-multiwall carbon nanotubes. *Environ Sci Pollut Res*. 22: 16721-16731.

Santos, L.H.M., Araújo, A.N., Fachini, A., Pena, A., Delerue-Matos, C., Montenegro, M.C.B.S.M. (2010). Ecotoxicological aspects related to the presence of pharmaceuticals in the aquatic environment. *Journal of Hazardous Materials,* 175(1-3): 45-95.

Sapawe, N., Jalil, A.A, Triwahyono, S. Shah, M. Jusoh, R. Salleh, N.F.M., Hameed B.H. and Karim, A.H. (2013). Cost-effective microwave rapid synthesis of zeolite Na A for removal of methylene blue. *Chem. Eng. J*., 229: 388–398.

Schaider, L.A., Ruthann, A.R., Ackerman, J.M., Dunagan, S.C., Brody, J.G. (2014). Pharmaceuticals, perfluorosurfactants, and other organic wastewater compounds in public drinking water wells in a shallow sand and gravel aquifer. *Sci. Total Environ*. 468–469: 384–393.

Schmidt, C.K., Brauch, H.J. (2008). N,N-dimethosulfamide as precursor for N-nitrosodimethylamine (NDMA) formation upon ozonation and its fate during drinking water treatment. *Environ. Sci. Technol.,* 42(17): 6340-6346.

Schwaiger, J., Ferling, H., Mallow, U., Wintermayr, H., Negele, R.D. (2004). Toxic effects of the non-steroidal anti-inflammatory drug diclofenac Part 1: histopathological alterations and bioaccumulation in rainbow trout. *Aquatic Toxicology*, 68 (2): 141-150.

Seydel, J.K., Wempe, E., Miller, G.H., Miller, L. (1972). Kinetics and mechanisms of action of trimethoprim and sulfonamides, alone or in combination, upon escherichia-coli. *Chemotherapy,* 17: 217–237.

Shen, R., Andrews, S.A. (2011). NDMA formation kinetics from three pharmaceuticals in four water matrices. *Water Research,* 45(17): 5687-5694.

Sheshde, R.K., Abbasizadeh, S., Nikou, M.R.K., Badii, K. and Sharafi, M.S. (2014). Liquid Phase adsorption kinetics and equilibrium of toluene by novel modified-diatomite. *Journal of Environmental Health Science and Engineering*, 12: 148-149. https://doi.org/10.1186/s40201-014-0148-9.

Shikuku, V. O., Donato, F. F., Kowenje, C. O., Zanella, R., & Prestes, O. D. (2015). A Comparison of Adsorption Equilibrium , Kinetics and Thermodynamics of Aqueous Phase Clomazone between Faujasite X and a Natural Zeolite from Kenya. *S. Afr. J. Chem*., 68: 245–252.

Shikuku, V.O., Kowenje, C.O., Ongeri, D.M.K., Zanella, R., Prestes, O.D. (2014). Removal of tebuconazole from wastewater by zeolite X: kinetics and thermodynamics studies. *Int. J. Eng. Res. Techn*., 3 (8) ISSN: 2278-0181.

Shikuku, V.O., Nyairo, W.N., K'owenje C.O. (2017). Fundamentals and sources of magnetic nanocomposites and their sorption properties: In Tawfik A. Saleh (Editor*) Advanced Nanomaterials for Water Engineering, Treatment and Hydraulics*. pp. 64. *IGI Global publishers*. ISBN13: 9781522521365.

Shimabuku, K. K., Kearns, J.P., Martinez, J.E., Mahoney.B., Moreno-Vasquez L., Summers, R.S. (2016). Biochar sorbents for sulfamethoxazole removal from surface water, stormwater, and wastewater effluent. *Water Research*, 96: 236-245.

Singer, A.C., Colizza, V., Schmitt, H., Andrews, J., Balcan, D., Huang, W. E., Keller, V.D.J., Vespignani, A., Williams, R.J. (2011). Assessing the Ecotoxicologic Hazards of a Pandemic Influenza Medical Response. *Environmental Health Perspectives*, 119(8): 1084-1090.

Singer, A.C., Nunn , M.A., Gould, E.A., Johnson, A. C. (2007). Potential risks associated with the proposed widespread use of Tamiflu. *Environ. Health Perspect*.,115 (1): 102–106.

Snyder, S.A., Westerhoff, P., Yoon, Y., Sedlak, D.L. (2003). Pharmaceuticals, personal care products, and endocrine disruptors in water: Implications for the water industry. *Environ. Eng. Sci.* 20: 449–469.

Song, Z., Lian, F., Yu, Z., Zhu, L., Xing, B., & Qiu, W. (2014). Synthesis and characterization of a novel MnO x -loaded biochar and its adsorption properties for Cu^{2+} in aqueous solution. *Chemical Engineering Journal*, 242: 36–42.

Soufan, M., Deborde, M., Legube, B. (2012). Aqueous chlorination of diclofenac: kinetic study and transformation products identification. *Water research*, 46(10): 3377-3386.

Stackelberg, P.E., Furlong, E.T., Meyer, M.T., Zaugg, S.D., Henderson, A.K., Reissman, D.B. (2004). Persistence of Pharmaceutical compounds and other organic Waste water contaminants in a convectional drinking water treatment plants. *Science of the Total Environment*, 329: 99-113.

Straub, J. O. (2009). An environmental risk assessment for oseltamivir (Tamiflu (R)) for sewage works and surface waters under seasonal-influenza- and pandemic-use conditions. *Ecotoxicology and Environmental Safety*, 72 (6): 1625-1634.

Sun, H.Y., Shi, X., Mao, J.D., Zhu, D.Q. (2010). Tetracycline sorption to coal and soil humic acids: An examination of humic structural heterogeneity. *Environ Toxicol Chem*, 29: 1934–1942.

Teixeira, M.R., Rosa, S.M., Sousa, V. (2011). Natural organic matter and disinfection by-products formation potential in water treatment. *Water Resources Management*, 25(12): 3005-3015.

Tenenbaum , I., Chefetz, B., Avisar, D. (2014). Physicochemical behavior of Tetracycline and 17α -Ethinylestradiol with wastewater sludge-derived humic substance. *Water Air Soil Pollut*., 225: 2155. DOI: 10.1007/s11270-014-2155-y

Ternes, T., Bonerz, M., Schmidt , T. (2001). Determination of neutral pharmaceuticals in wastewater and rivers by liquid chromatography-electrospray tandem mass spectrometry. *J. Chromatogr. A*, 938: 175–185.

Ternes, T.A., Stumpf, M., Mueller, J., Heberer, K., Wilken, R.D., Servos, M. (1999). Behavior and occurrence of estrogens in municipal sewage treatment plants. Investigations in Germany, Canada and Brazil. *Sci. Total Environ*. 225: 81–90.

Thacker, P.D. (2005). Pharmaceutical data elude researchers. *Environ Sci Technol* 39: 193A-194A

Thattai, S., Khurana, P., Boken, J., Prasad, S., Kumar, D. (2014). Nanoparticles and coreshell nanocomposite based new generation water remediation materials and analytical techniques: A review. *Microchemical Journal*, 116: 62-76.

Treybal, R.E. (1981). Mass-transfer Operations, 3rd ed., McGraw-Hill.

van de Steene, J.C., Lambert, W.E. (2008).Validation of a solid-phase extraction and liquid chromatography-electrospray tandem mass spectrometric method for the determination of nine basic pharmaceuticals in wastewater and surface water samples. *Journal Chromatography A*, 1182(2): 153–60.

van de Steene, J.C., Mortier, K.A., Lambert, W.E. (2006). Tackling matrix effects during development of a liquid chromatographic-electrospray ionisation tandem mass spectrometric analysis of nine basic pharmaceuticals in aqueous environmental samples. *Journal of Chromatogry A*, 1123(1): 71–81.

van de Ven, K., van Dongen, W., Maes, B.U.W., Esmans, E.L., Blust, R., de Coen, W.M. (2004). Determination of diazepam in aquatic samples by capillary liquid chromatography electrospray tandem mass spectrometry. *Chemosphere*, 57(8): 967–73.

Vazquez-Roig, P., Kasprzyk-Hordern, B., Blasco, C., Picó, Y. (2014). Stereoisomeric profiling of drugs of abuse and pharmaceuticals in wastewaters of Valencia (Spain). *Science of the Total Environment*, 494–495: 49–57.

Vieno, N., Sillanpää, M. (2014). Fate of diclofenac in municipal wastewater treatment plant—A review. *Environment International*, 69: 28-39.

von Gunten, U. (2003). Ozonation of drinking water: Part I. Oxidation kinetics and product formation. *Water Research*, 37(7): 1443-1467.

Wang, T., Su, J., Jin, X., Chen, Z., Megharaj, M., Naidu, R. 2013. Functional clay supported bimetallic nZVI/Pd nanoparticles used for removal of methyl orange from aqueous solution. *Journal of Harzardous Materials*, 262: 819-825.

Watkinson, A.J., Murby, E.J., Kolpin, D.W., Constanzo, S.D., (2009). The occurrence of antibiotics in an urban watershed: From wastewater to drinking water. *Journal of Science and the Total Environment*, 407: 2711-23.

Weber, W. J., and Morris, J. C. (1963). "Kinetics of Adsorption on Carbon from Solution." *J. San. Eng.: Am. Soc. Civ. Eng.* 89: 31-59.

Wei, D., Hao, H., Guo, W., Xu, W., Zhang, Y., Du, B., & Wei, Q. (2016). Biosorption of effluent organic matter onto magnetic biochar composite : Behavior of fluorescent components and their binding properties. *Bioresource Technology*, 214: 259–265.

Werimo, K., Bergwerff, A., Seinen, W. (2009). Residue levels of organochlorines and organophosphates in water, fish and sediments from Lake Victoria-Kenyan portion. *Journal of Aquatic Ecosystem Health & Management*, 12(3): 337 – 341.

Wick, A., Wagner, M., Ternes, T. A. (2011). Elucidation of the transformation pathway of the opium alkaloid codeine in biological wastewater treatment. *Environmental Science and Technology*, 45(8): 3374-3385.

Wiegel, S., Aulinger, A., Brockmeyer, R., Harms, H., Löffler, J., Reincke, H., Schmidt, R., Stachel, B., Von Tümpling, W., Wanke, A. (2004). Pharmaceuticals in the river Elbe and its tributaries. *Chemosphere*, 57: 107-126.

Wieren, E.M.V., Seymour, M.D., Peterson, J.W. (2012). Interaction of the fluoroquinolone antibiotic, ofloxacin, with titanium oxide nanoparticles in water: Adsorption and breakdown. *Science of the Total Environment*, 441: 1–9.

Wong, S., Appleberg, M., Ward, C. M., Lewis, D.R. (2004). Aspirin resistance in cardiovascular disease: a review. *European journal of vascular and endovascular surgery*, 27(5): 456-465.

Wood, T.P., Duvenage, C.S.J., Rohwer, E. (2015). The occurrence of anti-retroviral compounds used for HIV treatment in South African surface water. *Environmental Pollution*, 199: 235-243.

Wu, R., Liu, J.H., Zhao, L., Zhang, X., Xie, J., Yu, B., Ma, X., Yang, S.T., Wang, H., Liu, Y. (2014). Hydrothermal preparation of magnetic Fe_3O_4@C nanoparticles for dye adsorption. *Journal of Environmental Chemical Engineering*, 2: 907–913.

Yang, X., Flowers, R.C., Weinberg, H.S., Singer, P.C. (2011). Occurrence and removal of pharmaceuticals (PHCs) in an advanced wastewater reclamation plant. *Water Research*, 45(16): 5218-5228.

Yao, Y., Gao, B., Fang, J., Zhang, M., Chen, H., Zhou, Y., Yang, L. (2014). Characterization and environmental applications of clay – biochar composites. *Chemical Engineering Journal*, 242: 136–143.

Yu, W., Deng, L., Yuan, P., Liu, D., & Yuan, W. (2015). Preparation of hierarchically porous diatomite / MFI-type zeolite composites and their performance for benzene adsorption : The effects of desilication. *Chemical Engineering Journal*. http://doi.org/10.1016/j.cej.2015.02.065.

Yu, Y., Wu, L. (2012). Analysis of endocrine disrupting compounds, pharmaceuticals in

sewage sludge by gas chromatography-mass spectrometry. *Talanta*, 89: 258-263.

Yuan, P., Liu, D., Tan, D., Liu, K., Yu, H., & Zhong, Y. (2013). Microporous and Mesoporous Materials Surface silylation of mesoporous / macroporous diatomite (diatomaceous earth) and its function in Cu(II) adsorption : The effects of heating pretreatment. *Microporous and Mesoporous Materials*, 170: 9–19. http://doi.org/10.1016/j.micromeso.2012.11.030.

Zhang, D., Niu, H., Zhang, X., Meng, Z., Cai, Y. (2011). Strong adsorption of chlorotetracyline on magnetite nanoparticles. *J. Hazard. Mater.*, 192: 1088–1093.

Zhang, M., Gao, B., Varnoosfaderani, S., Hebard, A., Yao, Y., & Inyang, M. (2013). Bioresource Technology Preparation and characterization of a novel magnetic biochar for arsenic removal. *Bioresource Technology*, 130: 457–462. http://doi.org/10.1016/j.biortech.2012.11.132.

Zhang, X., Zhang, T. (2011). Occurrence, abundance, and diversity of tetracycline resistance genes in sewage treatment plants across China and other global locations. *Environ. Sci. Technol.*, *45*: 2598–2604.

Zhang, Y. Z. H., Liang, H. Z. M., & Lu, R. (2012). Adsorption of chromium (VI) from aqueous solution by the iron (III) -impregnated sorbent prepared from sugarcane bagasse, *Bioresource Technology*, 12: 463–472. http://doi.org/10.1007/s13762-012-0043-9.

Zhang, Y., Geißen, S. U., & Gal, C. (2008). Carbamazepine and diclofenac: removal in wastewater treatment plants and occurrence in water bodies. *Chemosphere*, 73(8): 1151-1161.

Zhao, Y., Geng, J., Wang, X., Gu, X., Gao, S. (2011). Adsorption of tetracycline onto goethite in the presence of metal cations and humic substances. *J Colloid Interface Sci*, 361: 247–251.

Zhu, J., Snow, D.D., Cassada, D.A., Monson, S.J., Spalding, R.F. (2010). Analysis of oxytetracycline, tetracycline, and chlortetracycline in water using solid-phase extraction and liquid chromatography-tandem mass spectrometry. *J. Chromatography. A*, 928: 177–186.

Zimmermann, S.G., Wittenwiler, M., Hollender, J., Krauss, M., Ort C., Siegrist, H., von Gunten, U. (2011). Kinetic assessment and modeling of an ozonation step for full-scale municipal wastewater treatment: Micropollutant oxidation, by- product formation and disinfection. *Water Research,* 45(2): 605-617.

Zuccato, E., Castiglioni, S., Bagnati, R., Melis, M., Fanelli, R., (2010). Source, occurrence and fate of antibiotics in the Italian aquatic environment. *J. Hazardous* Materials, 179: 1042-1048.

APPENDICES

Appendix 1: A photograph showing influent sampling from a WWTP in Kakamega

Appendix 2: A photograph showing effluent sampling from Nyalenda WWTP in Kisumu

Appendix 3: A photograph showing collection of sludge sample from Eldoret WWTP

Appendix 4: A photograph of Auji river in Kisumu at discharge point to Lake Victoria

Appendix 5: A phorograph showing HPLC analysis of pharmaceutical residues

Appendix 6: HPLC Chromatogram for raw waste water influent sample

Sample Information

C:\LabSolutions\Method folder\wash.lcmAcquired by : Admin

Sample Name: KWIN 1
Sample ID: KWIN 1
Time: 5:15:56 PM
20
C:\LabSolutions\Data\KIMOSOP\091015-33.lcd

Chromatogram

KWIN 1 C:\LabSolutions\Data\KIMOSOP\091015-33.lcd

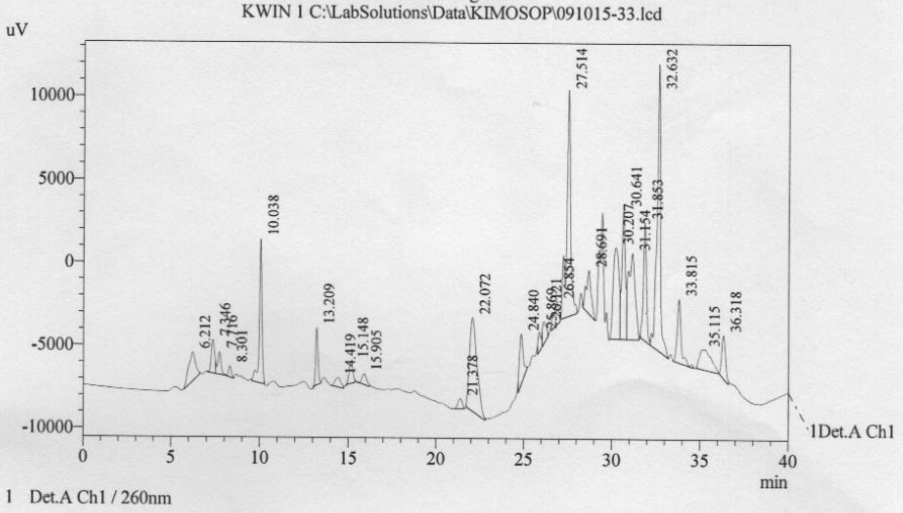

1 Det.A Ch1 / 260nm

PeakTable

Detector A Ch1 260nm

Name	Ret. Time	Area	Area %	ID#
	6.212	47058	2.826	
	7.346	26262	1.577	
	7.716	18601	1.117	
	8.301	7239	0.435	
	10.038	90585	5.439	
	13.209	30788	1.849	
	14.419	12924	0.776	
	15.148	20296	1.219	
	15.905	11577	0.695	
	21.378	11172	0.671	
	22.072	168494	10.118	
	24.840	44871	2.694	
	25.869	13740	0.825	
	26.121	18652	1.120	
	26.854	28661	1.721	
	27.514	215406	12.935	
	28.691	51004	3.063	
	30.207	122479	7.355	

Appendix 7: HPLC Chromatogram for treated waste water effluent sample

Sample Information

C:\LabSolutions\Method folder\wash.lcmAcquired by : Admin

Sample Name: BWEF 1
Sample ID: BWEF 1
Time: 1:03:20 AM
20
C:\LabSolutions\Data\KIMOSOP\091015-42.lcd

Chromatogram

BWEF 1 C:\LabSolutions\Data\KIMOSOP\091015-42.lcd

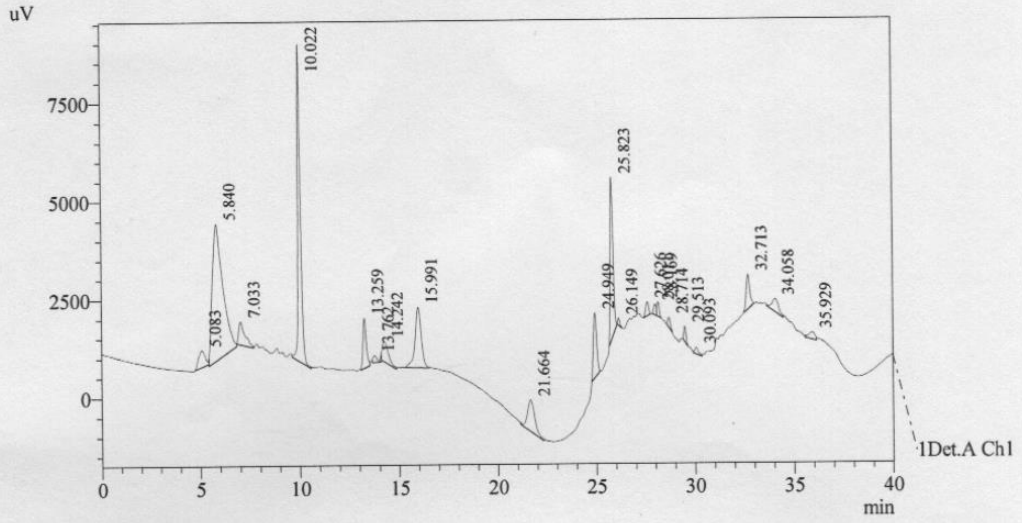

1 Det.A Ch1 / 260nm

PeakTable

Detector A Ch1 260nm

Name	Ret. Time	Area	Area %	ID#
	5.083	10169	2.451	
	5.840	128705	31.025	
	7.033	12561	3.028	
	10.022	79379	19.135	
	13.259	14626	3.526	
	13.762	2837	0.684	
	14.242	11060	2.666	
	15.991	33944	8.182	
	21.664	20811	5.017	
	24.949	19447	4.688	
	25.823	40906	9.861	
	26.149	1305	0.315	
	27.626	3723	0.897	
	28.011	2388	0.576	
	28.169	2995	0.722	
	28.714	2342	0.565	
	29.513	2915	0.703	
	30.093	2144	0.517	

Appendix 8: LC-MS/MS Chromatogram for carbamazepine

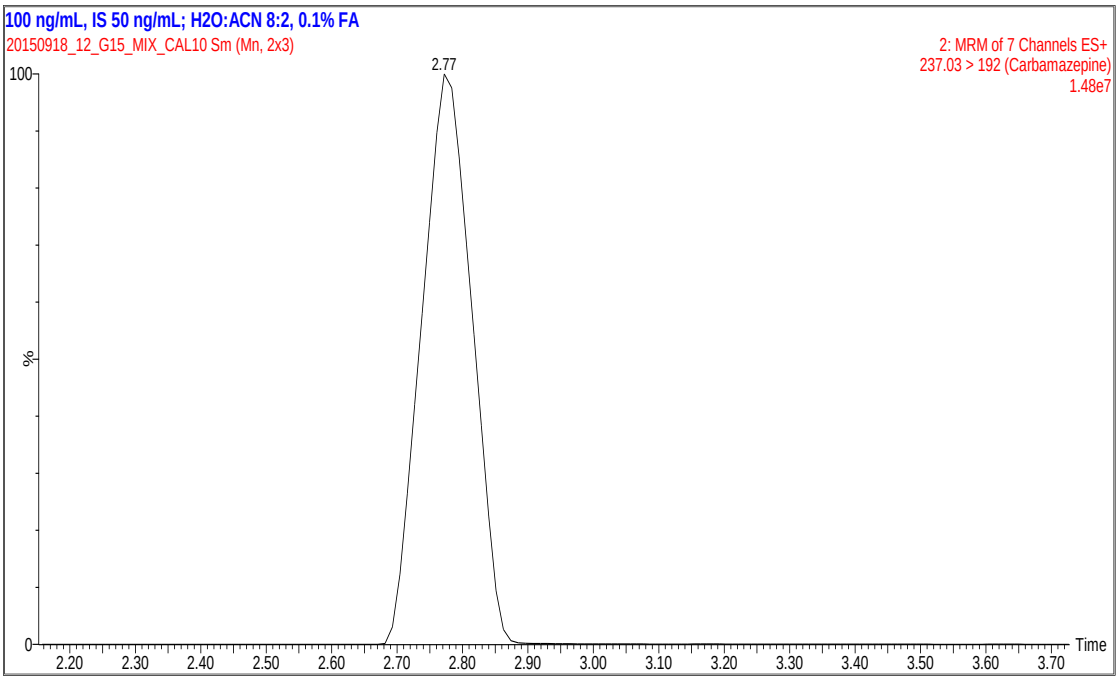

Appendix 9: LC-MS/MS Chromatogram for sulfamethoxazole

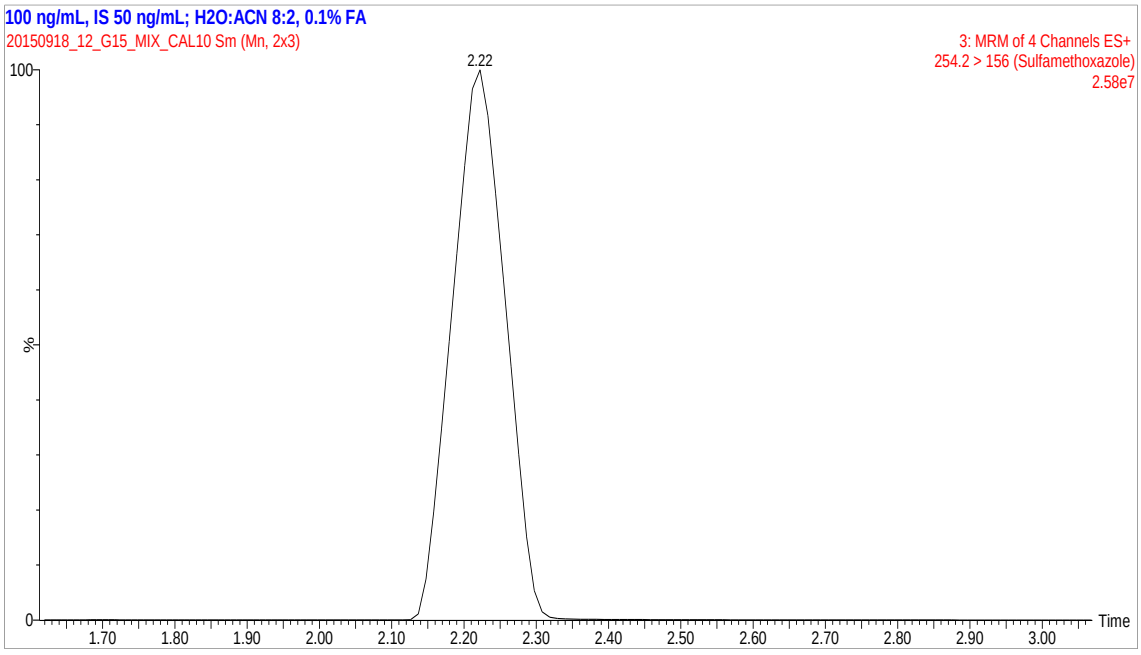

Appendix 10: XRF Data for carbonized baggase biochar

Sample : C
Operator: ADATI
Comment : Baggasse bio..
Group : easy
Date : 2017-01-05 13:03:14

Measurement Condition

Instrument: 800HS2	Atmosphere: Air	Collimator: 10(mm)	Spin: Off

Analyte	TG kV	uA	FI	Acq.(keV)	Anal.(keV)	Time(sec)	DT(%)
Ti-U	Rh 50	100-Auto	----	0 - 40	0.00-40.00	Live- 50	26
Na-Sc	Rh 15	756-Auto	----	0 - 20	0.00- 4.40	Live- 50	26

Qualitative Result

Element: Rh, K , Ca, Ti, Mn, Fe, Cu, Zn, Si

Peak List

Channel	Line	keV	Net Int.(cps/uA)	
Ti-U	RhLa	2.70	0.8560	
	RhLb2	2.96	0.7554	
	K Ka	3.32	1.8787	
	CaKa	3.68	1.9481	
	CaKb	4.00	0.2709	
	TiKa	4.52	0.2169	QF
	MnKa	5.88	1.3213	QF
	FeKa	6.40	5.5895	QF
	MnKb	6.50	0.2191	
	FeKb	7.04	0.8525	
	CuKa	8.00	0.2520	QF
	ZnKa	8.64	0.3954	QF
	RhKaC	19.20	3.6309	
	RhKa	20.18	0.7832	
	----	21.46	0.6310	
Na-Sc	----	0.94	0.0066	
	----	1.55	0.0093	
	SiKa	1.73	0.0158	QF
	RhLa	2.69	0.4167	
	RhLb2	2.96	0.3449	
	K Ka	3.32	0.6935	QF
	K Kb	3.59	0.0971	
	CaKa	3.69	0.6860	QF
	CaKb	4.02	0.0960	
	TiKa	4.51	0.0780	
	MnKa	5.90	0.2550	
	FeKa	6.40	0.9503	
	MnKb	6.49	0.0383	
	FeKb	7.07	0.1325	

Quantitative Result

Analyte	Result	(Std.Dev.)	Proc.-Calc.	Line	Int.(cps/uA)
Ca	37.521 %	(0.259)	Quan-FP	CaKa	0.6860
K	29.522 %	(0.199)	Quan-FP	K Ka	0.6935
Fe	18.528 %	(0.118)	Quan-FP	FeKa	5.5895
Mn	5.491 %	(0.081)	Quan-FP	MnKa	1.3213
Si	5.290 %	(0.286)	Quan-FP	SiKa	0.0158
Ti	2.207 %	(0.108)	Quan-FP	TiKa	0.2169
Zn	0.821 %	(0.034)	Quan-FP	ZnKa	0.3954
Cu	0.622 %	(0.040)	Quan-FP	CuKa	0.2520

Appendix 11: XRF Spectra of raw bio-oil

Sample : D
Operator: ADATI
Comment : Modified baggasse bio..
Group : easy
Date : 2017-01-05 13:07:28

Measurement Condition

Instrument: 800HS2 Atmosphere: Air Collimator: 10(mm) Spin: Off

Analyte	TG	kV	uA	FI	Acq.(keV)	Anal.(keV)	Time(sec)		DT(%)
Ti-U	Rh	50	13-Auto	----	0 - 40	0.00-40.00	Live-	50	25
Na-Sc	Rh	15	100-Auto	----	0 - 20	0.00- 4.40	Live-	50	26

Qualitative Result

Element: Cl, Fe, Mn, Zn, Rh, Pd, K , Ca

Peak List

Channel	Line	keV	Net Int.(cps/uA)	
Ti-U	ClKa	2.62	10.7341	
	----	3.32	0.5241	
	----	3.68	0.6219	
	FeKaESC	4.62	1.2496	
	MnKa	5.88	1.0285	QF
	FeKa	6.40	395.5108	QF
	MnKb	6.50	0.1543	
	FeKb	7.04	61.7200	
	ZnKa	8.60	0.7380	QF
	FeKaSUM	12.78	1.3903	
	RhKaC	19.14	6.9101	
	RhKa	20.14	5.1726	
	----	21.34	1.3163	
Na-Sc	ClKaESC	0.87	0.0622	
	ClKa	2.62	4.7097	QF
	ClKb	2.82	0.4041	
	PdLa	2.84	0.2293	
	PdLb1	2.97	0.2913	
	K Ka	3.32	0.1692	QF
	K Kb	3.59	0.0237	
	CaKa	3.69	0.2125	QF
	FeKaESC	4.64	0.2226	
	FeKa	6.40	56.2489	
	FeKb	7.06	8.4213	
	FeKaSUM	12.83	0.1744	

Quantitative Result

Analyte	Result	(Std.Dev.)	Proc.-Calc.	Line	Int.(cps/uA)
Fe	78.803 %	(0.153)	Quan-FP	FeKa	395.5108
Cl	19.201 %	(0.128)	Quan-FP	ClKa	4.7097
K	0.871 %	(0.040)	Quan-FP	K Ka	0.1692
Ca	0.709 %	(0.029)	Quan-FP	CaKa	0.2125
Mn	0.214 %	(0.014)	Quan-FP	MnKa	1.0285
Zn	0.201 %	(0.014)	Quan-FP	ZnKa	0.7380

Appendix 13: XRF Spectrum of unmodified bagasse

Sample : B
Operator: ADATI
Comment : Maize cob bio..
Group : easy
Date : 2017-01-05 12:54:26

Measurement Condition

Instrument: 800HS2 Atmosphere: Air Collimator: 10(mm) Spin: Off

Analyte	TG	kV	uA	FI	Acq.(keV)	Anal.(keV)	Time(sec)		DT(%)
Ti-U	Rh	50	27-Auto	----	0 - 40	0.00-40.00	Live-	49	25
Na-Sc	Rh	15	205-Auto	----	0 - 20	0.00- 4.40	Live-	50	24

Qualitative Result

Element: Rh, K , Fe, Zn, Cl, Pd

Peak List

Channel	Line	keV	Net Int.(cps/uA)	
Ti-U	RhLa	2.64	5.1848	
	----	2.92	0.6858	
	K Ka	3.32	5.9069	
	K Kb	3.60	0.9285	
	FeKaESC	4.64	0.3956	
	FeKa	6.40	99.8611	QF
	FeKb	7.04	15.4991	
	ZnKa	8.66	0.7530	QF
	RhKaC	19.12	8.6211	
	RhKa	20.16	2.9558	
	----	21.48	1.6821	
Na-Sc	ClKaESC	0.89	0.0324	
	ClKa	2.62	2.3671	QF
	ClKb	2.82	0.1894	
	PdLa	2.84	0.3467	
	PdLb1	2.98	0.2500	
	K Ka	3.31	2.1475	QF
	K Kb	3.60	0.3323	
	FeKa	6.40	15.7699	
	FeKb	7.06	2.3767	

Quantitative Result

Analyte	Result	(Std.Dev.)	Proc.-Calc.	Line	Int.(cps/uA)
Fe	53.940 %	(0.147)	Quan-FP	FeKa	99.8611
K	26.239 %	(0.182)	Quan-FP	K Ka	2.1475
Cl	19.426 %	(0.129)	Quan-FP	ClKa	2.3671
Zn	0.395 %	(0.024)	Quan-FP	ZnKa	0.7530

Appendix 15: XRF Spectrum carbonized maize cob

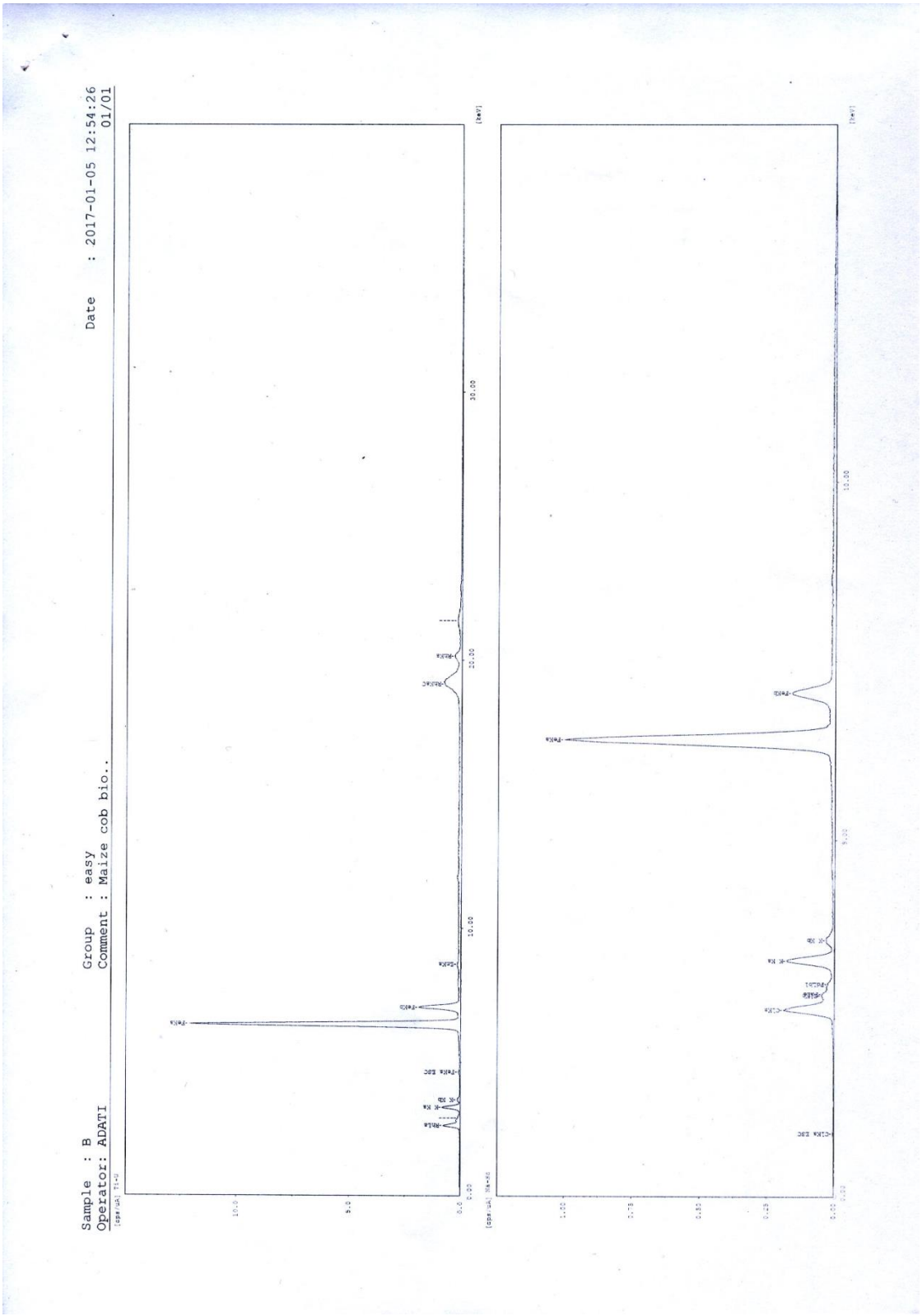

Sample : A
Operator: ADATI
Comment : Modified maize cob bio..
Group : easy
Date : 2017-01-05 12:49:26

Measurement Condition

Instrument: 800HS2	Atmosphere: Air	Collimator: 10(mm)	Spin: Off

Analyte	TG kV	uA	FI	Acq.(keV)	Anal.(keV)	Time(sec)	DT(%)
Ti-U	Rh 50	13-Auto	----	0 - 40	0.00-40.00	Live- 50	25
Na-Sc	Rh 15	100-Auto	----	0 - 20	0.00- 4.40	Live- 50	24

Qualitative Result

Element: Cl, K , Fe, Rh, Pd

Peak List

Channel	Line	keV	Net Int.(cps/uA)	
Ti-U	ClKa	2.62	12.4569	
	K Ka	3.32	1.5742	
	FeKaESC	4.64	1.2699	
	FeKa	6.40	354.2557	QF
	FeKb	7.04	56.3031	
	RhKaC	19.16	9.0793	
	RhKa	20.16	7.0456	
	----	21.48	1.8983	
Na-Sc	ClKaESC	0.87	0.0739	
	ClKa	2.62	5.2386	QF
	ClKb	2.82	0.4602	
	PdLa	2.84	0.3384	
	PdLb1	2.99	0.1607	
	K Ka	3.32	0.5608	QF
	K Kb	3.61	0.0868	
	FeKaESC	4.68	0.1779	
	FeKa	6.40	48.5848	
	FeKb	7.05	7.6674	
	FeKaSUM	12.82	0.1670	

Quantitative Result

Analyte	Result	(Std.Dev.)	Proc.-Calc.	Line	Int.(cps/uA)
Fe	74.879 %	(0.154)	Quan-FP	FeKa	354.2557
Cl	21.995 %	(0.139)	Quan-FP	ClKa	5.2386
K	3.126 %	(0.065)	Quan-FP	K Ka	0.5608

Appendix 17: XRF Spectra of microwave modified maize bio-char

Appendix 18: XRF Spectrum for Diatomaceous Earth

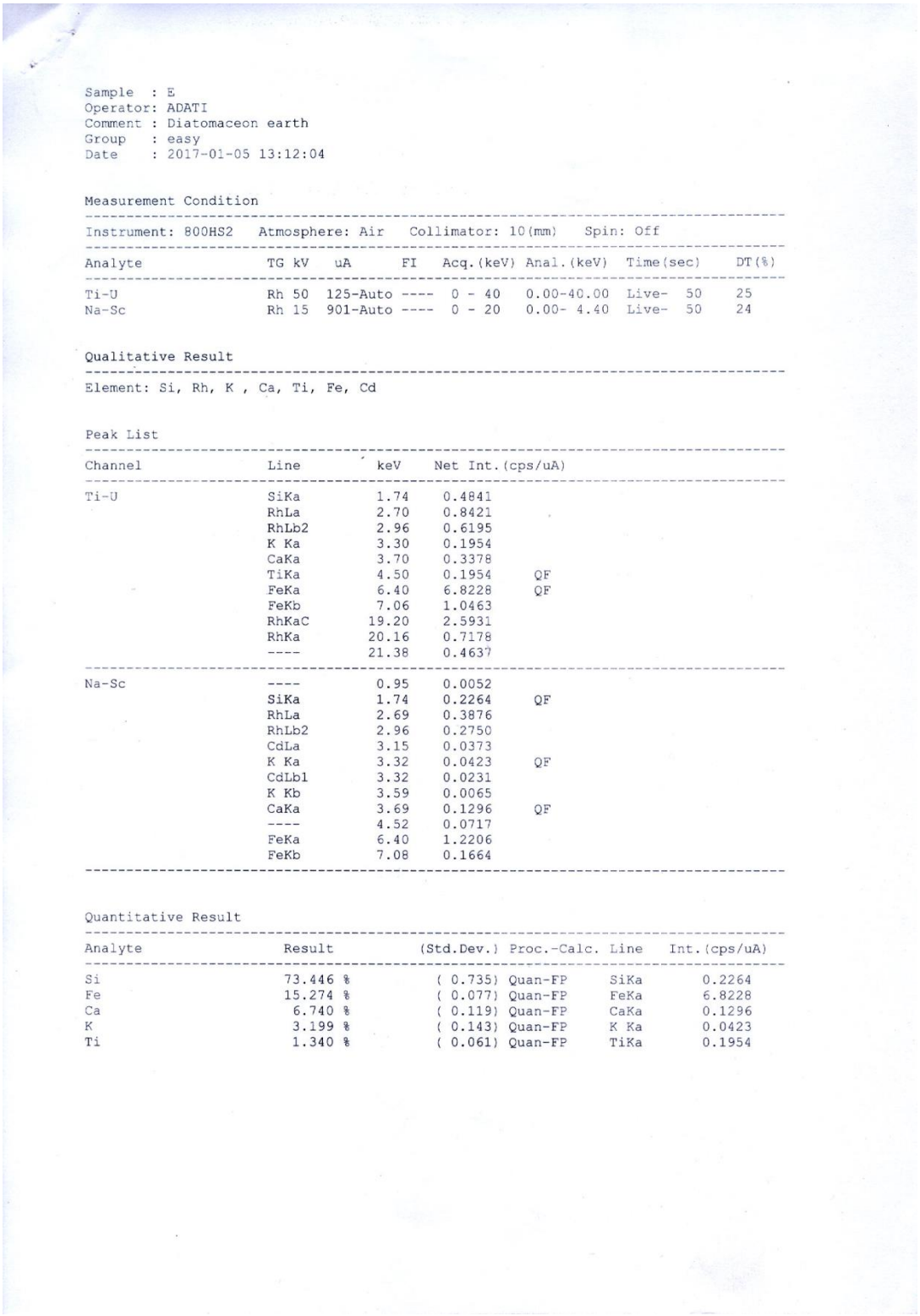

Sample : E
Operator: ADATI
Comment : Diatomaceon earth
Group : easy
Date : 2017-01-05 13:12:04

Measurement Condition

Instrument: 800HS2 Atmosphere: Air Collimator: 10(mm) Spin: Off

Analyte	TG kV	uA	FI	Acq.(keV)	Anal.(keV)	Time(sec)	DT(%)
Ti-U	Rh 50	125-Auto	----	0 - 40	0.00-40.00	Live- 50	25
Na-Sc	Rh 15	901-Auto	----	0 - 20	0.00- 4.40	Live- 50	24

Qualitative Result

Element: Si, Rh, K , Ca, Ti, Fe, Cd

Peak List

Channel	Line	keV	Net Int.(cps/uA)	
Ti-U	SiKa	1.74	0.4841	
	RhLa	2.70	0.8421	
	RhLb2	2.96	0.6195	
	K Ka	3.30	0.1954	
	CaKa	3.70	0.3378	
	TiKa	4.50	0.1954	QF
	FeKa	6.40	6.8228	QF
	FeKb	7.06	1.0463	
	RhKaC	19.20	2.5931	
	RhKa	20.16	0.7178	
	----	21.38	0.4637	
Na-Sc	----	0.95	0.0052	
	SiKa	1.74	0.2264	QF
	RhLa	2.69	0.3876	
	RhLb2	2.96	0.2750	
	CdLa	3.15	0.0373	
	K Ka	3.32	0.0423	QF
	CdLb1	3.32	0.0231	
	K Kb	3.59	0.0065	
	CaKa	3.69	0.1296	QF
	----	4.52	0.0717	
	FeKa	6.40	1.2206	
	FeKb	7.08	0.1664	

Quantitative Result

Analyte	Result	(Std.Dev.)	Proc.-Calc.	Line	Int.(cps/uA)
Si	73.446 %	(0.735)	Quan-FP	SiKa	0.2264
Fe	15.274 %	(0.077)	Quan-FP	FeKa	6.8228
Ca	6.740 %	(0.119)	Quan-FP	CaKa	0.1296
K	3.199 %	(0.143)	Quan-FP	K Ka	0.0423
Ti	1.340 %	(0.061)	Quan-FP	TiKa	0.1954

Appendix 19: XRF Spectrum for Diatomaceous Earth

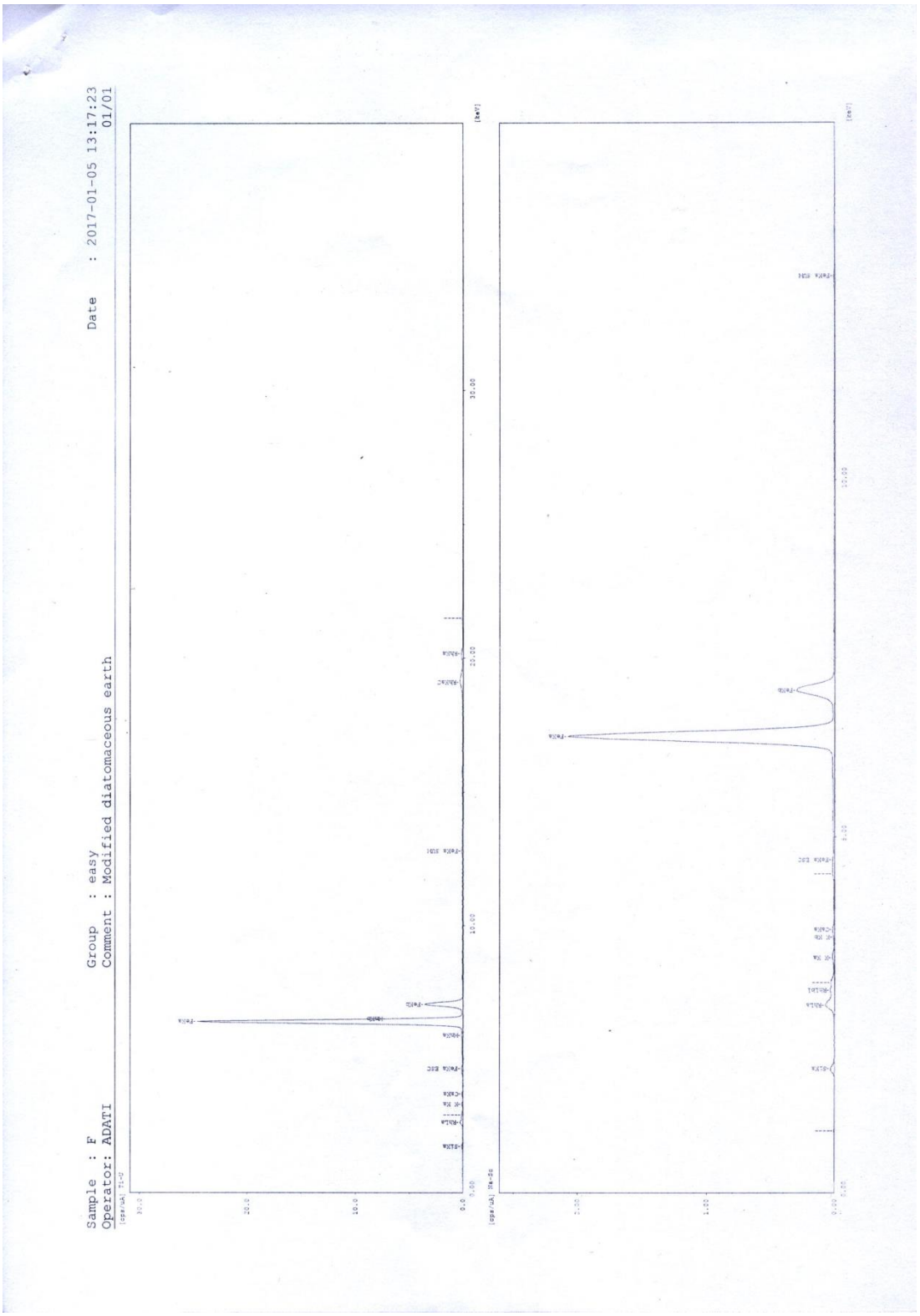

Appendix 20: XRF Data for Modified Diatomaceous Earth

Sample : F
Operator: ADATI
Comment : Modified diatomaceous earth
Group : easy
Date : 2017-01-05 13:17:23

Measurement Condition

Instrument: 800HS2 Atmosphere: Air Collimator: 10(mm) Spin: Off

Analyte	TG kV	uA	FI	Acq.(keV)	Anal.(keV)	Time(sec)	DT(%)
Ti-U	Rh 50	26-Auto	----	0 - 40	0.00-40.00	Live- 50	26
Na-Sc	Rh 15	157-Auto	----	0 - 20	0.00- 4.40	Live- 50	24

Qualitative Result

Element: Si, Rh, K , Ca, Fe, Mn

Peak List

Channel	Line	keV	Net Int.(cps/uA)	
Ti-U	SiKa	1.74	0.6448	
	RhLa	2.64	1.7034	
	----	2.92	0.7248	
	K Ka	3.32	0.5228	
	CaKa	3.70	0.4317	
	FeKaESC	4.64	0.8352	
	MnKa	5.88	0.7564	QF
	FeKa	6.40	205.0498	QF
	MnKb	6.50	0.1135	
	FeKb	7.04	31.0609	
	FeKaSUM	12.80	0.6358	
	RhKaC	19.10	2.9612	
	RhKa	20.18	1.9208	
	----	21.50	0.5141	
Na-Sc	----	0.87	0.0225	
	SiKa	1.74	0.3209	QF
	RhLa	2.63	0.8539	
	RhLb1	2.84	0.3577	
	----	2.95	0.3072	
	K Ka	3.30	0.1607	QF
	K Kb	3.59	0.0204	
	CaKa	3.70	0.1306	QF
	----	4.48	0.1439	
	FeKaESC	4.68	0.1288	
	FeKa	6.40	33.0991	
	FeKb	7.05	4.7326	
	FeKaSUM	12.85	0.1187	

Quantitative Result

Analyte	Result	(Std.Dev.)	Proc.-Calc.	Line	Int.(cps/uA)
Fe	71.108 %	(0.136)	Quan-FP	FeKa	205.0498
Si	26.443 %	(0.533)	Quan-FP	SiKa	0.3209
K	1.417 %	(0.053)	Quan-FP	K Ka	0.1607
Ca	0.757 %	(0.032)	Quan-FP	CaKa	0.1306
Mn	0.275 %	(0.014)	Quan-FP	MnKa	0.7564

Appendix 21: XRF Spectrum for Modified Diatomaceous Earth

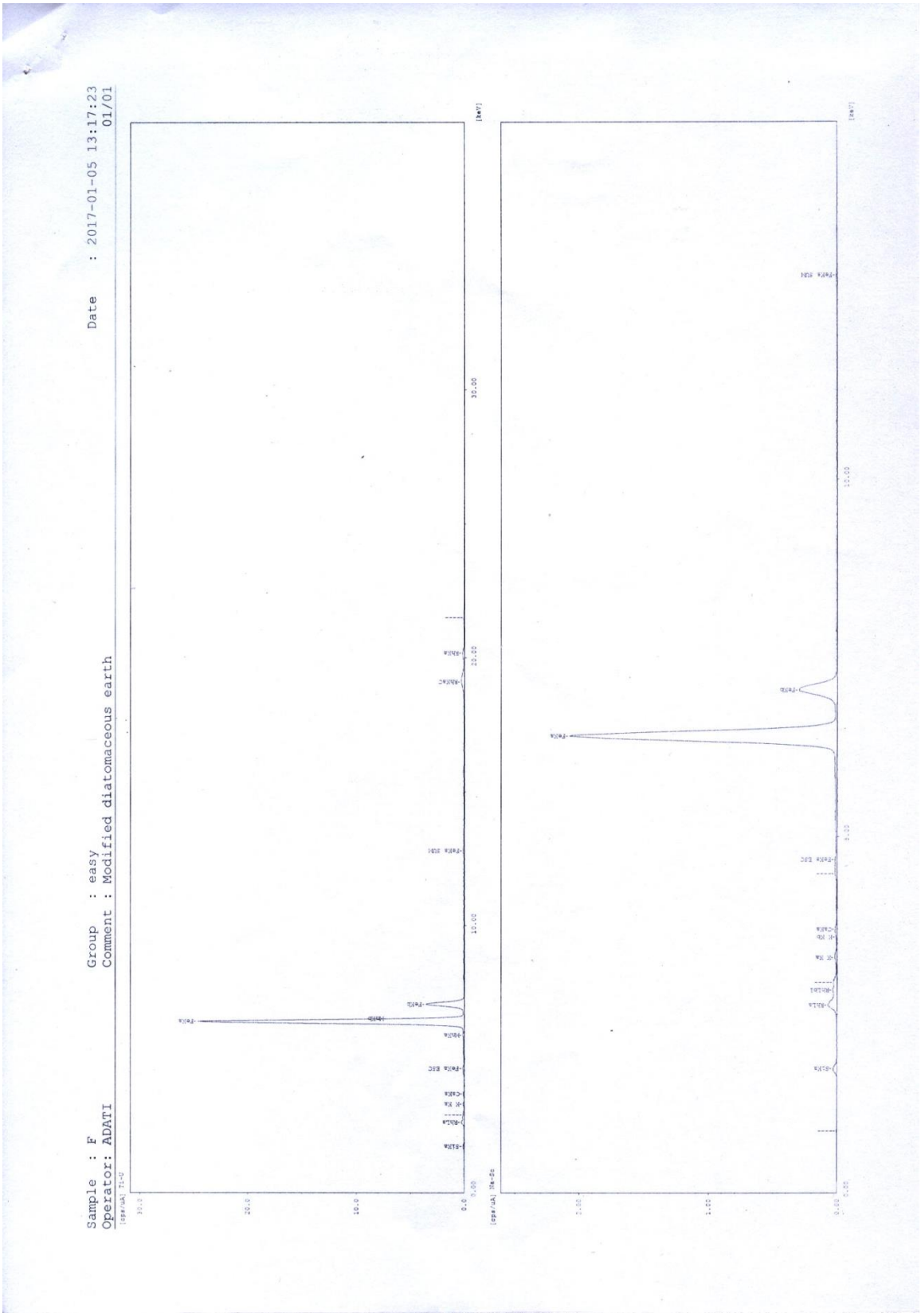

Appendix 22: SEM image of Carbonized Bagasse (CBG) biochar at a magnification of 5.00 KX

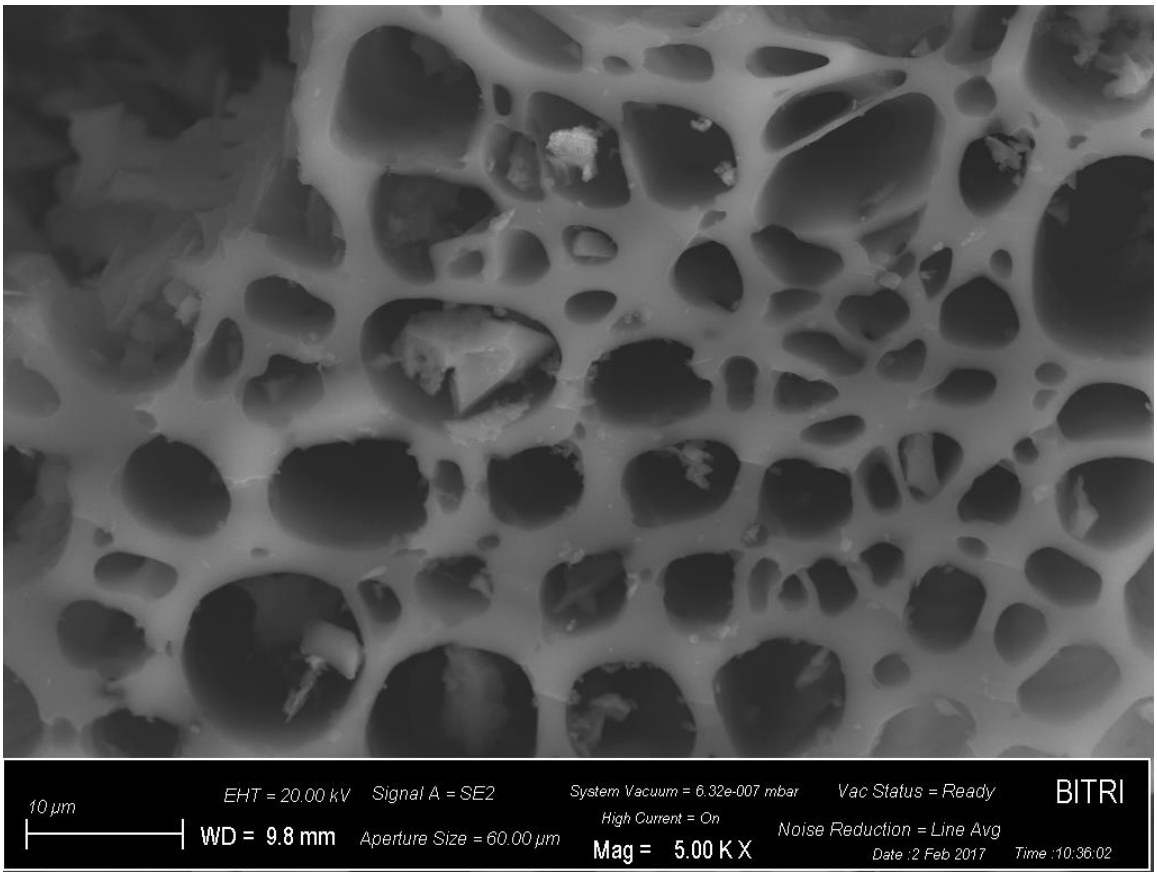

Appendix: 23 SEM image of Carbonized Bagasse (CBG) biochar at a magnification of 2.00 KX

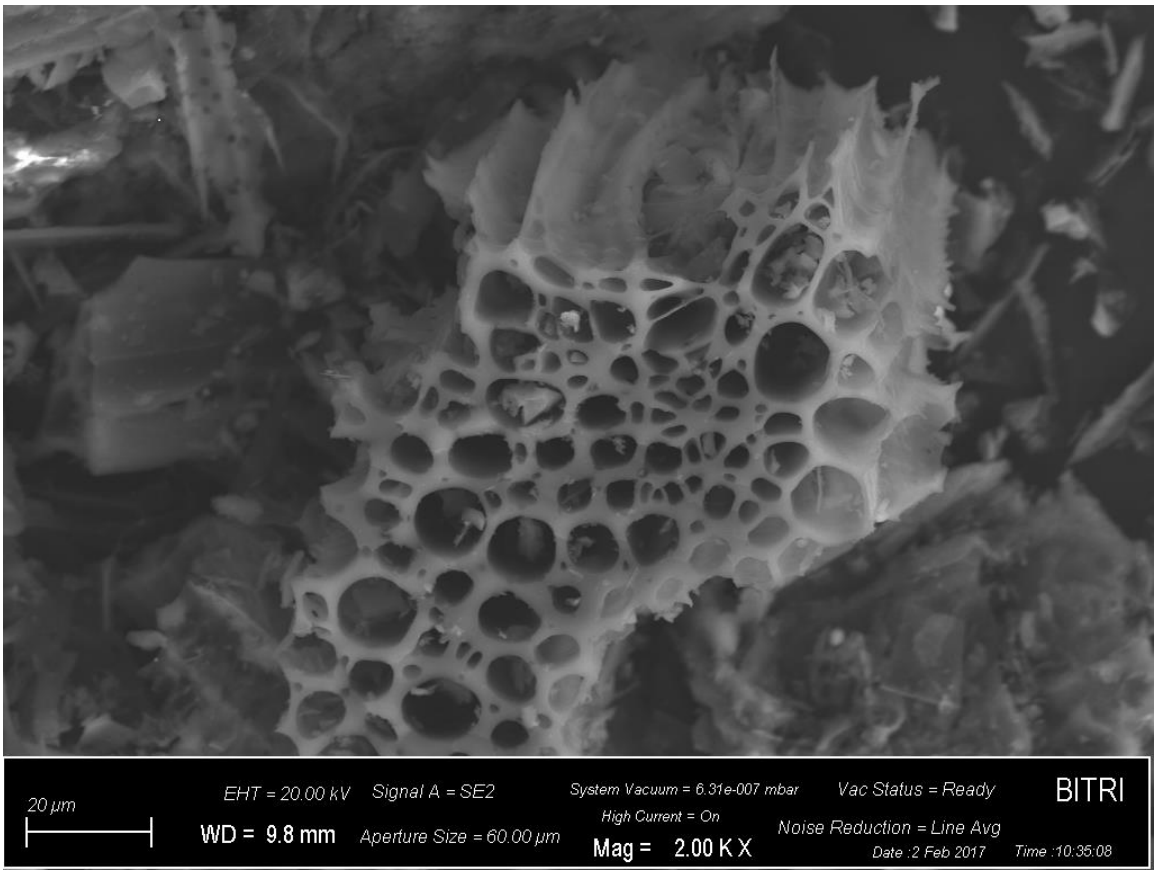

Appendix 24: SEM image of chemically engineered Carbonized Bagasse (α-Fe_2O_3-CBG) adsorbent composite at a magnification of 5.00KX

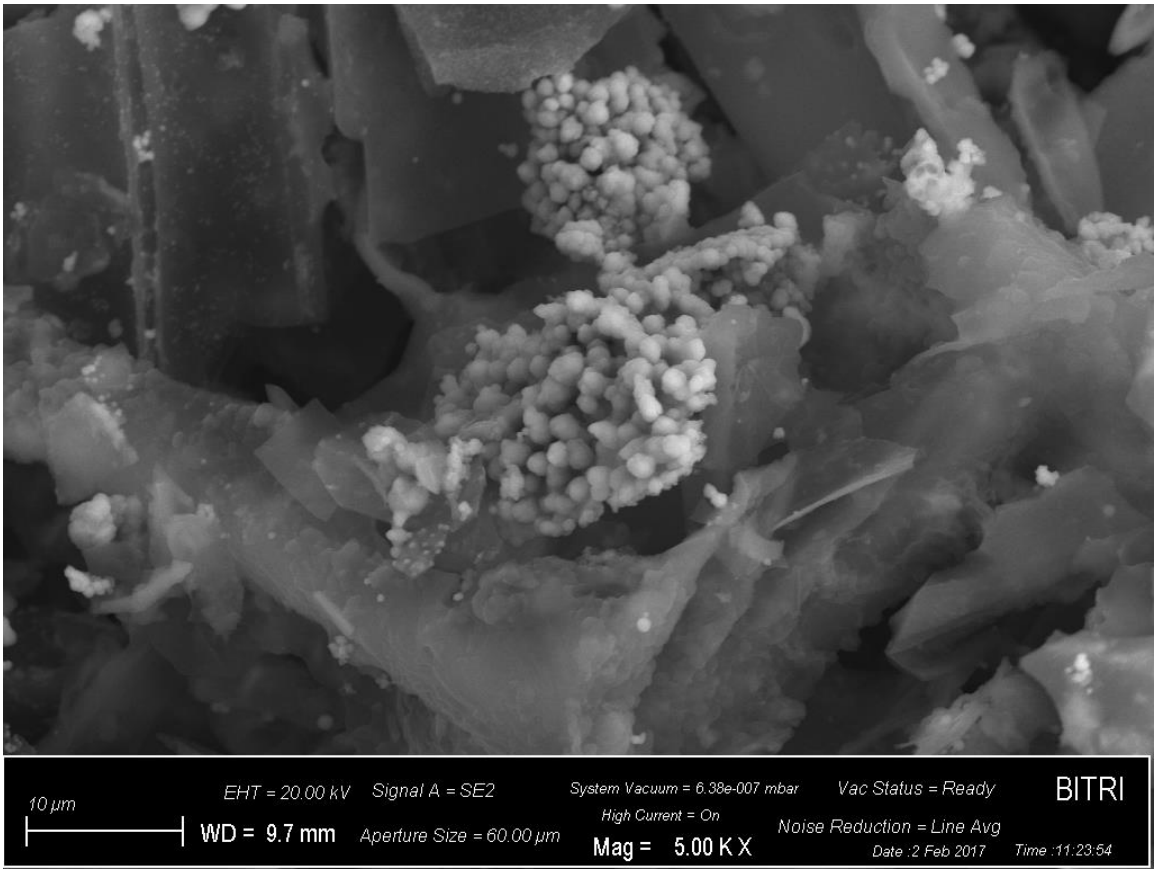

Appendix 25: SEM image of chemically engineered Carbonized Bagasse (α-Fe_2O_3-CBG) adsorbent at a magnification of 2.00 KX

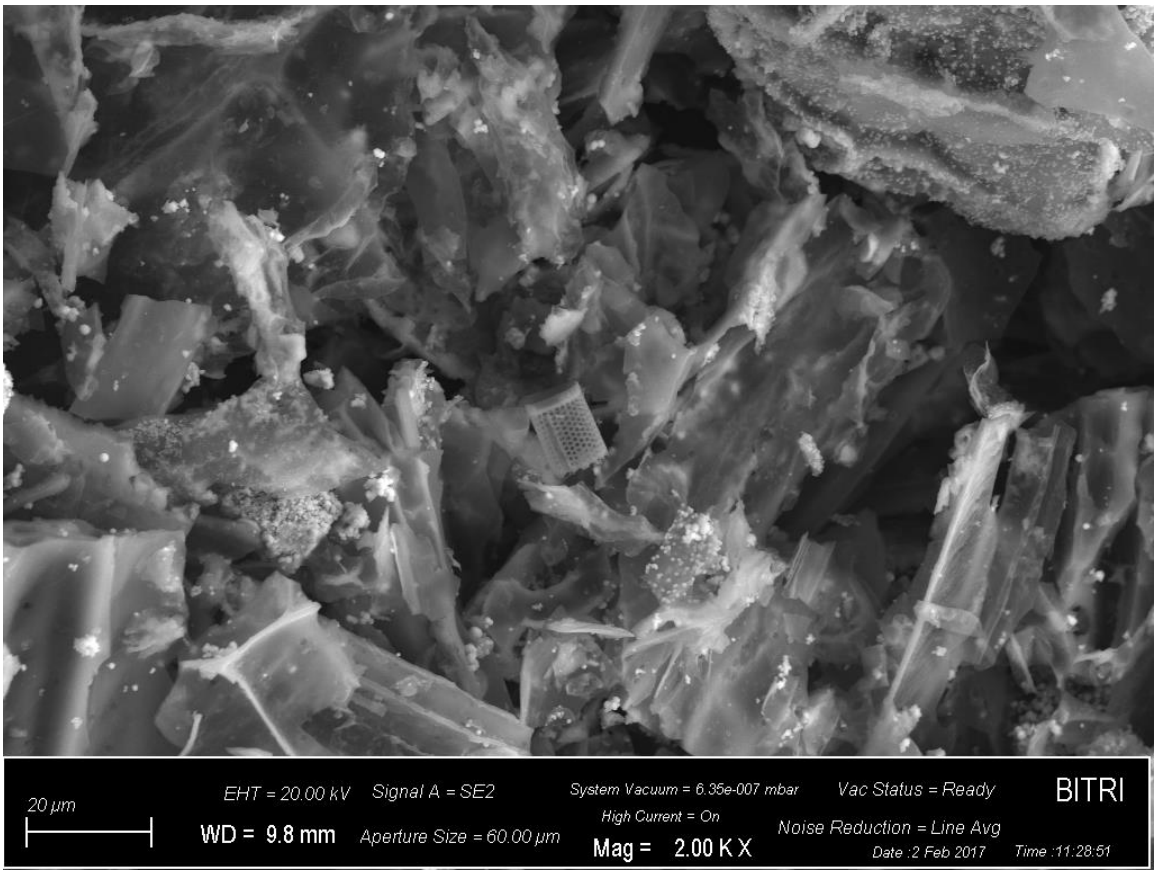

Appendix 26: SEM image of Carbonized Maize Cob (CMC) biochar adsorbent at a magnification of 1.00 KX

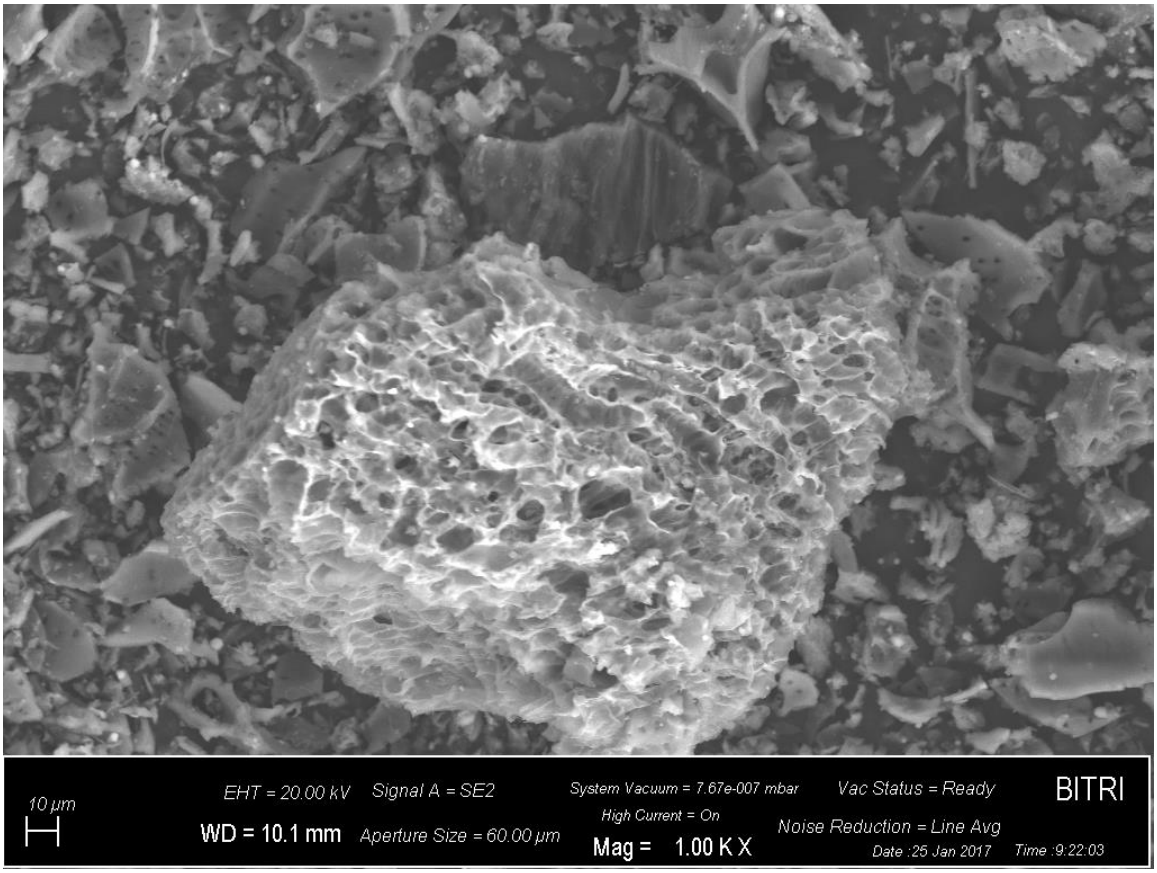

Appendix 27: SEM image of Modified Carbonized Maize Cob (β-FeO(OH)-CMC) adsorbent at a magnification of 1.05 KX

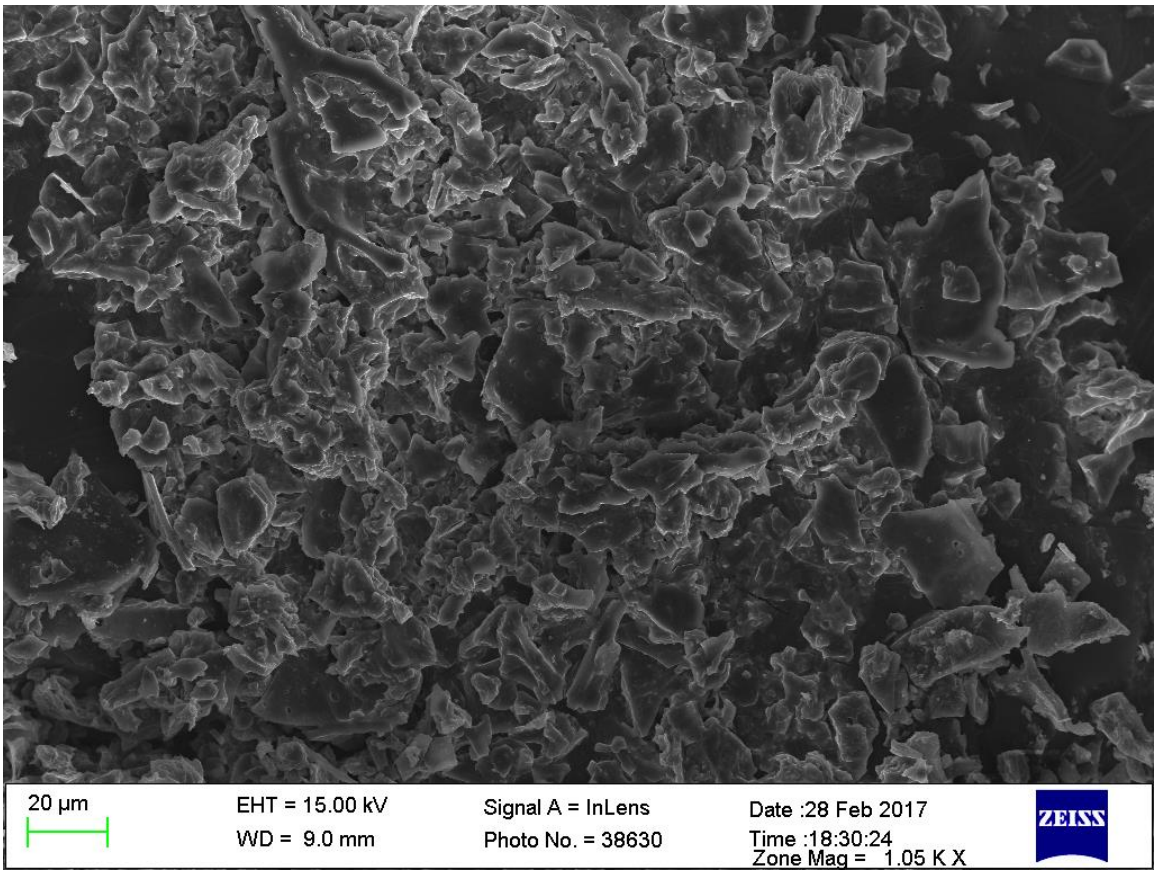

Appendix 28: SEM image of Diatomaceous Earth (DTE) adsorbent at a magnification of 4.00 KX

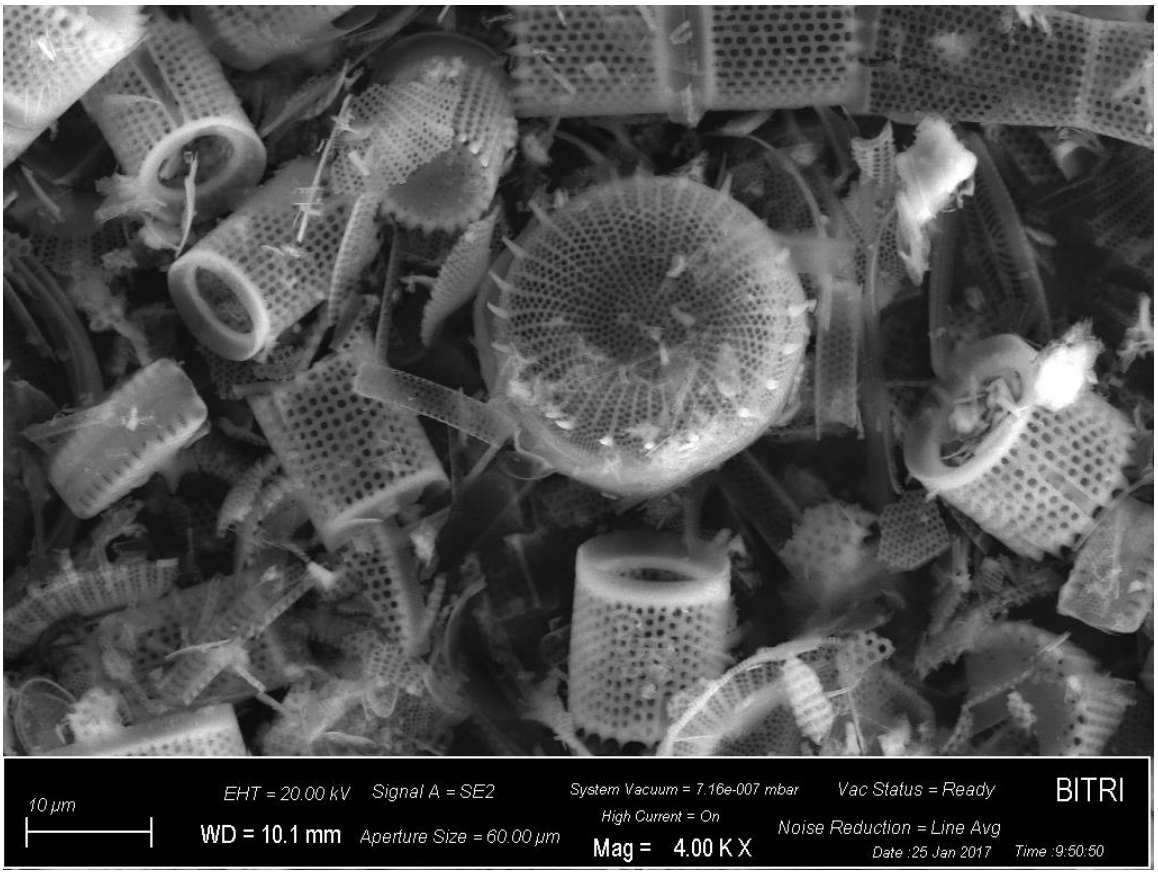

Appendix 29: SEM image of Diatomaceous Earth (DTE) adsorbent at a magnification of 10.00 KX

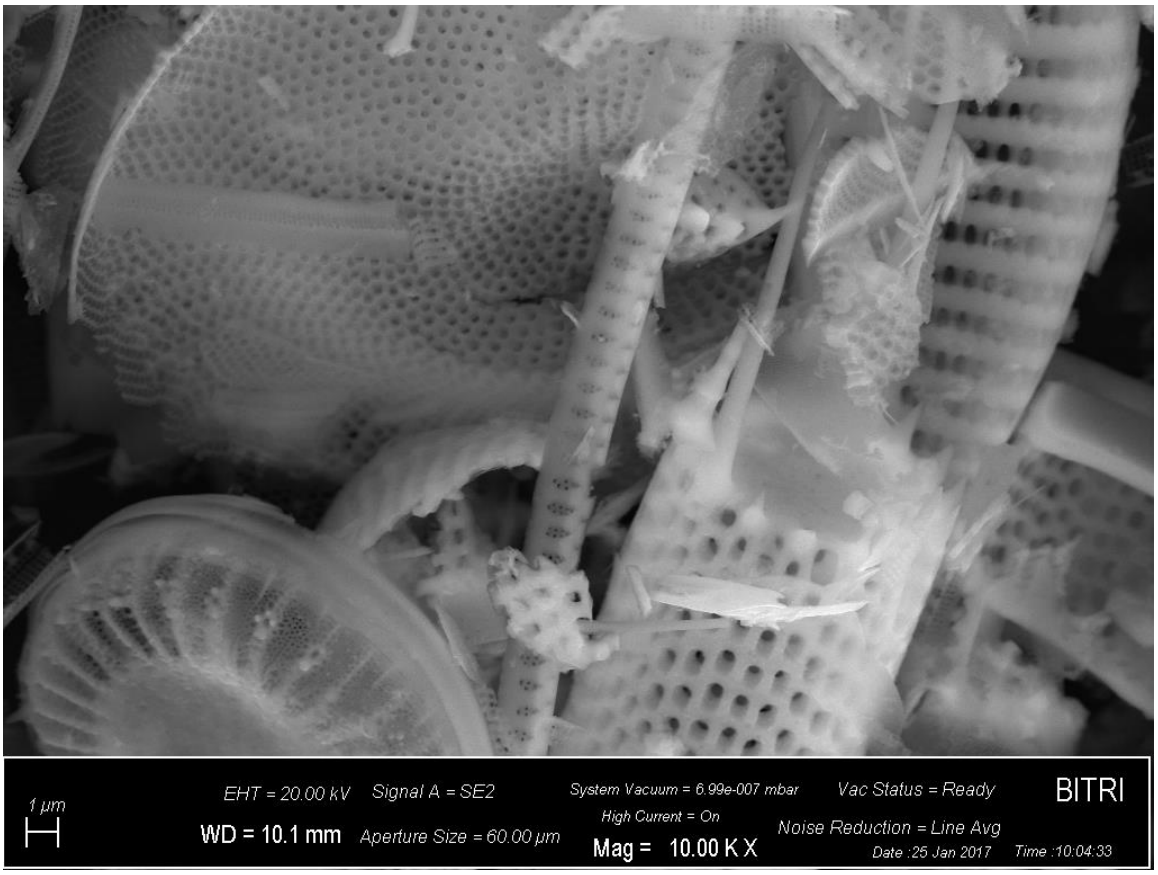

Appendix 30: SEM image of Modified Diatomaceous Earth (α-Fe_2O_3-DTE) composite at a magnification of 5.00 KX

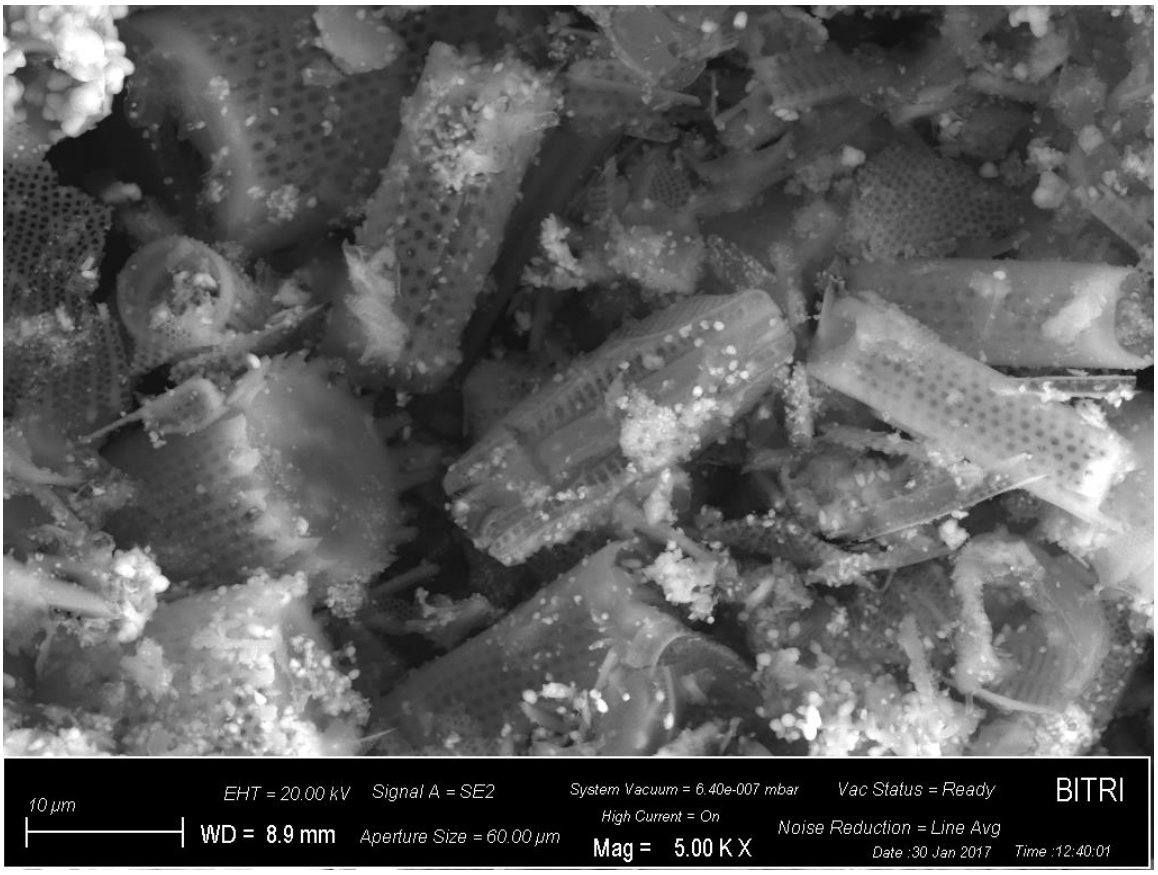

Appendix 31: SEM image of Modified Diatomaceous Earth (α-Fe_2O_3-DTE) composite at a magnification of 4.00KX

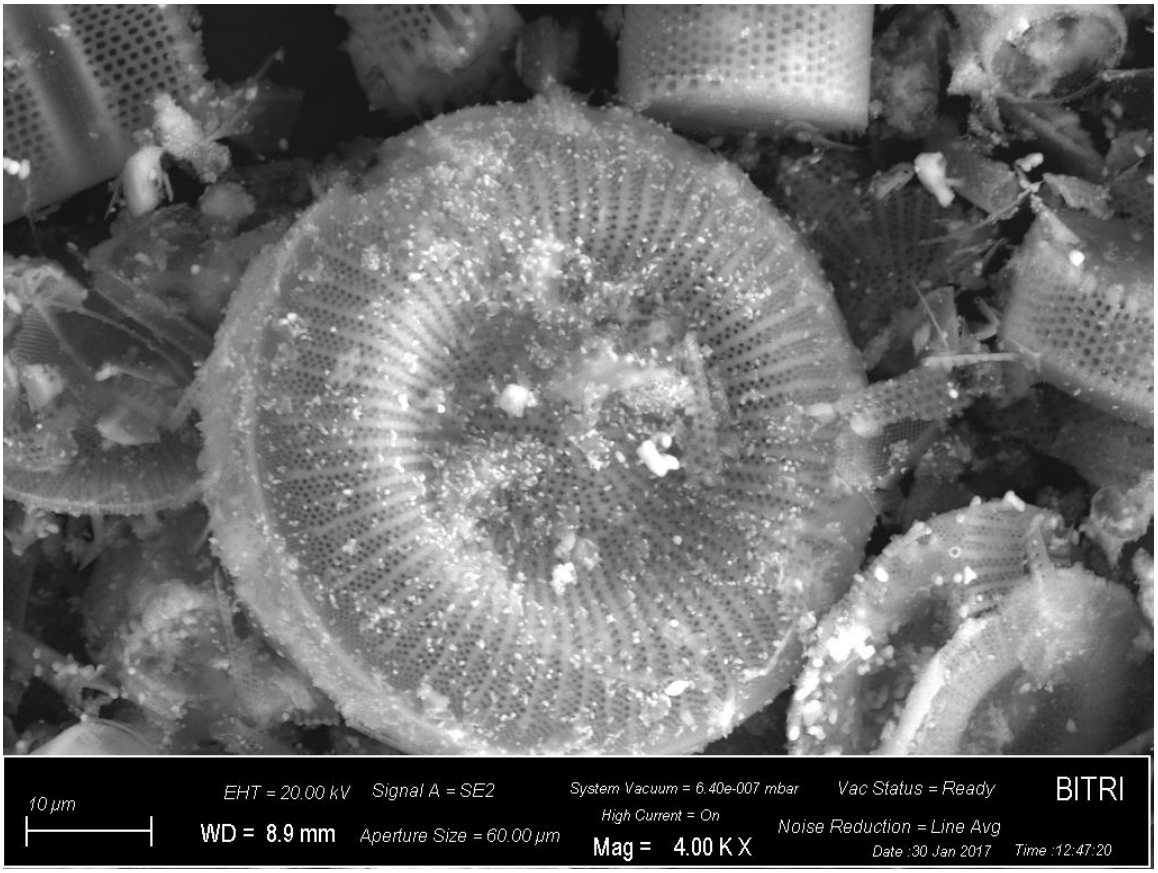

Appendix 32: XRD Spectrum for Carbonized Bagasse (CBG) Biochar

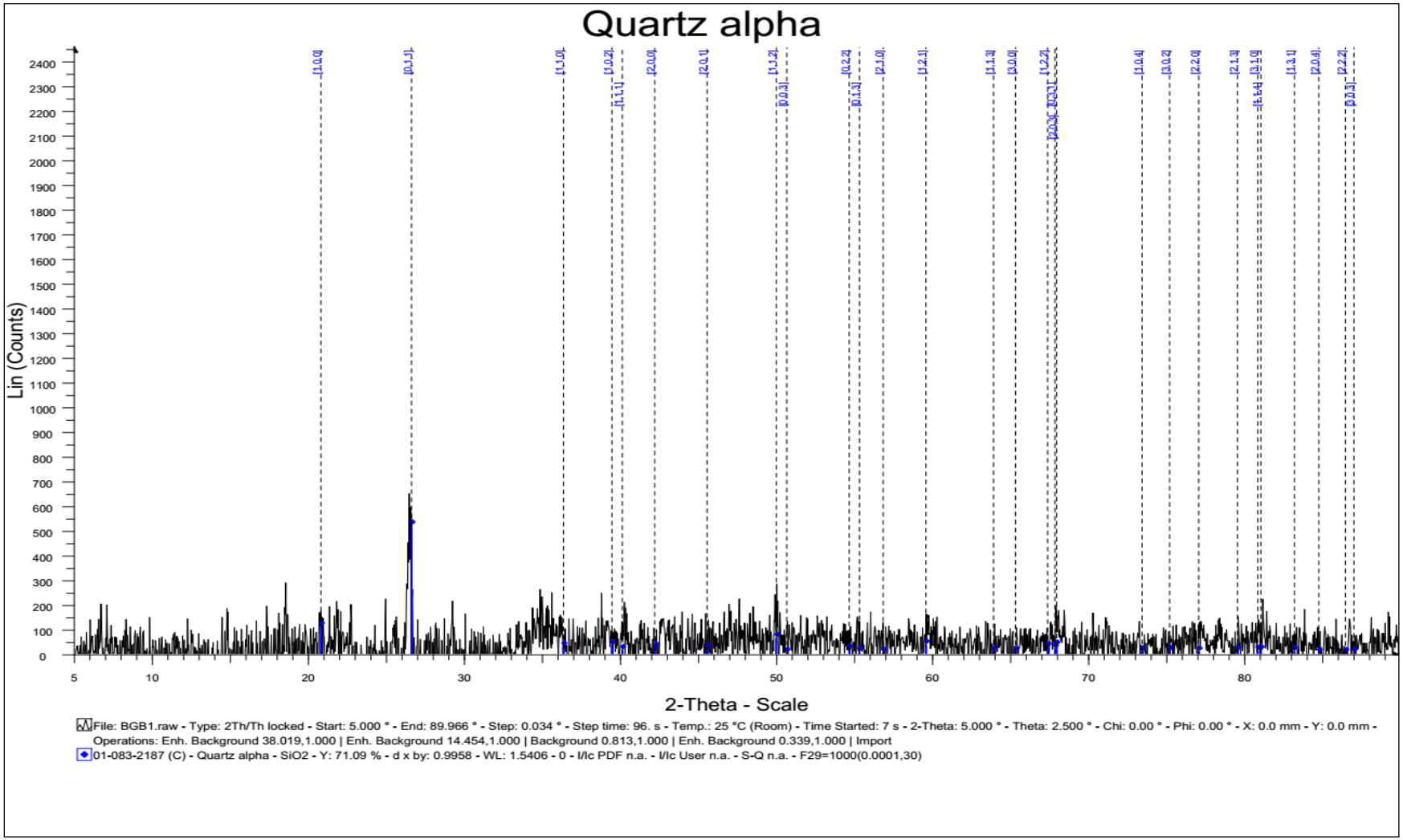

Appendix 33: XRD Spectrum for Modified for Carbonized Bagasse α-Fe_2O_3-CBG adsorbent

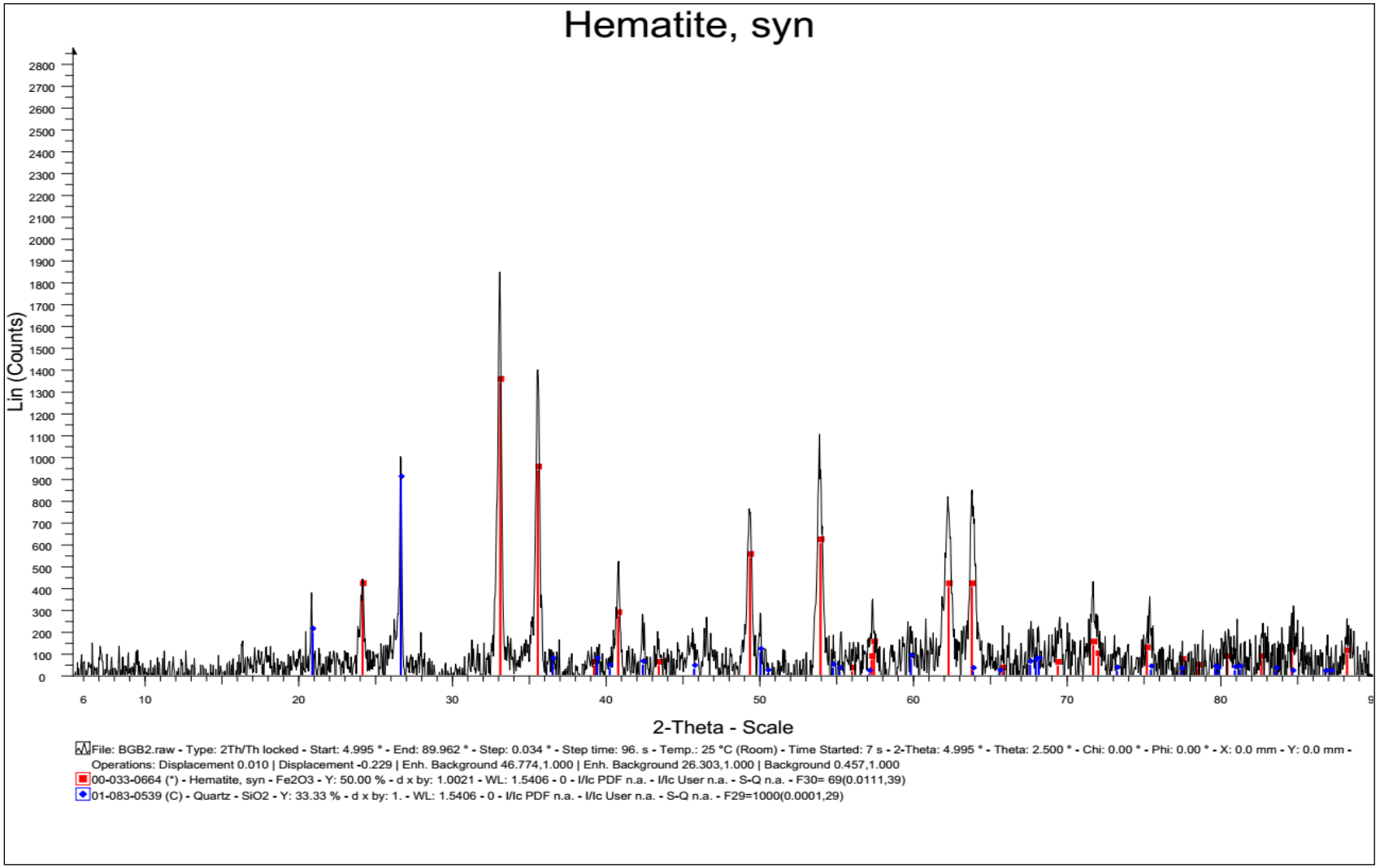

Appendix 34: XRD Spectrum for Carbonized Maize Cob (CMC) Biochar

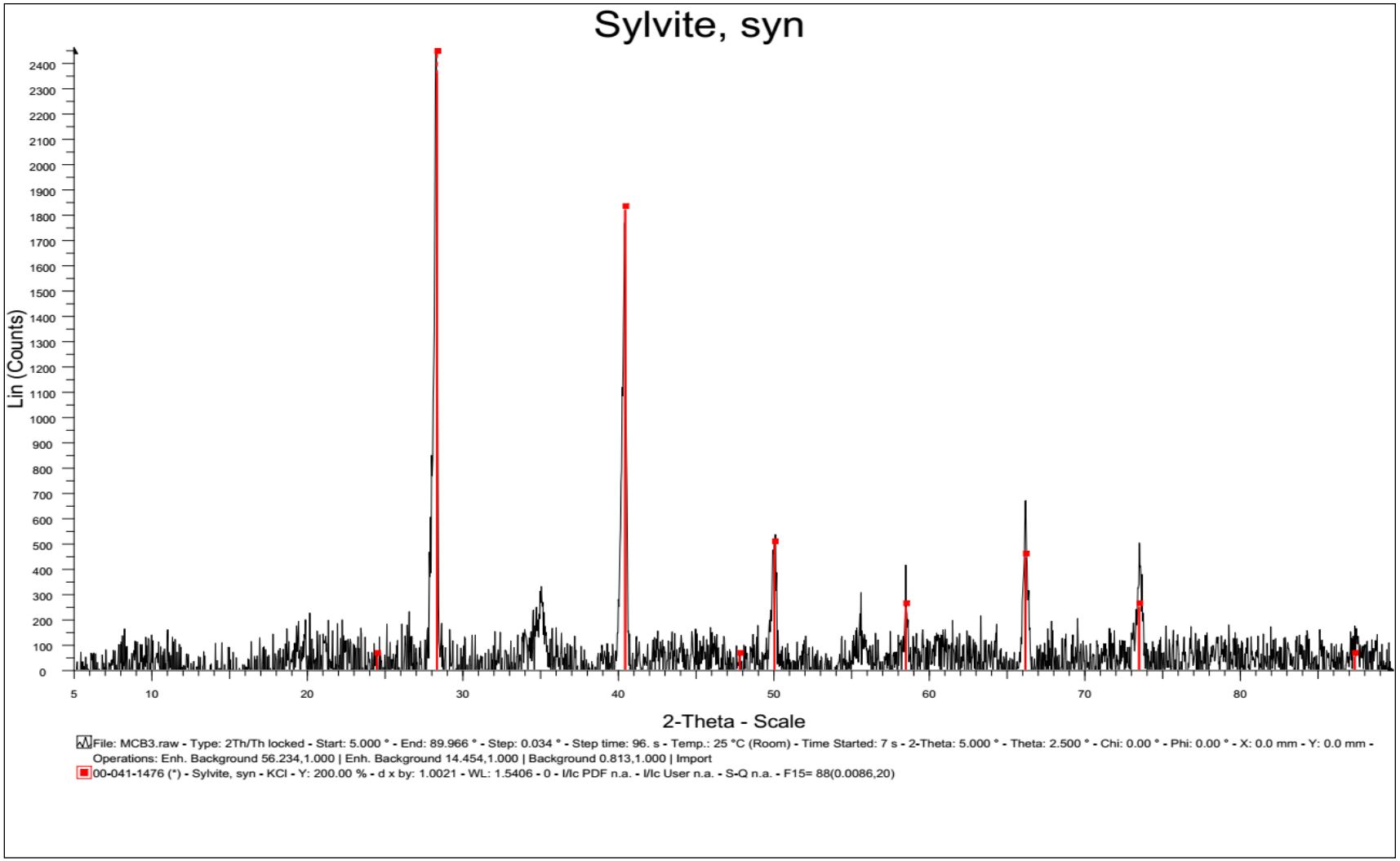

Appendix 35: XRD Spectrum for Modified for Carbonized Maize Cob β-FeO(OH)-CMC composite

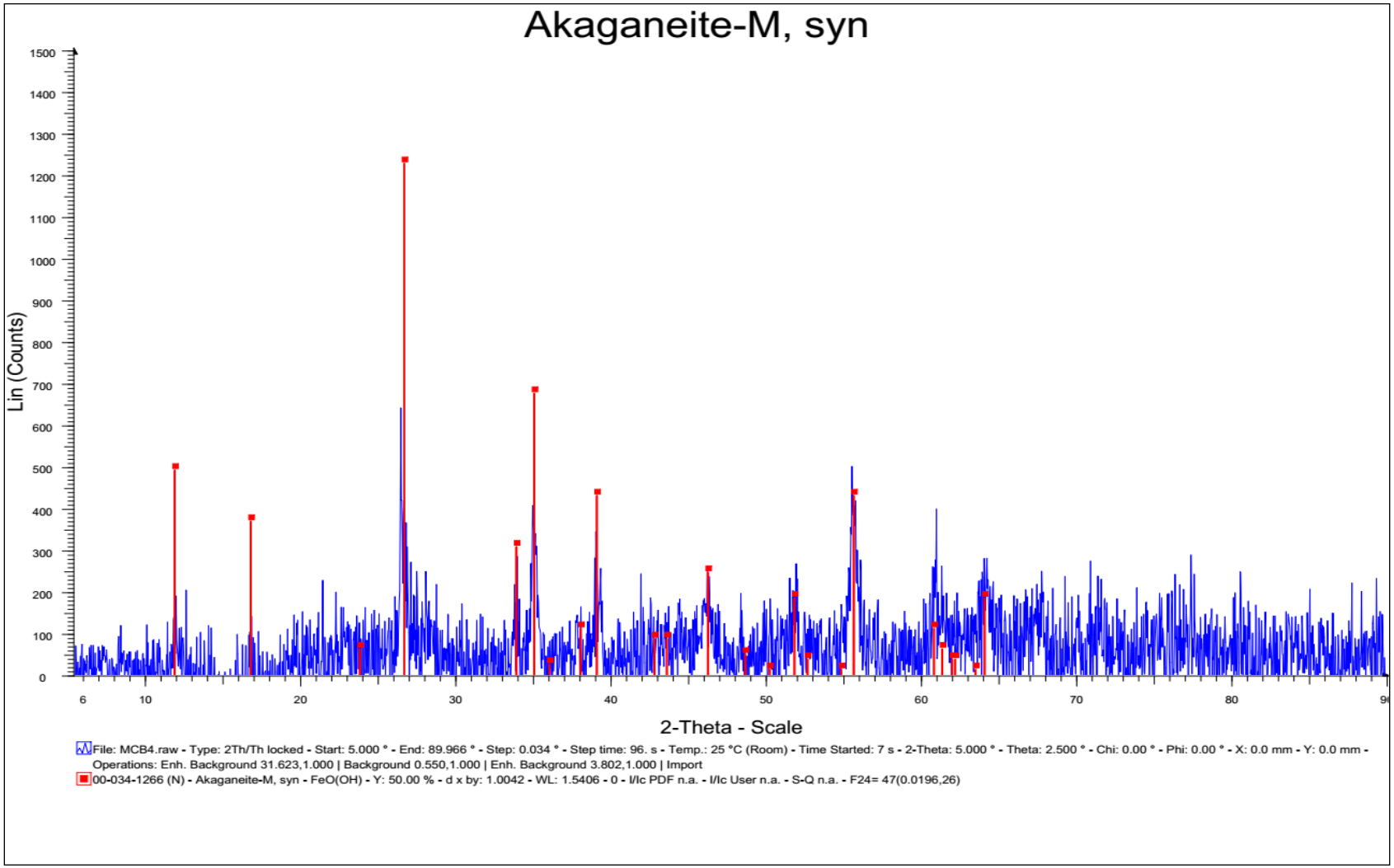

Appendix 36: XRD Spectrum for Diatomaceous Earth (DTE) adsorbent

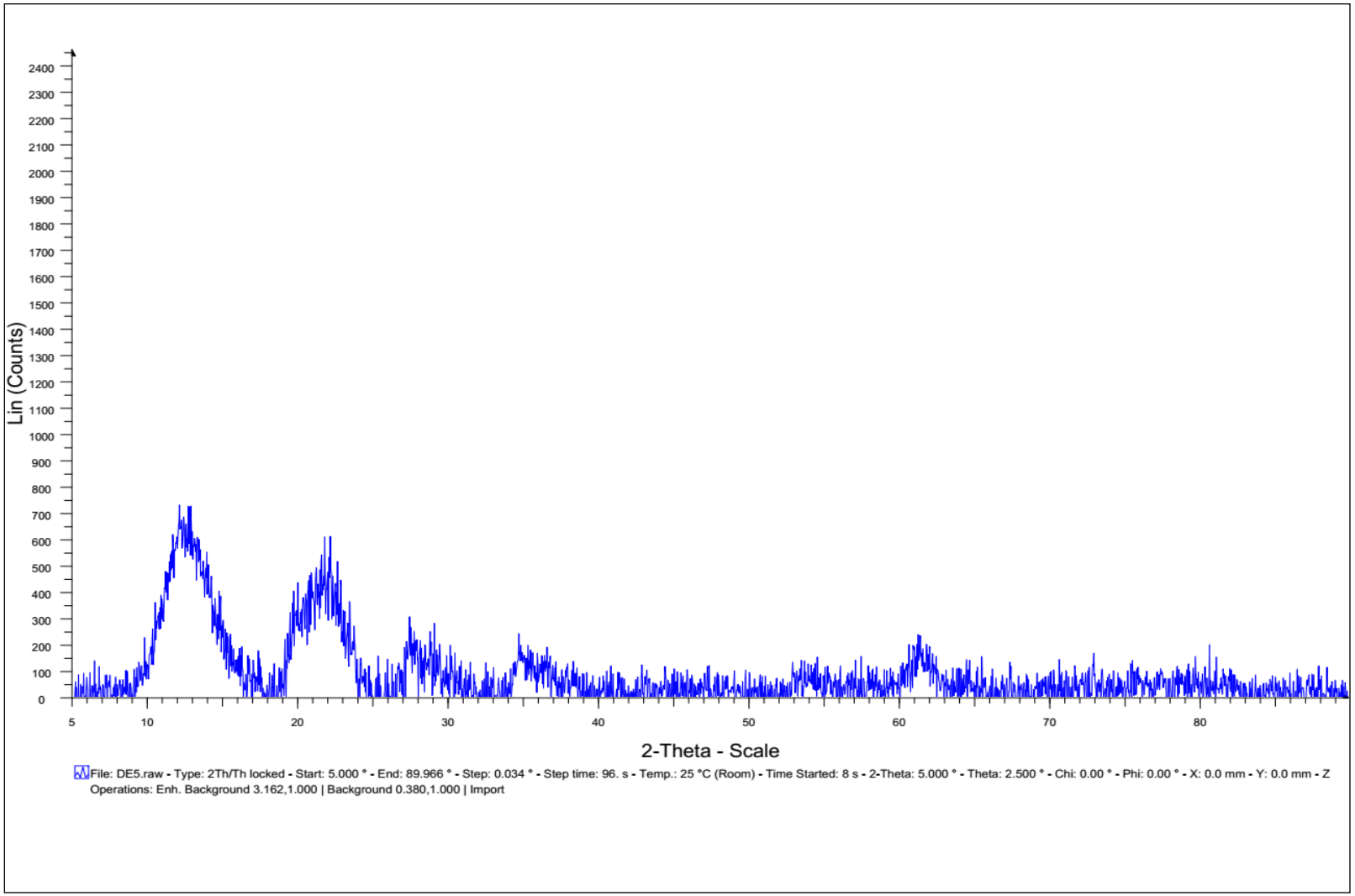

Appendix 37: XRD Spectrum for Modified Diatomaceous Earth α-Fe_2O_3-DTE composite